APPLICATION OF FISHER'S INFORMATION TO ANTENNA ARRAY DESIGN

Samuel D. Wire

November 1999

Radar Systems and Remote Sensing Laboratory Technical Report 12180-1

Radar Systems and Remote Sensing Laboratory
University of Kansas Center for Research, Inc.
2291 Irving Hill Road, Lawrence, Kansas 66045-2969, USA
785/864-4835 * Fax, 785/864-7789 * graham@rsl.ukans.edu

Agreement Dated February 23, 1996
Texas Instruments, Inc.
Dallas TX 75265

Wire, Samuel D. (M.S., Electrical Engineering)

Applications of Fisher's Information to Antenna Array Design

Thesis directed by Assistant Professor James Stiles

Electromagnetic sensors are often implemented to estimate the angle-of-arrival (AOA) of a scattered or emitted signal. An estimation algorithm uses the response from an antenna array to provide AOA estimates. Much research has been performed in developing estimators that minimize AOA estimate error. However, AOA estimate error can likewise be decreased by designing arrays that provide the maximum possible information to the estimation processor.

A concept is presented for using Fisher's Information to design conformal arrays that can provide an optimal response for estimating signal AOA. It will be shown that the resulting designs maximize the upper bound on AOA estimation accuracy, thus presenting an optimal array response to an arbitrary estimator. This concept accounts for measurement uncertainties including thermal noise, receiver channel imbalance, and incident wave polarization.

Contents

Chapter

Figures

Figure

Tables

Table

Chapter 1

Introduction

1.1 Background

Over the the past thirty years, estimation techniques to find the direction-of-arrival (DOA) of an incident plane wave upon an array of sensors has received considerable attention in the literature [9]. The publishings address all facets of direction finding, but one core issue appears again and again. Given data taken from an array of sensors measuring incident electromagnetic (EM) radiation, how should one process this data to compute the best possible estimate of the direction of the incident waveform(s)?

Functionally, direction finding systems can be divided into two parts: the DOA estimator (also called the DOA processor) and the antenna. Much of the hype has centered on improving the DOA processor. Great leaps have been made in computer processing power in the last two decades. This additional processing power has spawned new interest in classical estimation theory. Consequently, estimation algorithms that were considered impossible twenty or thirty years ago have now become feasable.

1.1.1 The Estimator

Estimators can be categorized into two principle groups: parametric and spectral-based methods. Consideration of these two types will be in regard to estimating DOA. Spectal-based methods of estimation generate a spectrum-type function of the parameter of interest (in this case a DOA angle) versus another parameter such as incoming signal power. For instance, if one incident waveform were present and the function were plotted, the peak in the plot would be tagged as the DOA of the incident wave. Parametric methods of estimation frequently require simultaneous solution of all unknown parameters as opposed to isolation of just one parameter. This means that besides needing to estimate the DOA angles ϕ and θ, additional unknown parameters such as the incident wave polarization angles χ and ψ may also require inclusion into the estimator.

Some of the popular spectral-based approaches to estimation are the classical beamformer (also known as Bartlett's beamformer) and MUSIC (MUltiple SIgnal Classification) methods. In classical beamforming, the array beam is steered in one direction and a measurement of the array output is taken. After all the desired directions are scanned and measured, the direction(s) with the maximum array signal power is(are) deemed the DOA estimate(s). For additional information on beamformers, see reference [19].

MUSIC methods are generally superior to beamformers for direction finding. Basic MUSIC estimators operate on the eigenvectors of the cross correlation matrix of the measurements taken from the array. The eigenvectors are used in the generation of a spectrum function. The angle for which the spectrum function is maximized becomes the DOA estimate. The MUSIC algorithms are considered statistically consistent because the DOA estimates they provide will ideally

converge to the actual DOA value when the number of data samples approximates infinity. Details on the MUSIC algorithm can be found in two works by the originator, Ralph Schmidt [12, 13].

Parametric estimators are the other category of estimators. They use statistical signal processing methods to make estimates and can be classified into two main types, Bayesian and classical (non-Bayesian). Classical and Bayesian estimators both utilize probability density functions (PDF) in calculating an estimate. However, the Bayesian approach starts with an a priori PDF from which an a posteriori PDF is obtained by applying Bayes rule. In classical estimation, no a priori PDF exists or none is designated. Consequently, an a posteriori PDF cannot be defined. Instead, one has the PDF of the measurements conditioned on the parameter to estimate. This is called a likelihood function, upon which the maximum likelihood (ML) estimator is based. An ML estimate is the value of the parameter which maximizes the likelihood function. On the other hand, a maximum a posteriori (MAP) estimator bases its estimates on an a posteriori PDF. An MAP estimate is the value of the parameter which maximizes the a posteriori PDF. The classic work in the field of parametric estimators is by Harry Van Trees [18]. A more recent work was authored by Steven Kay [8].

One goal central to all DOA estimators is to make the most accurate direction finding estimates possible. To accomplish this goal, the estimator must make maximum use of the array data presented to it. Stated differently, the estimator must extract the maximum information about direction of arrival from the total information given. The total information will include undesired information such as noise or jamming interference as well as the desired information (that information which is relevant to locating the emitter/scatterer).

1.1.2 The Antenna

The second part of a direction finding system is the antenna. In many instances, the antenna consists of multiple sensors or elements collectively called an array. Arrays are utilized for many reasons, but two key reasons are gain and steering. Arrays provide elevated gain compared with single element antennas. Arrays also permit custom formation and steering of beam patterns.

Because arrays can be very difficult to design, substantial effort has been focused at improving synthesis methods which can be programmed and executed by computer. In 1946, long before the advent of computing power as we know it today, C. L. Dolph published one of the first works on linear array synthesis [4]. Dolph's work used the Chebyshev polynomial to formulate a beam pattern with sidelobes of equal height. The element spacing in Dolph's array was one-half wavelength. Because equal height sidelobes gather unwanted clutter and other interference, they are disadvantageous. Recognizing that sidelobes that taper off from the mainlobe would reduce clutter, T. T. Taylor published a synthesis method (which came to be known as the Taylor one-parameter design [14]) for beam patterns with a sidelobe envelope that approximates the envelope of a sinc function $\frac{\sin(x)}{x}$. The sinc function envelope tapers off at the rate $\frac{1}{x}$. The disadvantage of the Taylor one-parameter pattern is inefficiency. Developed as a compromise between the Dolph-Chebyshev and Taylor one-parameter synthesis methods, the Taylor $\bar{n}$ distribution obtains the higher efficiency of Dolph-Chebyshev while retaining the advantages of a tapered distribution like the Taylor one-parameter [15].

A more recent technique by Bayliss [3] applies the principles of the Taylor $\bar{n}$ distribution to a difference pattern. This work has come to be known as Bayliss pattern synthesis and sees use in linear as well as planar array design.

Planar array pattern synthesis borrows much from linear array pattern synthesis. Typically, the product of two linearly synthesized patterns are used to create the planar array pattern [5]. For a planar array with waveguide elements, a Taylor $\bar{n}$ distribution is applied along the waveguide slots, and another Taylor $\bar{n}$ distribution is applied across the slots, and the two are multiplied together to synthesize the complete pattern.

1.2 Motivation

As seen by the literature, most array synthesis techniques currently focus on forming a specific beam pattern by phasing and/or placing the individual sensors in some calculated manner. These techniques are frequently applied to linear and planar array development and, over the years, have proven to produce working designs. However, conformal array development using these techniques is much more challenging. Therefore many array designers avoid the use of the conformal array where possible. Unfortunately, some array designers cannot avoid the use of a conformal array, because the application requires an array which conforms to a surface, such as the wing of an aircraft or the nose cone of a missile. Because most synthesis techniques are aimed at linear and planar array design, designers are often left with nothing but their own resourcefulness when designing conformal arrays.

There are a number of reasons that conformal array design is an arduous task [7]. First, many synthesis techniques rely on a principle known as the array multiplication principle. This principle states that the beam pattern of an array is the product of the beam pattern of an array of isotropic elements and the beam pattern of an individual element. This does not apply to conformal arrays because one cannot factor out an individual element pattern out of the total

radiation pattern. Second, mutual coupling can be severe and difficult to analyze because of the extreme asymmetry of structures like cones and because of multiple coupling paths between array elements (as in the case of a cylinder, where coupling paths can be clockwise and counterclockwise). Third, cross polarization effects arise because of the different pointing directions for elements on curved surfaces. Other reasons also exist, but this is merely a sampling.

Additionally, while present synthesis techniques can provide maximum array gain in a specified direction, those same techniques may not synthesize an array that gathers maximum direction finding information. Hence, a DOA processor may not make the best estimate of the DOA.

Because of these motivations, a new technique for synthesizing direction finding arrays is proposed. This technique will use principles from estimation theory to determine the best locations for the individual sensors in a direction finding array. The method will also indicate which sensor locations supply the maximum amount of information for direction finding. Should these locations be used in an array design, the resulting array will be "tuned" in a direction finding sense, and, therefore will provide the DOA estimator with the most information possible to make DOA estimates.

1.3 Research Objectives and Scope

The primary objective which forms the basis for this research is:

To find an information oriented metric for use as a parameter in the design of direction finding arrays.

In addition to the primary objective, there are several secondary objectives we hope to accomplish.

(1) Evaluate the new information measure in the design of a conformal array on a complex body

(2) Account for three important measurement uncertainties - thermal noise, receiver channel imbalance, and incident wave polarization

(3) Ascertain the performance of the information measure for designing direction finding arrays

The purpose of objective 1 is to test the new information metric on a model that is as realistic as possible. While a linear or planar array could be used as a model for this work, choosing a conformal array integrated with a more complex structure will confer additional credibility to the final results. This is due to the difficulty in designing conformal arrays with traditional array synthesis techniques.

It is desired that the model will include three important measurement uncertainties - thermal (additive) noise, receiver channel imbalance (multiplicative noise), and incident wave polarization. This is the intent of objective 2. Additive noise is often included in the models of most direction finding estimation problems. However, multiplicative noise, which appears in the form of channel imbalance at the receiver, is rarely taken into account. This is one possible reason some estimation algorithms do not achieve their theoretical performance level.

Many arrays are designed with identically polarized sensors. On one hand, this simplifies the estimation problem. On the other, it hurts the accuracy of the entire direction finding system because polarization is an additional characteristic which can be used to help make estimates of all types of target parameters. It has been shown by Weiss [20] that diversely polarized arrays in direction finding systems permit better DOA estimates than systems with uniformly polarized arrays. Therefore, the array model used in this research will need to account for incident

wave polarization to obtain maximum accuracy.

The worth of an array designed with the new technique must be judged by some criteria. A quantitative criteria is preferable, but in this case a qualitative criteria was used because of schedule constraints. The criteria used is as follows: If the sensor locations determined by the technique are **not** obvious and predictable, then the technique holds promise. On the contrary, if the sensor locations determined by the technique are obvious and predictable, then the technique may be useless.

The key to understanding the criteria is to understand the phrase "obvious and predictable." By "obvious and predictable," an array design is something the designer could have easily determined without the use of the new technique. Examples of "obvious and predictable" include arrays with elements placed for maximum separation or arrays with evenly spaced elements. Arrays with a symetrical look could also be classified as such.

Therefore, if the new design technique indicates element locations which are unusual or **not** obvious and predictable, it could mean that the so called obvious and predictable arrays are sub-optimum in terms of DOA determination. On the other hand, if the new design technique yields arrays which are obvious and predictable, then the new technique achieves no advantages and can be disregarded.

1.3.1 The Approach to be Taken

The list below summarizes the steps which will be taken in chapters to follow.

(1) Choose an array element model. This choice is made in Chapter 2.

(2) Apply Mie's electromagnetic scattering solution to the conducting sphere

array model. This is done in Chapter 3.

(3) Derive an observation model from probability theory. This is shown in Chapter 4.

(4) Obtain the Fisher's Information Matrix from the Mie scattering solution. This step happens in Chapter 5.

(5) Design an array based on Fisher's Information. This will be illustrated in Chapter 6.

(6) Examine the resulting element locations for the array designed with Fisher's Information. This occurs in Chapter 7.

Let us begin by choosing a physical model for an array design.

Chapter 2

The Conformal Array Model

2.1 The Structural Model

A physical structure to carry the array sensors will be need to be chosen. While many structures may suffice, the selected structure must fulfill several criteria.

(1) The structure must demonstrate a realistic electromagnetic scattering response.

(2) The response of the antenna elements placed on the structure must depend upon the shape of the conformal structure.

(3) The structure must have a simple scattering solution.

The simple scattering solution of criteria 3 need not be a closed form solution. However, for the purpose of a model, a closed form solution without numerical integration is desirable because it will require far less computer time to generate solutions.

The first and third criteria are contradictory in that many times simple electromagnetic problems are not realistic and, just as often, realistic electromagnetic problems are not simple. Some examples of conformal shapes that would

make realistic models include the nose cone of a missile or the wing of a airplane. Both of these shapes are commonly found in practice. However, closed form electromagnetic scattering solutions do not exist for these complex shapes. Since a conformal shape with a simple mathematical description is desired, a compromise will be necessary. The conducting cylinder and the conducting sphere meet all our requirements. Both shapes are conformal and both have closed form scattering solutions. Either structure would work, but the conducting sphere offers two dimensions of curvature, and therefore was selected as the physical structure for the conformal array design to come.

The conducting sphere has two features which make it a suitable structure for the array model. First, a closed form scattering solution exists and is known as the Mie scattering solution. It can be found in several textbooks including Harrington [6] and Balanis [1]. Second, it is a simple shape with an equally simple description in the spherical coordinate system.

2.2 The Sensor Model

In the previous section, a physical structure for the array was selected. This physical structure will carry the individual sensor elements which comprise the array. The conducting sphere was chosen in part because of its known, existing scattering solution. Any sensors added to the conducting sphere will obviously change the electric field such that the scattering solution defined in Balanis [1] is no longer valid. But if very small monopole elements are added to the sphere, the scattering solution for the electric field will not change significantly. Consequently, the Mie scattering solution is still considered a good approximation to the electric field. This type of solution for the electric field is called a perturbation solution. By using electrically small monopoles and a perturbation solution, the closed form

Mie solution still applies.

2.3 The Application Model

While there are many possible uses for a direction finding array, the primary application targeted by this research is airborne direction finding. It is important that the model relates to a real world situation. With this in mind, the following scenario will serve as an application model.

Figure 2.1 depicts the model. The conducting sphere will serve as an airborne vehicle or aircraft. It is flying along at an elevation h above the ground. Assume the aircraft (sphere) is looking for emitters on the ground in an oval shaped viewing area. This oval shaped area represents the a priori knowledge we hold about the location of the emitter. We can assume the emitter is located within the oval viewing area and not somewhere else. This assumption will rule out any ridiculous calculations made by the DOA processor that may indicate the emitter is located somewhere outside of the oval (while this in fact could be true due to circumstances such as multipath, in the interest of simplicity, we will limit the problem to the case where the emitter is located in the general direction we are looking).

The radii of the elliptical oval are a and b where $a = 2b$. The sphere is not positioned directly above the center of the ellipse but rather is offset along the z axis by precisely z_{off} from the center. Note that the $+z$ axis faces left and the $+x$ axis faces down in this model. This arrangement is intentional and will help to shorten later calculations. The center of the (x, y, z) coordinate system is located in the center of the sphere. The center of the (x', y', z') coordinate system is located in the center of the ellipse.

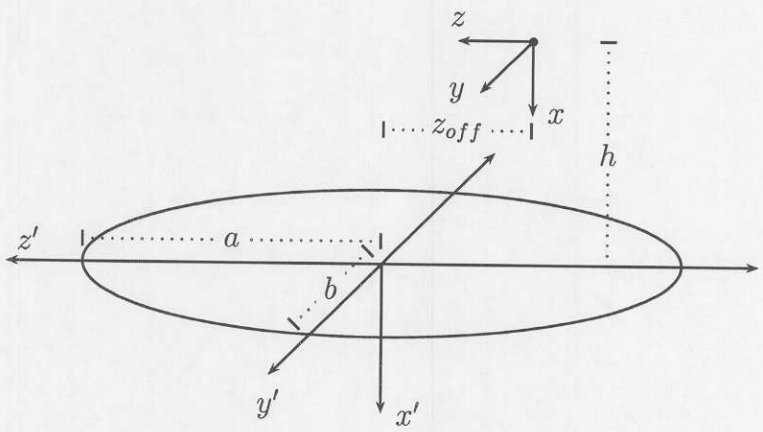

Figure 2.1: Application Model.

Chapter 3

The Mie Scattering Solution for a Conducting Sphere

3.1 Scattering Solution

As stated in Chapter 2, the electromagnetic scattering solution for a conducting sphere is known and can be readily found in Harrington [6] or Balanis [1]. The derivation below closely follows that in Balanis [1].

A uniform plane wave is incident upon a conducting sphere. The plane wave is propagating in the $+z$ direction and is polarized in the $+x$ direction as shown in Figure 3.1. The total electric field at a given point outside the sphere is the sum of the incident and scattered fields. In the spherical coordinate system, the total electric field can be broken down into range, azimuth, and elevation components. Since the azimuth and elevation components of the electric field at the surface of the sphere do not couple into the elements, they may be considered zero. Therefore, the total electric field consists of the radial component only.

The radial component of the total electric field may be found with Equation 3.1 below:

$$E_r^t = \frac{1}{j\omega\mu\varepsilon}\left(\frac{\partial^2}{\partial r^2}A_r^t + \beta^2 A_r^t\right) \tag{3.1}$$

where:

j is the imaginary number $\sqrt{-1}$.

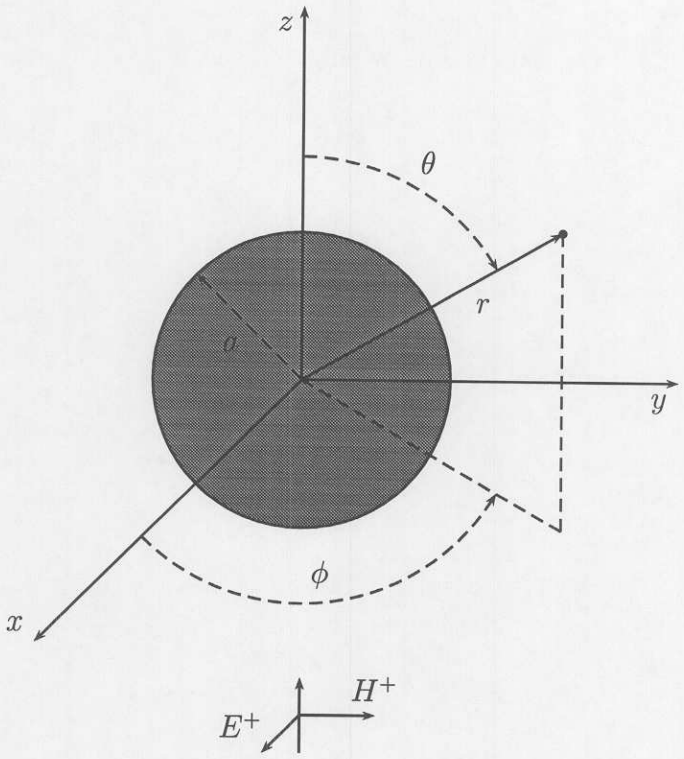

Figure 3.1: Uniform plane wave incident on a conducting sphere.

ω is the angular velocity in rad/s.

μ is the permeability of free space equal to $4\pi \times 10^{-7}$ H/m.

ϵ is the permittivity of free space equal to 8.854×10^{-12} F/m.

β is the wavenumber defined by $\frac{\omega}{c}$ with units of rad/m.

r is the distance from the center of the sphere.

A_r^t is the total magnetic vector potential.

The total magnetic vector potential A_r^t can be found by:

$$A_r^t = E_0 \frac{\cos\phi}{\omega} \sum_{n=1}^{\infty} [a_n \hat{J}_n(\beta r) + b_n \hat{H}_n^{(2)}(\beta r)] P_n^1(\cos\theta) \tag{3.2}$$

Here:

E_0 is the scalar amplitude of the incident waveform.

r is the range associated with position.

ϕ is the azimuth angle associated with position.

θ is the elevation angle associated with position.

ω is again the angular velocity in rad/s.

$\hat{J}_n(\beta r)$ is the spherical Bessel function of the first kind defined by:

$$\hat{J}_n(\beta r) = \sqrt{\frac{\pi\beta r}{2}} J_{n+\frac{1}{2}}(\beta r) \tag{3.3}$$

$J_n(\beta r)$ is referred to as the Bessel function of the first kind of order n.

$\hat{H}_n(\beta r)$ is the spherical Hankel function of the second kind defined by:

$$\hat{H}_n^{(2)}(\beta r) = \sqrt{\frac{\pi\beta r}{2}} H_{n+\frac{1}{2}}^{(2)}(\beta r) \tag{3.4}$$

where:

$$H_n^{(2)}(\beta r) = J_n(\beta r) - jY_n(\beta r) \tag{3.5}$$

is the Hankel function of the second kind. Again, n denotes the order.

P_n^1 is the associated Legendre function of the first kind. Associated Legendre functions of the first kind are defined as:

$$P_n^m = (-1)^m \frac{(1-x^2)^{\frac{m}{2}}}{2^n n!} \frac{d^{m+n}(x^2-1)^n}{dx^{m+n}} \tag{3.6}$$

n is known as the order of the associated Legendre function.

m is called the type of the associated Legendre function.

The coefficients a_n and b_n are:

$$a_n = j^{-n} \frac{2n+1}{n(n+1)} \tag{3.7}$$

$$b_n = -a_n \frac{\frac{\partial}{\partial(\beta r)}\left\{\hat{J}_n(\beta a)\right\}}{\frac{\partial}{\partial(\beta r)}\left\{\hat{H}_n^{(2)}(\beta a)\right\}} \tag{3.8}$$

3.2 Transformed Scattering Solution

The equations in Section 3.1 find the total electric field at a specified location for a specified incident wave with a specified polarization. The location is a predetermined spherical coordinate (r, θ, ϕ); the incident wave is propagating in the $+z$ direction with $+x$ polarization. However, the incident waveform can approach the sphere from any direction with any polarization. Therefore, a more general solution that allows for arbitrary incident waveform direction and polarization is necessary.

The sphere is a symmetric object. When a sphere is viewed from different directions, no matter which view is taken, it still looks like a sphere. This symmetry permits some simplification. The original problem of finding a general solution for the total electric field for an arbitrary incident wave simplifies to one of finding a coordinate transformation which transforms the arbitrary direction of the incident waveform into an incident waveform traveling in the $+z$ direction with $+x$ polarization.

Because electromagnetic fields obey the law of superposition, it is convenient to find the horizontal and vertical components of electric field and later add them together to get the total electric field.

3.2.1 Vertical Component of Electric Field

The total vertical component of the electric field will be comprised of a scattered field component and an incident field component. The scattered com-

ponent for the case of a conducting sphere can be found with the Mie scattering solution just presented. The incident field component can be found utilizing wave polarization techniques. Let us find the scattered component first.

3.2.1.1 Vertical Component of the Scattered Electric Field

To find the vertical scattered component of the electric field, the original location angles must be transformed into new location angles (θ_e, ϕ_e) which fit the sphere scattering model. In other words, after rotating the incident wave from its original location to the location defined by the sphere scattering model ($+z$ propagating, $+x$ polarized), the original point in space has now taken a different position. This newly tranformed point in space is the location where the electric field is to be calculated.

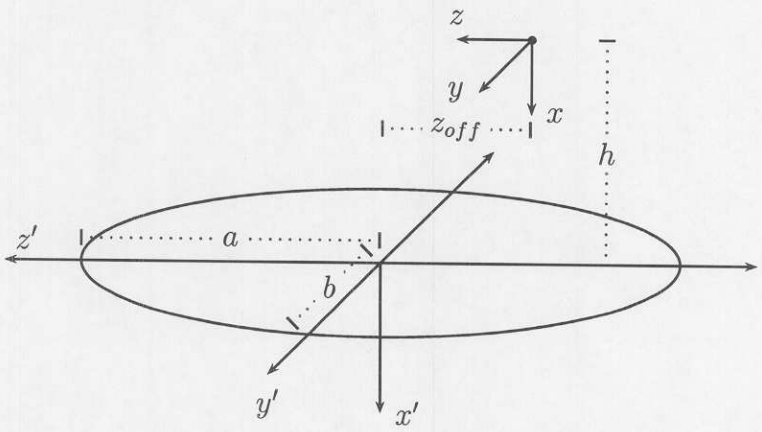

Figure 3.2: Application Model.

Mathematically speaking, define two coordinate systems - one primed $(\hat{x}', \hat{y}', \hat{z}')$ and one unprimed $(\hat{x}, \hat{y}, \hat{z})$. Figure 2.1 from Chapter 2 is reproduced again here as Figure 3.2 for easy reference. Let the primed coordinate system represent the Mie

scattering solution coordinate system; call this the Mie space. Let the unprimed coordinate system represent the coordinate system where any incident waveform direction and polarization are possible; call this global space. Within these two coordinate systems, define the following:

$\hat{r}_i$ = the waveform incidence vector in the global coordinate system.

$\hat{h}_i$ = the horizontal polarization component of the electric field.

$\hat{v}_i$ = the vertical polarization component of the electric field.

$\hat{r}_e$ = the element position in global space.

$\hat{r}'_e$ = the element position in Mie space.

ϕ_e = the azimuth angle of the element position.

θ_e = the elevation angle of the element position.

ϕ_i = the azimuth angle of the DOA of the incident wave.

θ_i = the elevation angle of the DOA of the incident wave.

Refer to Figure 3.3 for element position and DOA angle definitions.

Now that all parameters have been defined, let us derive the coordinate transformation.

$$\hat{r}_i = \cos\phi_i \sin\theta_i \hat{x} + \sin\phi_i \sin\theta_i \hat{y} + \cos\theta_i \hat{z} \tag{3.9}$$

$$\hat{h}_i = -\sin\phi_i \hat{x} + \cos\phi_i \hat{y} \tag{3.10}$$

$$\hat{v}_i = \cos\phi_i \cos\theta_i \hat{x} + \sin\phi_i \cos\theta_i \hat{y} - \sin\theta_i \hat{z} \tag{3.11}$$

$$\hat{r}_e = \cos\phi_e \sin\theta_e \hat{x} + \sin\phi_e \sin\theta_e \hat{y} + \cos\theta_e \hat{z} \tag{3.12}$$

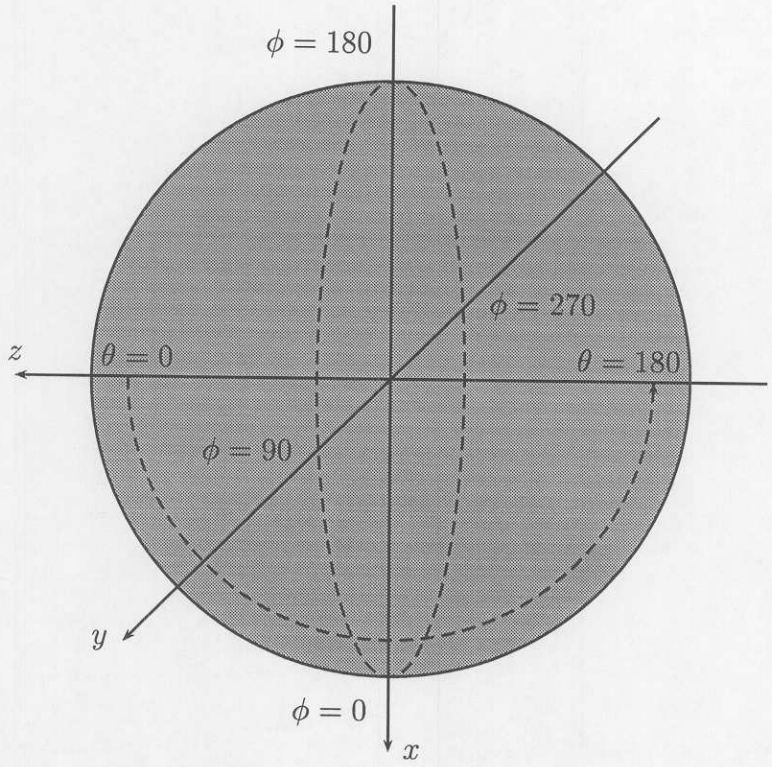

Figure 3.3: Angle Definitions.

$$\hat{r}'_e = \cos\phi'_e \sin\theta'_e \hat{x} + \sin\phi'_e \sin\theta'_e \hat{y} + \cos\theta \hat{z} \tag{3.13}$$

Because the incident waveform must propagate in the $+z$ direction with $+x$ polarization, set

$$\hat{r}_i = \hat{z}' \tag{3.14}$$

$$\hat{v}_i = \hat{x}' \tag{3.15}$$

$$\hat{h}_i = \hat{y}' \tag{3.16}$$

Because the element positions in the primed and unprimed coordinate systems must be equal, set

$$\hat{r}'_e = \hat{r}_e \tag{3.17}$$

Take the dot product of both sides with $\hat{z}'$

$$\hat{r}'_e \cdot \hat{z}' = \hat{r}_e \cdot \hat{z}' \tag{3.18}$$

Substituting for $\hat{z}'$ on the right from 3.14

$$\hat{r}'_e \cdot \hat{z}' = \hat{r}_e \cdot \hat{r}_i \tag{3.19}$$

Substituting for $\hat{r}_i$ with 3.9 and simplifying both sides

$$\cos\theta'_e = \cos(\phi_e - \phi_i)\sin\theta_e \sin\theta_i + \cos\theta_e \cos\theta_i \tag{3.20}$$

Wherever θ appears in Equation 3.2, it appears as $\cos\theta$. The result of Equation 3.20 can be directly inserted into Equation 3.2 without further solving to find θ_e.

At this point, it is important to make a change in the notation of Equation 3.20. The notation $\cos\theta'_e$ in equation 3.20 will be replaced with $\cos\theta^v_e$ where the v stands for vertical. This is done solely to aid in keeping track of horizontal and vertical variables. The equation will now appear as

$$\cos\theta^v_e = \cos(\phi_e - \phi_i)\sin\theta_e \sin\theta_i + \cos\theta_e \cos\theta_i \tag{3.21}$$

Now let us find $\cos\phi^v_e$. Begin by dotting both sides of Equation 3.17 with y' and x' respectively.

$$\hat{r}'_e \cdot \hat{x}' = \hat{r}_e \cdot \hat{x}' \tag{3.22}$$

$$\hat{r}'_e \cdot \hat{y}' = \hat{r}_e \cdot \hat{y}' \tag{3.23}$$

Carrying out the dot product on the left and substituting on the right for $\hat{x}'$ and $\hat{y}'$ with Equation 3.15 and Equation 3.16 respectively

$$\cos\phi'_e \sin\theta'_e = \hat{r}_e \cdot \hat{v}_i \tag{3.24}$$

$$\sin\phi'_e \sin\theta'_e = \hat{r}_e \cdot \hat{h}_i \tag{3.25}$$

Dividing Equation 3.25 by Equation 3.24

$$\tan\phi'_e = \frac{\hat{r}_e \cdot \hat{y}'}{\hat{r}_e \cdot \hat{x}'} \tag{3.26}$$

However, we set out to find $\cos\phi$, not $\tan\phi$. From the definition of cosine:

$$\cos\alpha = \frac{x}{\sqrt{x^2 + y^2}} \tag{3.27}$$

where x is now the denominator of Equation 3.26 and y is the numerator.

$$\cos\phi'_e = \frac{\hat{r}_e \cdot \hat{y}'}{\sqrt{(\hat{r}_e \cdot \hat{x}')^2 + (\hat{r}_e \cdot \hat{y}')^2}} \tag{3.28}$$

Substituting and simplifying yields:

$$\cos\phi'_e = \frac{\cos(\phi_e - \phi_i)\sin\theta_e \cos\theta_i - \cos\theta_e \sin\theta_i}{\sqrt{\sin^2\phi_e - \phi_i \sin^2\theta_e + (\cos(\phi_e - \phi_i)\sin\theta_e \cos\theta_i - \cos\theta_e \sin\theta_i)^2}} \tag{3.29}$$

Once again, it is important to make a change of notation. In Equation 3.29, $\cos\phi'_e$ will be replaced with $\cos\phi^v_e$ where the v stands for vertical. This is done

solely to aid in keeping track of horizontal and vertical variables. The equation will now appear as

$$\cos\phi_e^v = \frac{\cos(\phi_e - \phi i)\sin\theta_e\cos\theta_i - \cos\theta_e\sin\theta_i}{\sqrt{\sin^2\phi_e - \phi_i\sin^2\theta_e + (\cos(\phi_e - \phi_i)\sin\theta_e\cos\theta_i - \cos\theta_e\sin\theta_i)^2}} \quad (3.30)$$

When $\cos\phi_e^v$ and $\cos\theta_e^v$ are inserted into Equation 3.2 and the result of Equation 3.2 is inserted into Equation 3.1, the resulting output is the vertical component of the sphere scattered electric field, denoted E_r^v.

3.2.1.2 Vertical Component of the Incident Electric Field

To find the vertical component of the total electric field, one must include not only the vertical component of the scattered wave, but also the vertical component of the incident wave. To find the vertical field component of the incident wave, we will rely on mathematics from the concept of polarization in plane waves.

It is commonly known that waves in the far field of a radiator approximate plane waves. The electric field vector lies in the plane of the wave and is orthogonal to the direction of wave propagation. For a fixed point in space and as a function of time, the electric field vector will rotate in either a clockwise or counterclockwise manner and the tip of the electric field vector will trace out one of three possible shapes: a line, a circle, or an ellipse. These three shapes result in three types of polarization respectively: linear, circular, and elliptical. Linear and circular polarizations are special cases of the more general elliptical polarization.

As defined by Ulaby [16, 17], the electric field vector of a wave propagating in the $+z$ direction lies in the $x - y$ plane and can be represented by horizontal and vertical components (see Figure 3.4).

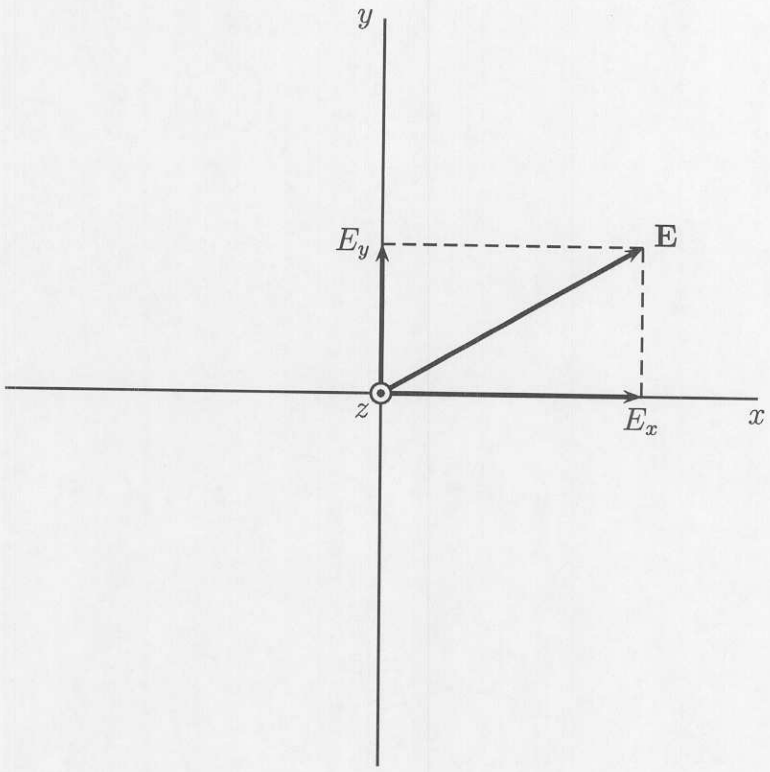

Figure 3.4: Electric field vector for a plane wave propagating in the $+z$ direction

$$\mathbf{E}(z) = E_x(z)\hat{\mathbf{x}} + E_y(z)\hat{\mathbf{y}} \tag{3.31}$$

where

$$\begin{aligned} E_x(z) &= A_x \exp^{ikz} \\ &= a_x \exp^{-i\delta_x} \exp^{ikz} \end{aligned} \tag{3.32}$$

$$\begin{aligned} E_y(z) &= A_y \exp^{ikz} \\ &= a_y \exp^{-i\delta_y} \exp^{ikz} \end{aligned} \tag{3.33}$$

Here, A_x and A_y are the complex amplitudes of $E_x(z)$ and $E_y(z)$. Both A_x and A_y consist of a magnitude a_x or a_y and a phase angle δ_x or δ_y respectively. The corresponding instantaneous field is then

$$\begin{aligned}\mathbf{E}(z,t) &= \mathrm{Re}\left[\mathbf{E}(z)\exp^{-i\omega t}\right] \\ &= \mathrm{Re}\left[E_x(z)\exp^{-i\omega t}\,\hat{\mathbf{x}} + E_y(z)\exp^{-i\omega t}\,\hat{\mathbf{y}}\right] \\ &= \mathrm{Re}\left[E_x(z)\exp^{-i\omega t}\,\hat{\mathbf{x}}\right] + \mathrm{Re}\left[E_y(z)\exp^{-i\omega t}\,\hat{\mathbf{y}}\right] \\ &= a_x\cos(kz-\omega t-\delta_x)\hat{\mathbf{x}} + a_y\cos(kz-\omega t-\delta_y)\hat{\mathbf{y}}\end{aligned} \tag{3.34}$$

Two quantities are of interest when examining the instantaneous electric field: intensity and direction. Intensity is found by the modulus $|\mathbf{E}(z,t)|$

$$\begin{aligned}|\mathbf{E}(z,t)| &= \left[E_x^2(z,t) + E_y^2(z,t)\right]^{\frac{1}{2}} \\ &= \left[a_x^2\cos^2(kz-\omega t-\delta_x) + a_y^2\cos^2(kz-\omega t-\delta_y)\right]^{\frac{1}{2}}\end{aligned} \tag{3.35}$$

while direction is given by the inclination angle ψ

$$\psi(z,t) = \arctan\left(\frac{E_y(z,t)}{E_x(z,t)}\right) \tag{3.36}$$

Elliptical polarization can be characterized by defining a few angles. In Figure 3.5, the angle between the major axis (ξ) of the ellipse and the x axis is called the rotation angle ψ. It is related to wave parameters a_x, a_y, and δ by

$$\tan 2\psi = (\tan 2\alpha)\cos\delta \tag{3.37}$$

The angle defined by Equation 3.38 is called the ellipticity angle and is represented by the letter χ.

$$\tan\chi = \pm\frac{a_\xi}{a_\eta} = \pm\frac{1}{R} \tag{3.38}$$

Ellipticity χ is related to wave parameters a_x, a_y, δ by

$$\sin 2\chi = (\sin 2\alpha)\sin\delta \tag{3.39}$$

R is called the axial ratio. It is sometimes used as an alternative to the ellipticity angle and is defined as $R = \frac{a_\xi}{a_\eta}$.

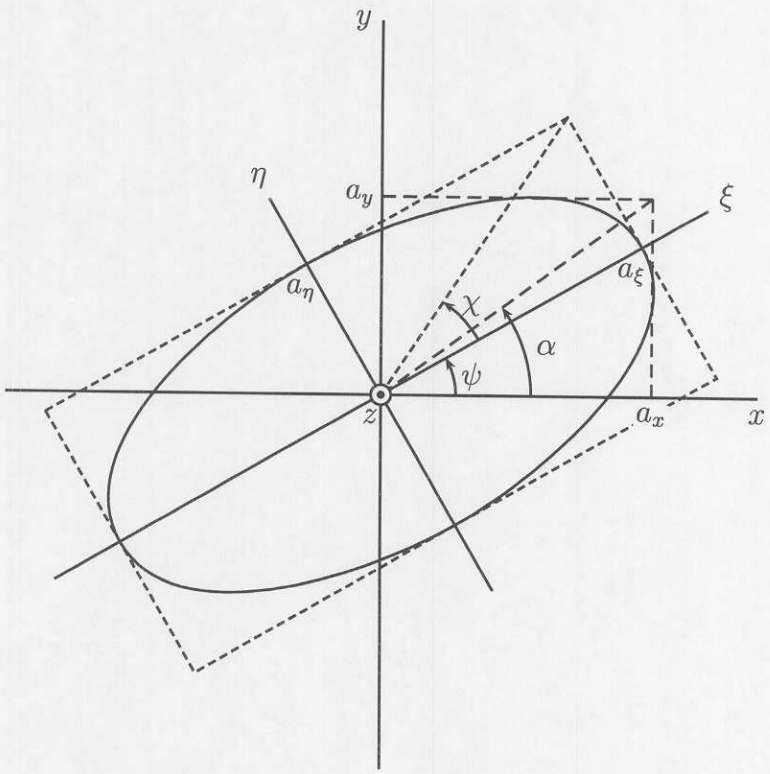

Figure 3.5: Polarization ellipse in the $x-y$ plane. The wave is traveling in the z direction (out of page).

For many antenna problems, it is more convenient to adopt a spherical coordinate system much like the one defined previously in chapter 2. In Figure

3.6, the electric field of the incident wave can still be represented by horizontal and vertical polarization components.

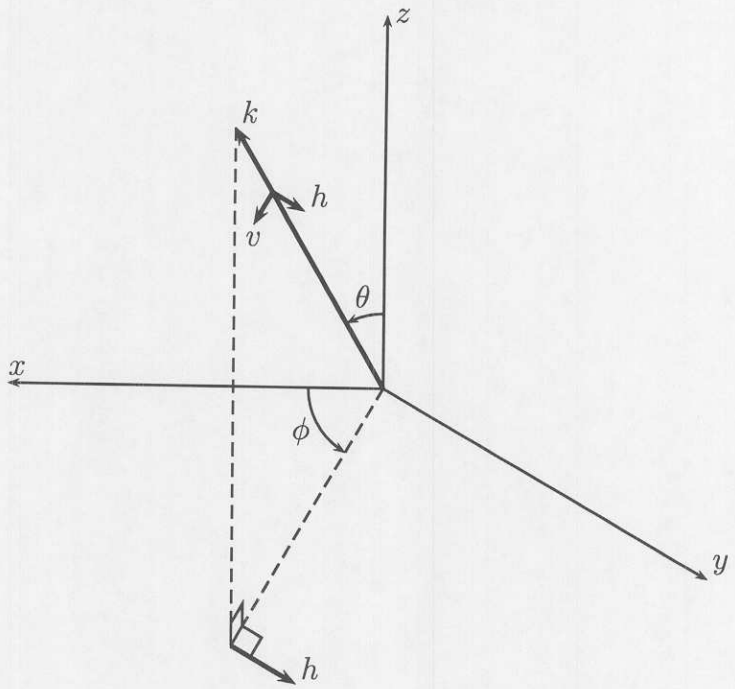

Figure 3.6: Plane wave propagating in direction $\mathbf{k}$ with E-vector components E_v and E_h defined as $\mathbf{h} = (\mathbf{k} \times \mathbf{z})/|\mathbf{k} \times \mathbf{z}|$ and $\mathbf{v} = \mathbf{h} \times \mathbf{k}$.

The electric field vector E may be defined as in [17] where the coordinate system $(\hat{\mathbf{k}}, \hat{\mathbf{v}}, \hat{\mathbf{h}})$ corresponds with $(\hat{\mathbf{r}}, \hat{\theta}, \hat{\phi})$ of a standard spherical coordinate system.

$$\mathbf{E} = (E_v \hat{\mathbf{v}} + E_h \hat{\mathbf{h}}) \exp^{ik\hat{\mathbf{k}} \cdot \mathbf{r}} \tag{3.40}$$

where

$$\hat{\mathbf{h}} = \frac{\hat{\mathbf{z}} \times \hat{\mathbf{k}}}{|\hat{\mathbf{z}} \times \hat{\mathbf{k}}|} = -\sin\phi\hat{\mathbf{x}} + \cos\phi\hat{\mathbf{y}} \tag{3.41}$$

and

$$\hat{\mathbf{v}} = \hat{\mathbf{h}} \times \hat{\mathbf{k}} = \cos\theta\cos\phi\hat{\mathbf{x}} + \cos\theta\sin\phi\hat{\mathbf{y}} - \sin\theta\hat{\mathbf{z}} \tag{3.42}$$

Adopting a matrix form and suppressing the phase factor from Equation 3.40, $\mathbf{E}$ becomes

$$\mathbf{E} = \begin{bmatrix} E_v \\ E_h \end{bmatrix} \tag{3.43}$$

In this case, E_v and E_h are similar to the Cartesian case except all the x subscripts are changed to v subscripts and the y subscripts are replaced with h subscripts. This leaves

$$E_v = a_v \exp^{-i\delta_v}, \tag{3.44}$$

$$E_h = a_h \exp^{-i\delta_h}, \tag{3.45}$$

$$\delta = \delta_h - \delta_v, \tag{3.46}$$

$$\tan\alpha = \frac{a_v}{a_h} \tag{3.47}$$

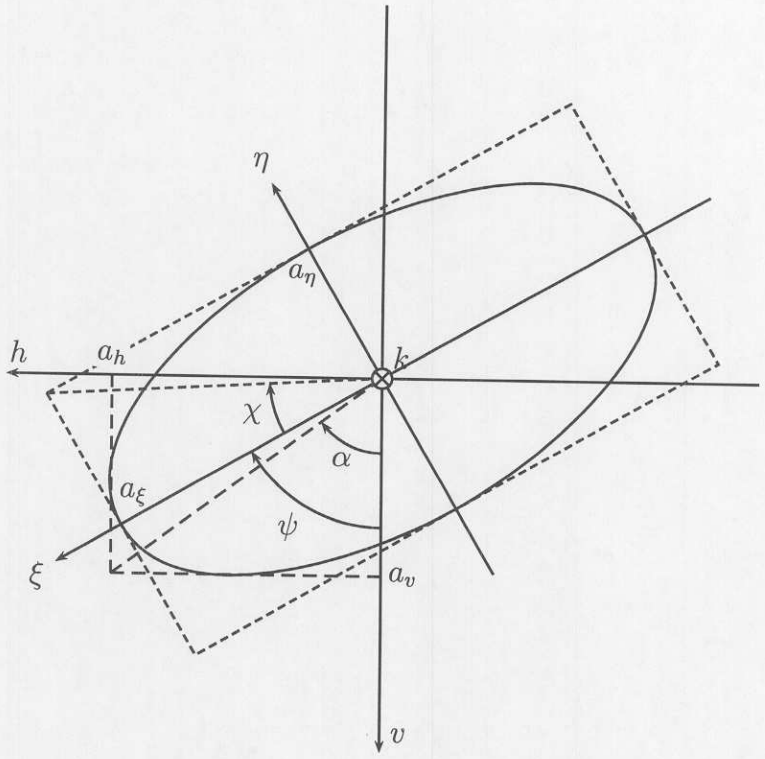

Figure 3.7: Polarization ellipse in the $v-h$ plane. The wave is traveling in the k direction (out of page).

and the polarization angles χ and ψ remain the same as Equation 3.39 and 3.37. The polarization ellipse for the $v-h$ plane is shown in Figure 3.7.

Now that we have an understanding of polarization we can find the vertical polarization component of the incident wave. We represent it here as:

$$E_v^i = a_v e^{+j\frac{\delta}{2}} \tag{3.48}$$

where

$$a_v = \sqrt{\frac{1}{2}(1+\cos 2\psi \cos 2\chi)} \tag{3.49}$$

$$\delta = \arcsin\left[\frac{\sin 2\chi}{2a_v a_h}\right] \tag{3.50}$$

By multiplying E_v^i from Equation 3.48 with E_r^v, the vertical component of the total electric field is obtained.

3.2.2 Horizontal Component of the Electric Field

By following a process similar to the vertical case, the horizontal component of the radial electric field may be found. The new position angles $\cos\theta_e^h$ and $\cos\phi_e^h$ are

$$\cos\theta_e^h = \cos(\phi_e - \phi_i)\sin\theta_e \sin\theta_i + \cos\theta_e \cos\theta_i \tag{3.51}$$

$$\cos\phi_e^h = \frac{-\sin(\phi_e - \phi i)\sin\theta_e}{\sqrt{\sin^2\phi_e - \phi_i \sin^2\theta_e + (\cos(\phi_e - \phi_i)\sin\theta_e \cos\theta_i - \cos\theta_e \sin\theta_i)^2}} \tag{3.52}$$

It is noteworthy to recognize that Equation 3.21 and Equation 3.51 are exactly equal. Similar to the vertical case, inserting the results of Equations 3.51 and 3.52 into Equation 3.2 and the result from Equation 3.2 into Equation 3.1 yields the horizontal component of the sphere scattering solution E_r^h.

But to arrive at the horizontal component of the electric field, one must account for the magnitude and phase of the original incident wave. The horizontal polarization component of the incident wave is

$$E_h^i = a_h e^{-j\frac{\delta}{2}} \tag{3.53}$$

where:

$$a_h = \sqrt{\frac{1}{2}(1 - \cos 2\psi \cos 2\chi)} \tag{3.54}$$

$$\delta = \arcsin\left[\frac{\sin 2\chi}{2a_v a_h}\right] \tag{3.55}$$

By multiplying E_h^i from Equation 3.48 with E_r^h, the horizontal component component of the total electric field is obtained.

3.2.3 Total Electric Field

The total electric field is found by multiplying and adding the different components found previously as follows:

$$E_r = E_v^i E_r^v + E_h^i E_r^h \tag{3.56}$$

Chapter 4

The Observation Model and PDF

4.1 Some Background in Modeling and Estimation Theory

The fundamental 3D direction finding problem involves estimating the elevation and azimuth angles (θ, ϕ) of an incident waveform from data provided by an array of E.M. sensors. One common way to model such an array is with a function of random variables.

$$\mathbf{R} = g(\mathbf{A}) \quad \text{where} \qquad \mathbf{A} = \{\phi_i, \theta_i, \chi, \psi\} \tag{4.1}$$

Here, the function $g(\quad)$ takes state vector $\mathbf{A}$ as an input and gives vector $\mathbf{R}$ as a result. The azimuth angle of the incident wave is represented by ϕ_i, the elevation angle of the incident wave is represented by θ_i, the ellipticity angle associated with incident waveform polarization is represented by χ, and the rotation angle associated with incident waveform polarization is represented by ψ.

Equation 4.1 says that given a state vector $\mathbf{A}$ as input, the output from the array should be $\mathbf{R}$. However, this situation is exactly opposite of the direction finding problem. In the direction finding problem, the output $\mathbf{R}$ from the array is given, and the goal is to find $\mathbf{A}$. Stated more rigorously, given a measurement from the array $\mathbf{R}$, find an estimate of $\mathbf{A}$, denoted $\hat{\mathbf{A}}$. An estimate $\hat{\mathbf{A}}$ can be found

by taking the inverse of the function $g(\quad)$.

$$\hat{\mathbf{A}} = g^{-1}(\mathbf{R}) \tag{4.2}$$

Equation 4.2 often provides accurate estimates of $\mathbf{A}$ if model $g(\quad)$ is linear. However, if $g(\quad)$ is nonlinear, then estimates for $\mathbf{A}$ can be grossly inaccurate. Along with the inaccuracy, multiple solutions to the inversion could exist. Or worse, no solutions to the inversion may exist. It is easy to see that model inversion works quite well for well-posed deterministic linear systems. For random nonlinear systems, a better suited technique would be statistical in nature.

Most statistical based methods are grounded in estimation theory. One method of estimation is the maximum likelihood (ML) estimate. With the maximum likelihood estimate, one seeks to find $\mathbf{A}$, a vector of random variables,

$$\mathbf{A} = \begin{bmatrix} \Phi \\ \Theta \\ X \\ \Psi \end{bmatrix} \tag{4.3}$$

which maximizes the likelihood function defined as:

$$\Lambda \triangleq p(\mathbf{R}|\mathbf{A}) \tag{4.4}$$

where $p(\mathbf{R}|\mathbf{A})$ is the PDF of the measurements conditioned on the parameters to estimate [2, 18]. When no prior knowledge exists about the parameters in state vector $\mathbf{A}$, the maximum likelihood (ML) estimate is a good choice for an estimator. However, if a priori knowledge about the parameters in $\mathbf{A}$ exists, the ML estimate will not take advantage of it.

For instance, assume for the moment that the conducting sphere discussed in Chapter 2 is an aircraft. As it flys along it is searching for an emitter on the ground

(its antenna array is pointed to a spot on the ground in front of the aircraft). This implies that there is a priori knowledge about any and all incident waves striking the antenna array. This a priori knowledge is simply that the emitter is located within some spot on the ground which is the size of the beamwidth of the array.

If ML estimation is applied in the situation above, the ML estimator will make no a priori assumptions about the location of the emitter. Consequently, the estimator will assume that every possible direction in 3D space is equally likely to be the correct DOA estimate. Therefore, the ML estimator may decide the DOA of the incoming wave is somewhere outside of the spot given by a priori information. That sort of estimate can be grossly inaccurate. What is needed is an estimator which utilizes the a priori information to help in making DOA estimates. Estimators such as this exist and a common one is called the maximum a posteriori (MAP) estimator.

The MAP estimator utilizes an a posteriori PDF

$$p(\mathbf{A}|\mathbf{R}) = \frac{p(\mathbf{R}|\mathbf{A})p(\mathbf{A})}{p(\mathbf{R})} \tag{4.5}$$

The object is to find the value of $\mathbf{A}$ which maximizes the a posteriori PDF [18]. Taking the logarithm of Equation 4.5 eases the computation of the maximum in cases where exponentials are involved (e.g. Gaussian).

$$\ln p(\mathbf{A}|\mathbf{R}) = \ln p(\mathbf{R}|\mathbf{A}) + \ln p(\mathbf{A}) - \ln p(\mathbf{R}) \tag{4.6}$$

Because the last term in Equation 4.6, $p(\mathbf{R})$, is not a function of $\mathbf{A}$, it can be considered a constant which can be ignored when maximizing. This leaves:

$$l(\mathbf{A}) = \ln p(\mathbf{R}|\mathbf{A}) + \ln p(\mathbf{A}) \tag{4.7}$$

By taking partial derivatives with respect to each A_i in $\mathbf{A}$, equating to zero, and

solving

$$\frac{\partial l(\mathbf{A})}{\partial A_i} = \frac{\partial \ln p(\mathbf{R}|\mathbf{A})}{\partial A_i} + \frac{\partial \ln p(\mathbf{A})}{\partial A_i} \tag{4.8}$$

the maximum for each parameter A_i can be found. It will be seen in Chapter 5 how closely this relates to Fisher's information. Until then, remember that MAP estimators utilize a priori information. Because the type of array we have chosen to design will be pointed in a specific direction (a priori information is available), the MAP estimator is a logical choice for the work to be done.

4.2 The Observation Model

Given a set of observations, the goal of array signal processing is to estimate some parameter or parameters from the information contained in those observations. An observation model is typically selected to help demonstrate system behavior. Ideally, the chosen model will explain how the observations are obtained from the system input.

While the goal of this research is not to design a better processor, an observation model is nonetheless useful in explaining system behavior. The observations from each element in our array can be modeled as follows:

$$R_n = s_n(\mathbf{A})(1 + N_n) + W_n \tag{4.9}$$

where:

n refers to antenna element n

$\mathbf{A}$ is the state vector $\mathbf{A} = \{\Phi, \Theta, X, \Psi\}$

s_n is the model's prediction of the EM field

N_n is multiplicative noise for modeling channel imbalances

W_n is additive noise for modeling thermal noise

R_n is the observation or measurement of the EM field at element n

It is important to note that R_n , s_n , N_n , W_n are complex values with both a real and imaginary part ($N = N_r + jN_i$). N_r, N_i, W_r, W_i are independent, zero-mean white-gaussian random variables. Therefore:

$$R = (s_r + js_i)(1 + Nr + jNi) + W_r + jW_i \tag{4.10}$$

$$= s_r + s_rN_r + js_rN_i + js_i + js_iN_r - s_iN_i + W_r + jW_i \tag{4.11}$$

Separating real and imaginary components

$$R_r = s_r + s_rN_r - s_iN_i + W_r \tag{4.12}$$

$$R_i = s_i + s_iN_r + s_rN_i + W_i \tag{4.13}$$

In matrix form,

$$\mathbf{R} = \mathbf{m} + \mathbf{sN} \tag{4.14}$$

where $\mathbf{R} = [R_r \quad R_i]^T$, $\mathbf{m} = [s_r \quad s_i]^T$, $\mathbf{N} = [N_r \quad N_i \quad W_r \quad W_i]^T$, and

$$\mathbf{S} = \begin{bmatrix} s_r & -s_i & 1 & 0 \\ s_i & s_r & 0 & 1 \end{bmatrix} \tag{4.15}$$

4.3 The Noise PDF

In Section 4.2, the noise in the observation model was separated into its real and imaginary components. Given that information and that each component is zero-mean white-gaussian noise, the PDF of the noise vector N is

$$p(\mathbf{N}) = \frac{1}{(2\pi)^2 \det \Sigma_{\mathbf{N}}{}^{\frac{1}{2}}} \exp\left[-\frac{1}{2}\mathbf{N}^T\Sigma_{\mathbf{N}}\mathbf{N}\right] \tag{4.16}$$

Here:

$$\Sigma_{\mathbf{N}} = \begin{bmatrix} \sigma_1^2 & 0 & 0 & 0 \\ 0 & \sigma_2^2 & 0 & 0 \\ 0 & 0 & \sigma_3^2 & 0 \\ 0 & 0 & 0 & \sigma_4^2 \end{bmatrix} \tag{4.17}$$

where:

$$\sigma_1^2 = E\left[n_r^2\right] \tag{4.18}$$

$$\sigma_2^2 = E\left[n_i^2\right] \tag{4.19}$$

$$\sigma_3^2 = E\left[w_r^2\right] \tag{4.20}$$

$$\sigma_4^2 = E\left[w_i^2\right] \tag{4.21}$$

and $|\Sigma_{\mathbf{n}}|$ is the determinant of $\Sigma_{\mathbf{n}}$. To make a simplication, the real and imaginary parts of the additive white noise variance are assumed equal ($\sigma_4^2 = \sigma_3^2$). This leaves

$$\Sigma_{\mathbf{N}} = \begin{bmatrix} \sigma_1^2 & 0 & 0 & 0 \\ 0 & \sigma_2^2 & 0 & 0 \\ 0 & 0 & \sigma_3^2 & 0 \\ 0 & 0 & 0 & \sigma_3^2 \end{bmatrix} \tag{4.22}$$

4.4 The Conditional PDF

Because the noise PDF's are gaussian, the conditional PDF $p(\mathbf{R_r^n}, \mathbf{R_i^n})$ is likewise Gaussian. Recall that the PDF of a multivariate Gaussian distribution is [11, 8]

$$p(\mathbf{x}) = \frac{1}{(2\pi)^{\frac{N}{2}} |\mathbf{C}_x|^{\frac{1}{2}}} \exp\left[-\frac{1}{2}(\mathbf{x} - \mu_x)^T \mathbf{C}_x^{-1}(\mathbf{x} - \mu_x)\right] \tag{4.23}$$

The conditional PDF for a single antenna element n is then

$$p\left(R_r^n, R_i^n | A\right) = \frac{1}{(2\pi)^2 \left|\Sigma_R\right|^{\frac{1}{2}}} \exp\left[-\frac{1}{2}(\mathbf{R}-\mathbf{m})\Sigma_R^{-1}(\mathbf{R}-\mathbf{m})\right] \tag{4.24}$$

where

$$\begin{aligned}
\Sigma_{\mathbf{R}} &= \mathbf{S}\Sigma_{\mathbf{R}}\mathbf{S}^{\mathbf{T}} \\
&= \begin{bmatrix} S_r & -S_i & 1 & 0 \\ S_i & S_r & 0 & 1 \end{bmatrix} \begin{bmatrix} \sigma_1^2 & 0 & 0 & 0 \\ 0 & \sigma_2^2 & 0 & 0 \\ 0 & 0 & \sigma_3^2 & 0 \\ 0 & 0 & 0 & \sigma_3^2 \end{bmatrix} \begin{bmatrix} S_r & S_i \\ -S_i & S_r \\ 1 & 0 \\ 0 & 1 \end{bmatrix} \\
&= \begin{bmatrix} S_r^2\sigma_1^2 + S_i^2\sigma_2^2 + \sigma_3^2 S_r S_i \sigma_1^2 - S_r S_i \sigma_2^2 \\ S_r S_i \sigma_1^2 - S_r S_i \sigma_2^2 S_i^2 \sigma_1^2 + S_r^2 \sigma_2^2 + \sigma_3^2 \end{bmatrix}
\end{aligned} \tag{4.25}$$

$\mathbf{m}$ and $\mathbf{S}$ are functions of A. Because the array consists of N total elements, the conditional PDF for the array is

$$p(\mathbf{R}|\mathbf{A}) = \prod_{n=1}^{N} p(\mathbf{R}_n|\mathbf{A}) \tag{4.26}$$

defining $\mathbf{R}$ as

$$\mathbf{R} = \left\{R_r^1, R_i^1, R_r^2, R_i^2, ..., R_r^N, R_i^N\right\} \tag{4.27}$$

Therefore

$$p(\mathbf{R}|\mathbf{A}) = \frac{1}{(2\pi)^N \prod_{n=1}^{N} \left|\Sigma_R^n\right|^{\frac{1}{2}}} \exp\left[-\frac{1}{2}\sum_{n=1}^{N}(\mathbf{R}_n - \mathbf{m}_n)^T \Sigma_{R_n}^{-1}(\mathbf{R}_n - \mathbf{m}_n)\right] \tag{4.28}$$

4.5 The Apriori PDF

By comparison to the conditional PDF, the PDF for the a priori information is relatively easy to find. Recognizing that the ellipticity and rotation angles χ

and ψ are statistically independent of each other and of the incidence angles ϕ_i and θ_i, the PDF of A is just:

$$p(\mathbf{A}) = p(\phi_i, \theta_i)p(\chi)p(\psi) \tag{4.29}$$

where the PDF of the location angles $p(\phi_i, \theta_i)$, the PDF of the ellipticity angle $p(\chi)$, and the PDF of the rotation angle $p(\psi)$ are found below.

4.5.1 The PDF $p(\phi_i, \theta_i)$

Finding the PDF $p(\phi_i, \theta_i)$ is a two step procedure. First, we will find the PDF of the antenna illumination area in the (y', z') plane. This PDF will be denoted by $p(y', z')$. Next, we will transform the PDF $p(y', z')$ from terms of y', z' to terms (ϕ_i, θ_i). This transformed PDF is $p(\phi_i, \theta_i)$.

Why do we bother to find the PDF in terms of (y', z')? It is much easier to describe the probability of emitter/scatterer location in the (y', z') plane. For instance, we can both conceptually visualize and mathematically describe a uniform emitter/scatterer location probability in the (y', z') plane. Then a simple random variable transformation will permit rewriting $p(y', z')$ as $p(\phi_i, \theta_i)$.

Originally, it was assumed that all locations within the beam width of the antenna pattern would be equally likely to be the location of an emitter or scatterer. The locations are uniformly distributed across the beam pattern. The beam pattern itself would be assumed elliptical. Figure 4.5.1 is a plot of the uniformly distribution over the beam pattern. Any location within the distribution has an equal probability of occurrence. Any location outside the limits formed by the beam pattern would have no chance of occurring.

The uniform PDF was chosen primarily because of its simple mathematical description. It wasn't until later that we found the uniform distribution to be

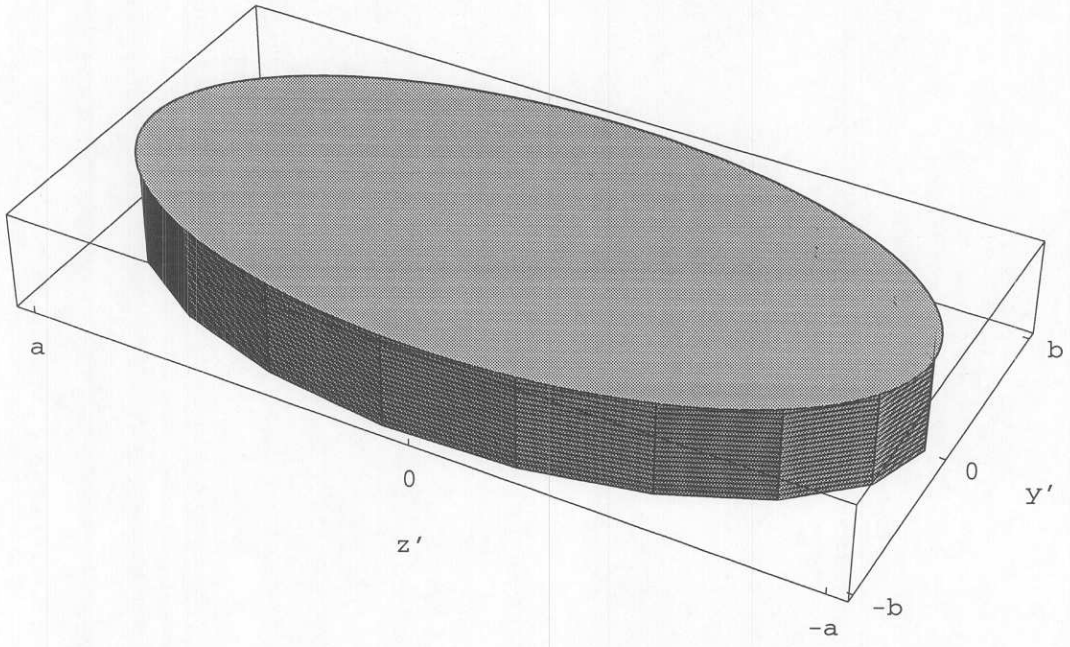

Figure 4.1: Apriori PDF $p(y', z')$

a poor choice for the PDF $p(y', z')$. We could not perform the differentiation of a uniform PDF required in later calculations. The uniform PDF has sharp discontinuities much like a step function and is therefore nondifferentiable. As a result, a different distribution had to be selected.

One distribution which does not display any discontinuities is the Gaussian distribution. It can be argued that the Gaussian PDF is also an appropriate choice for the emitter/scatterer location because antennae can be built with a beam pattern that is most sensitive in the center of the pattern and tapering off as the distance from center increases. Figure 4.5.1 shows the Gaussian a priori PDF $p(y', z')$.

The application model from Figure 2.1 will help to derive $p(y', z')$. From the figure, the vector $\bar{r}$ is

$$\bar{r} = -h\hat{x} - y'\hat{y} - (z' - z_{off})\hat{z} \tag{4.30}$$

The unit vector $\hat{r}$ is simply

$$\hat{r} = \frac{\bar{r}}{|\bar{r}|} \tag{4.31}$$

where

$$|\bar{r}| = \sqrt{h^2 + (y')^2 + (z' - z_{off})^2} \tag{4.32}$$

By the definition of ϕ_i and θ_i

$$\hat{r} = \cos\phi_i \sin\theta_i \hat{x} + \sin\phi_i \sin\theta_i \hat{y} + \cos\theta_i \hat{z} \tag{4.33}$$

Equating like terms

$$\cos\phi_i \sin\theta_i = \frac{-h}{|\bar{r}|} \tag{4.34}$$

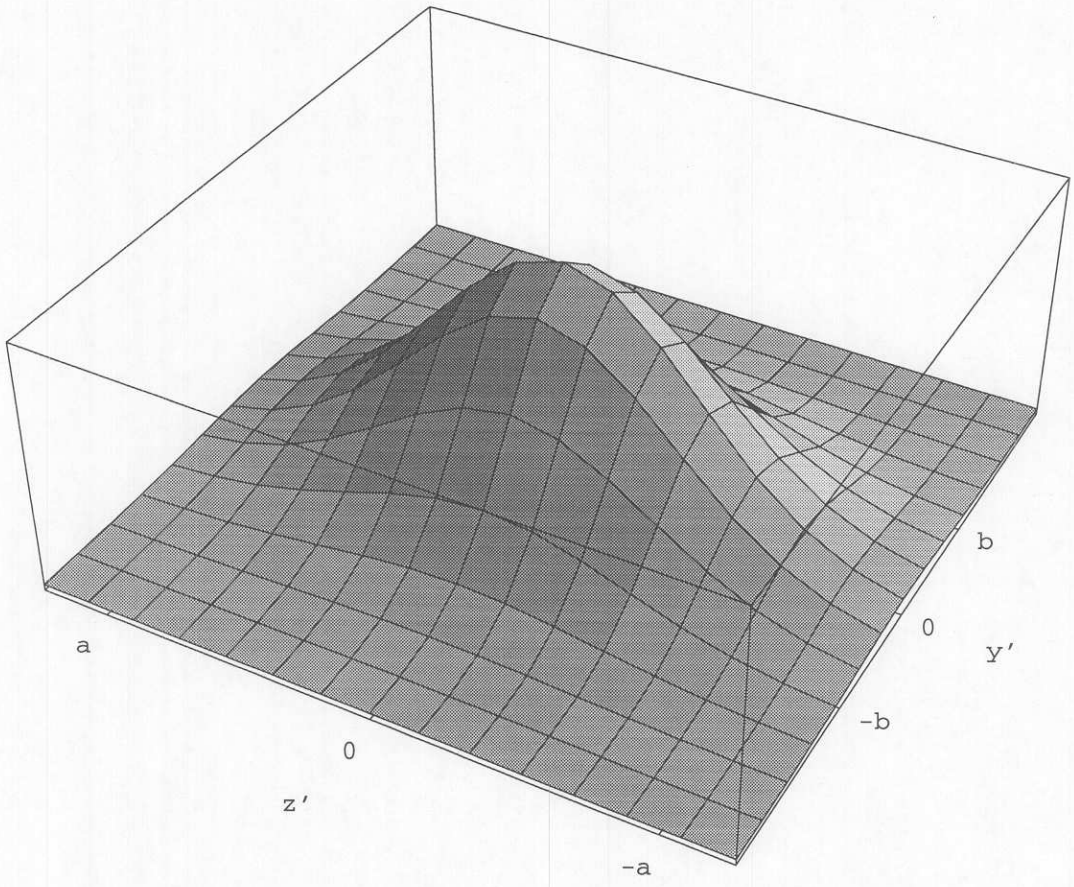

Figure 4.2: Apriori PDF $p(y', z')$

$$\sin\phi_i \sin\theta_i = \frac{-y'}{|\bar{r}|} \tag{4.35}$$

$$\cos\theta_i = \frac{-(z' - z_{off})}{|\bar{r}|} \tag{4.36}$$

Solving Equation 4.36 for θ_i

$$\boxed{\theta_i = \arccos\left(\frac{-(z' - z_{off})}{|\bar{r}|}\right)} \tag{4.37}$$

This result will be useful later. Dividing Equation 4.34 by Equation 4.35 yields

$$\tan\phi_i = \frac{-y'}{-h} \tag{4.38}$$

Solving for ϕ_i

$$\boxed{\phi_i = \arctan\left(\frac{-y'}{-h}\right)} \tag{4.39}$$

where the negative signs are kept to determine the proper quadrant. y' may be written in terms of ϕ_i and θ_i. Solving Equation 4.34 for $|\bar{r}|$ and Equation 4.35 for y'

$$|\bar{r}| = \frac{-h}{\cos\phi_i \sin\theta_i} \tag{4.40}$$

$$y' = -|\bar{r}| \sin\phi_i \sin\theta_i \tag{4.41}$$

Substituting for $|\bar{r}|$

$$\boxed{y' = h\tan\phi_i} \tag{4.42}$$

z' may also be written in terms of ϕ_i and θ_i. Solving Equation 4.36 for z'

$$z' = -|\bar{r}| \cos\theta_i + z_{off} \tag{4.43}$$

and again substituting for $|\bar{r}|$

$$\boxed{z' = \frac{h}{\cos\phi_i \tan\theta_i} + z_{off}} \tag{4.44}$$

The gaussian PDF for emitter/scatterer location can be directly written as

$$p\left(y', z'\right) = \frac{\exp\left[\frac{1}{2}\left(\frac{y'}{\sigma_{y'}}\right)^2 - \frac{1}{2}\left(\frac{z'}{\sigma_{z'}}\right)\right]}{2\pi\sigma_{y'}\sigma_{z'}} \tag{4.45}$$

Because the PDF in Equation 4.45 is in terms of (y', z') and the desired PDF $p(\theta_i, \phi_i)$ must be in terms of (θ_i, ϕ_i), a linear transformation is needed to transform the PDF from one set of random variables into another. This transformation makes use of a Jacobian matrix where

$$p(\theta_i, \phi_i) = p(y', z')\,|J| \tag{4.46}$$

where

$$|J| = \begin{vmatrix} \frac{\partial y'}{\partial \theta_i} & \frac{\partial y'}{\partial \phi_i} \\ \frac{\partial z'}{\partial \theta_i} & \frac{\partial z'}{\partial \phi_i} \end{vmatrix} = \frac{-h^2}{\sin^2\theta_i \cos^3\phi_i} \tag{4.47}$$

At last

$$p(\theta_i, \phi_i) = \frac{-h^2}{\sin^2\theta_i \cos^3\phi_i} \frac{\exp\left[\frac{-(h\tan\phi_i)^2}{2\sigma_{y'}^2} - \frac{\left(\frac{h}{\cos\phi_i\tan\theta_i} + z_{off}\right)^2}{2\sigma_{z'}^2}\right]}{2\pi\sigma_{y'}\sigma_{z'}} \tag{4.48}$$

Because it will be necessary to integrate over the PDF just found, the integration limits must be determined. The area over which to integrate is an elliptical pattern similar to that of the beam pattern. If the ellipse is defined with a radius of a in the z-direction and a radius of b in the y direction, the area of integration will appear as Figure 4.5.1 shows. First, define the range of integration over ϕ_i as

$$\phi_i^{b1} \leq \phi_i \leq \phi_i^{b2} \tag{4.49}$$

ϕ_i^{b1} and ϕ_i^{b2} are determined by

$$\phi_i^{b1} = \pi - \arctan\frac{b}{h} \tag{4.50}$$

$$\phi_i^{b2} = \pi + \arctan\frac{b}{h} \tag{4.51}$$

The limits of integration for θ_i can also be bounded with two angles

$$\theta_i^{b1} \leq \theta_i \leq \theta_i^{b2} \tag{4.52}$$

The bounding angles in this case are functions of ϕ_i. Recalling Equation 4.37

$$\theta_i = \arccos\left(\frac{-\left(z_b' - z_{off}\right)}{|\bar{r}|}\right) \tag{4.53}$$

z_{off} and $\bar{r}$ are known. It is necessary to find z_b' in terms of ϕ_i and the other knowns. Starting with the equation for the ellipse

$$\frac{(z_b')^2}{a^2} + \frac{(y_b')^2}{b^2} = 1 \tag{4.54}$$

Solving for z_b'

$$z_b' = \pm\sqrt{a^2\left(1 - \frac{(y_b')}{b^2}\right)} \tag{4.55}$$

remembering that y_b' is Equation 4.42

$$y_b' = h\tan\phi_i \tag{4.56}$$

Substituting for y_b' in z_b' Equation 4.55 yields

$$z_b' = \pm\sqrt{a^2\left(1 - \frac{h^2\tan^2\phi_i}{b^2}\right)} \tag{4.57}$$

Using the positive case for θ_i^{b1} and the negative case for θ_i^{b2}

$$\theta_i^{b1} = \arccos\left[\frac{z_{off} + \sqrt{a^2\left(1 - \frac{h^2\tan^2\phi_i}{b^2}\right)}}{\sqrt{h^2 + h^2\tan^2\phi_i + \left[z_{off} + \sqrt{a^2\left(1 - \frac{h^2\tan^2\phi_i}{b^2}\right)}\right]}}\right] \tag{4.58}$$

$$\theta_i^{b2} = \arccos\left[\frac{z_{off} - \sqrt{a^2\left(1 - \frac{h^2\tan^2\phi_i}{b^2}\right)}}{\sqrt{h^2 + h^2\tan^2\phi_i + \left[z_{off} - \sqrt{a^2\left(1 - \frac{h^2\tan^2\phi_i}{b^2}\right)}\right]}}\right] \tag{4.59}$$

we arrive at the limits for θ_i.

4.5.2 PDF of χ and ψ

The symbols χ and ψ represent the polarization of the incident waveform. The PDF of the incident waveform polarization is assumed to be uniform. All polarization states are equally likely to occur.

To derive the PDF's for χ and ψ, start by letting θ and ϕ be spherical coordinates describing the location on the surface of a sphere of radius 1. By the definition of the PDF, the probability of the location being within some region defined by

$$\theta_1 - \frac{\triangle\theta}{2} < \theta < \theta_1 + \frac{\triangle\theta}{2} \tag{4.60}$$

$$\phi_1 - \frac{\triangle\phi}{2} < \phi < \phi_1 + \frac{\triangle\phi}{2} \tag{4.61}$$

is approximately

$$p(\theta_1, \phi_1)\triangle\theta\triangle\phi \tag{4.62}$$

if $\triangle\theta$ and $\triangle\phi$ are very small.

If the PDF describing this location results in a uniform distribution across the surface of the sphere, then the probability of the location being within the region defined by Equations 4.60 and 4.61 is found by dividing the area of the region by the area of the sphere

$$\frac{\text{area of region}}{\text{area of sphere}} = \frac{\sin\theta_1\triangle\theta\triangle\phi}{4\pi} \tag{4.63}$$

And by equating 4.62 and 4.63

$$p(\theta_1, \phi_1) = \frac{\sin\theta_1}{4\pi} \tag{4.64}$$

or, in general, since θ_1 and ϕ_1 are arbitrary

$$p(\theta, \phi) = \frac{\sin\theta}{4\pi} \tag{4.65}$$

Because the coordinates of the Poincare sphere are not given in terms of θ and ϕ, the PDF of Equation 4.65 must be transformed into a PDF with terms of χ and ψ. By definition of the Poincare sphere

$$\phi = 2\psi \qquad\qquad \theta = \frac{\pi}{2} - 2\chi \tag{4.66}$$

rearranging

$$\psi = \frac{\phi}{2} \qquad\qquad \chi = \frac{\pi}{4} - \frac{\theta}{2} \tag{4.67}$$

where

$$\frac{-\pi}{4} < \chi < \frac{\pi}{4} \qquad\qquad \frac{-\pi}{2} < \psi < \frac{\pi}{2} \tag{4.68}$$

$p(\theta, \phi)$ can be transformed to $p(\chi, \psi)$ by the Jacobian

$$p(\chi, \psi) = \frac{p(\theta, \phi)}{|J|} \tag{4.69}$$

where

$$|J| = \begin{vmatrix} \frac{\partial\psi}{\partial\theta} & \frac{\partial\psi}{\partial\phi} \\ \frac{\partial\chi}{\partial\theta} & \frac{\partial\chi}{\partial\phi} \end{vmatrix} = \begin{vmatrix} 0 & \frac{1}{2} \\ -\frac{1}{2} & 0 \end{vmatrix} = \frac{1}{4} \tag{4.70}$$

Substituting the knowns into Equation 4.69

$$p(\chi, \psi) = \frac{p(\theta, \phi)}{|J|} = \frac{\frac{\sin\theta}{4\pi}}{\frac{1}{4}} = \frac{\sin\theta}{\pi} \tag{4.71}$$

replacing θ with $\frac{\pi}{2} - 2\chi$

$$p(\chi, \psi) = \frac{\sin\left(\frac{\pi}{2} - 2\chi\right)}{\pi} = \frac{\cos 2\chi}{\pi} \tag{4.72}$$

Because χ and ψ are independent, separation into marginal PDF's leaves

$$p(\chi) = \cos(2\chi) \tag{4.73}$$

$$p(\psi) = \frac{1}{\pi} \tag{4.74}$$

Recalling Equation 4.29, the general formula for the a priori PDF is

$$p(\mathbf{A}) = p(\phi_i, \theta_i)p(\chi)p(\psi) \tag{4.75}$$

Now, performing the substitutions, the a priori PDF becomes

$$p(\mathbf{A}) = -\frac{\cos 2\chi}{\pi} \frac{h^2}{\sin^2\theta_i \cos^2\phi_i} \frac{\exp\left[\frac{-(h\tan\phi_i)^2}{2\sigma_{y'}^2} - \frac{\left(\frac{h}{\cos\phi_i \tan\theta_i} + z_{off}\right)^2}{2\sigma_{z'}^2}\right]}{2\pi\sigma_{y'}\sigma_{z'}} \tag{4.76}$$

Chapter 5

Deriving Fisher's Information for the Conducting Sphere

5.1 The Theory

When choosing an estimator for a particular application, one generally tries to satisfy one or more criteria. Estimator performance is one such criteria. The performance of an estimator is best evaluated by the use of a metric. The error variance of the estimator is often used as a measure of performance. An estimator with small error variance over multiple estimates is said to perform better than an estimator with large error variance. In other words, the lower the error variance, the better the estimator.

While the error variance provides a metric for comparing estimators, it would be even more convenient if a bound existed which shows the best performance possible. This bound would be a lower bound and would predict the smallest error variance one could hope to acheive. As it turns out, many such variance bounds exist, but the Cramer Rao lower bound (CRLB) is one of the simplest to find [8].

Given an a posteriori PDF $p(\theta|\mathbf{R})$ where the object is to estimate θ, the PDF must first satisfy

$$E\left[\frac{\partial \ln p(\theta|\mathbf{R})}{\partial \theta}\right] = 0 \tag{5.1}$$

for all θ. If so, then the variance of an estimator $\hat{\theta}$ must satisfy

$$VAR(\hat{\theta}) \geq \frac{1}{-E\left[\frac{\partial^2 \ln p(\theta|\mathbf{R})}{\partial \theta^2}\right]} \tag{5.2}$$

This is the CRLB for the PDF $p(\theta|\mathbf{R})$ when estimating one parameter. It is also known as the CRLB for the scalar case. It is important to note that the denominator in Equation 5.2 is named the Fisher's Information and is often designated by $I(\theta)$.

If estimating more than one parameter, then the CRLB for the vector case applies. Given an a posteriori PDF $p(\mathbf{A}|\mathbf{R})$, the object now is to estimate the parameters in the state vector $\mathbf{A}$. As given in Equation 4.3, $\mathbf{A}$ is

$$\mathbf{A} = [\phi_i \quad \theta_i \quad \chi \quad \psi]^T \tag{5.3}$$

The CRLB now becomes

$$VAR(A_i) \geq \left[\mathbf{I}^{-1}(\mathbf{A})\right]_{ii} \tag{5.4}$$

where $\mathbf{I}(\mathbf{A})$ is the $p \times p$ Fisher's Information Matrix defined as

$$[\mathbf{I}(\mathbf{A})]_{ij} = -E\left[\frac{\partial^2 \ln p(\mathbf{A}|\mathbf{R})}{\partial A_i \partial A_j}\right] \quad \text{for} \quad i = 1, 2, ..., p \quad j = 1, 2, ..., p \tag{5.5}$$

or, rewritten as

$$[\mathbf{I}(\mathbf{A})]_{ij} = E\left[\frac{\partial \ln p(\mathbf{A}|\mathbf{R})}{\partial A_i} \frac{\partial \ln p(\mathbf{A}|\mathbf{R})}{\partial A_j}\right] \quad \text{for} \quad i = 1, 2, ..., p \quad j = 1, 2, ..., p \tag{5.6}$$

or, rewritten again as

$$\mathbf{I}(\mathbf{A}) = E\left\{\left(\nabla_{\mathbf{A}}\left[\ln p(\mathbf{A}|\mathbf{R})\right]\right)\left(\nabla_{\mathbf{A}}\left[\ln p(\mathbf{A}|\mathbf{R})\right]\right)^T\right\} \tag{5.7}$$

Continuing with the form in Equation 5.6, recall that Bayes' Rule allows one to write the aposterior PDF $p(\mathbf{A}|\mathbf{R})$ as

$$p(\mathbf{A}|\mathbf{R}) = \frac{p(\mathbf{R}|\mathbf{A})p(\mathbf{A})}{p(\mathbf{R})} \tag{5.8}$$

Due to the exponentials involved with Gaussian PDF's, it is helpful to take the natural logarithm of Equation 5.8 and rewrite it as

$$\ln p(\mathbf{A}|\mathbf{R}) = \ln p(\mathbf{R}|\mathbf{A}) + \ln p(\mathbf{A}) - \ln p(\mathbf{R}) \tag{5.9}$$

MAP estimation requires finding $\mathbf{A_i}$ which maximizes the a posteriori PDF $p(\mathbf{A}|\mathbf{R})$. Since the last term in Equation 5.9 is not a function of $\mathbf{A}$, it can be ignored when maximizing. This will simplify the maximization process by eliminating the need to find the PDF $p(\mathbf{R})$. The real bonus when applying this simplification is that it doesn't change the estimate for $\mathbf{A}$. The estimate is identical whether $p(\mathbf{R})$ is included or left out when maximizing. With this knowledge, Equation 5.6 can be rewritten by substituting $p(\mathbf{R}|\mathbf{A})p(\mathbf{A})$ for the a posteriori PDF $p(\mathbf{A}|\mathbf{R})$.

$$E\left[\frac{\partial}{\partial A_i}\left\{\ln\left(p(\mathbf{R}|\mathbf{A})p(\mathbf{A})\right)\right\}\frac{\partial}{\partial A_j}\left\{\ln\left(p(\mathbf{R}|\mathbf{A})p(\mathbf{A})\right)\right\}\right] \tag{5.10}$$

By rearranging and simplying

$$E\left[\frac{\partial \ln p(\mathbf{R}|\mathbf{A})}{\partial A_i}\frac{\partial \ln p(\mathbf{R}|\mathbf{A})}{\partial A_j}\right] + E\left[\frac{\partial \ln p(\mathbf{A})}{\partial A_i}\frac{\partial \ln p(\mathbf{A})}{\partial A_j}\right] \tag{5.11}$$

we see that the total Fisher's Information is just the Fisher's Information of the observed data plus the Fisher's Information of the a priori model. While the expected values in Equation 5.11 appear to be the same, the expected value in the Fisher's Information of the observed data is the expected value over both $\mathbf{R}$ and $\mathbf{A}$ because of the conditional probability function. The expected value in the Fisher's Information of the a priori model is simply the expectation over $\mathbf{A}$.

5.2 Fisher's Information of the Observed Data

Having defined Fisher's Information in the previous section, we are left with the nontrivial task of finding the Fisher's Information Matrix for the conducting sphere problem. We start by finding the Fisher's Information of the the observed data $p(\mathbf{R}|\mathbf{A})$. Our guiding equation is the first part of Equation 5.11.

$$E\left[\frac{\partial \ln p(\mathbf{R}|\mathbf{A})}{\partial A_i}\frac{\partial \ln p(\mathbf{R}|\mathbf{A})}{\partial A_j}\right] \tag{5.12}$$

It is obvious when looking at Equation 5.12 that the first task to is to find the conditional probability $p(\mathbf{R}|\mathbf{A})$. This was done in Chapter 4 and is reproduced below for convenience.

$$p(\mathbf{R}|\mathbf{A}) = \frac{1}{(2\pi)^N \prod_{n=1}^{N} |\Sigma_{R_n}|^{\frac{1}{2}}} \exp\left[-\frac{1}{2}\sum_{n=1}^{N}(\mathbf{R}_n - \mathbf{m}_n)^T \Sigma_{R_n}^{-1}(\mathbf{R}_n - \mathbf{m}_n)\right] \tag{5.13}$$

According to Equation 5.12, the next step is to take the natural logarithm.

$$\ln p(\mathbf{R}|\mathbf{A}) = -N\ln(2\pi) - \frac{1}{2}\sum_{n=1}^{N}\ln|\Sigma_{R_n}| - \frac{1}{2}\sum_{n=1}^{N}(\mathbf{R}_n - \mathbf{m}_n)^T \Sigma_{R_n}^{-1}(\mathbf{R}_n - \mathbf{m}_n) \tag{5.14}$$

After completing the natural logarithm, the partial derivative $\frac{\partial}{\partial A_i}$ with respect to each element in the vector $\mathbf{A}$ must be determined. A_i can be any of the elements in the vector $\mathbf{A}$ - either ϕ, θ, χ, or ψ.

$$\begin{aligned}\frac{\partial}{\partial A_i}\ln p(\mathbf{R}|\mathbf{A}) = &-\frac{1}{2}\sum_{n=1}^{N}\frac{\partial \ln|\Sigma_{R_n}|}{\partial S_r}\frac{\partial S_r}{\partial A_i} - \frac{1}{2}\sum_{n=1}^{N}\frac{\partial \ln|\Sigma_{R_n}|}{\partial S_i}\frac{\partial S_i}{\partial A_i} \\ &- \frac{1}{2}\sum_{n=1}^{N}\frac{\partial}{\partial S_r}\left[(\mathbf{R}_n - \mathbf{m}_n)^T \Sigma_{R_n}^{-1}(\mathbf{R}_n - \mathbf{m}_n)\right]\frac{\partial S_r}{\partial A_i} \\ &- \frac{1}{2}\sum_{n=1}^{N}\frac{\partial}{\partial S_i}\left[(\mathbf{R}_n - \mathbf{m}_n)^T \Sigma_{R_n}^{-1}(\mathbf{R}_n - \mathbf{m}_n)\right]\frac{\partial S_i}{\partial A_i}\end{aligned} \tag{5.15}$$

Here S_r and S_i represent the real and imaginary parts of E_r. Note that there are six different partial derivatives which need to be found. We will start by finding the partial derivatives of E_r with respect to each element in the vector $\mathbf{A}$. Once the partial derivatives are found, they can be easily split into their real and imaginary parts

$$\frac{\partial S_r}{\partial A_i} + \frac{\partial S_i}{\partial A_i} = \frac{\partial E_r}{\partial A_i} \tag{5.16}$$

5.2.1 Partial Derivative of E_r with Respect to ϕ_i

E_r represents the electric field found by the Mie Scattering Solution in Chapter 2. The partial derivative of E_r with respect to ϕ_i can be found by multiple applications of the chain rule. Recall from Equation 3.56, the total electric field at a given point on the surface of a conducting sphere is

$$E_r = E_v^i E_r^v + E_h^i E_r^h \tag{5.17}$$

To begin, we will apply the chain rule to Equation 5.17. E_v^i and E_h^i are not functions of ϕ_i. They become multiplication constants.

$$\begin{aligned} \frac{\partial E_r}{\partial \phi_i} &= \frac{\partial}{\partial \phi_i}\left\{E_v^i E_r^v + E_h^i E_r^h\right\} \\ &= E_v^i \frac{\partial E_r^v}{\partial \phi_i} + E_h^i \frac{\partial E_r^h}{\partial \phi_i} \end{aligned} \tag{5.18}$$

Remember E_r^v from Equation 3.1. Its derivative is

$$\begin{aligned} \frac{\partial E_r^v}{\partial \phi_i} &= \frac{\partial}{\partial \phi_i}\left\{\frac{1}{j\omega\mu\epsilon}\left[\frac{\partial^2}{\partial r^2}A_r^v + \beta^2 A_r^v\right]\right\} \\ &= \frac{1}{j\omega\mu\epsilon}\frac{\partial}{\partial \phi_i}\left\{\frac{\partial^2}{\partial r^2}A_r^v\right\} + \beta^2 \frac{\partial}{\partial \phi_i}\left\{A_r^v\right\} \end{aligned} \tag{5.19}$$

A_r^v is known from Equation 3.2 as the vertical component of the magnetic vector potential. Taking its derivative with respect to ϕ_i, we have

$$\begin{aligned}
&\frac{\partial}{\partial\phi_i}\{A_r^v\} \\
&= \frac{\partial}{\partial\phi_i}\left\{E_0\frac{\cos\phi_e^v}{\omega}\sum_{n=1}^{\infty}\left[a_n\hat{J}_n(\beta r)+b_n\hat{H}_n^{(2)}(\beta r)\right]P_n^1(\cos\theta_e^v)\right\} \\
&= \frac{E_0}{\omega}\frac{\partial}{\partial\phi_i}\{\cos\phi_e^v\}\sum_{n=1}^{\infty}\left[a_n\hat{J}_n(\beta r)+b_n\hat{H}_n^{(2)}(\beta r)\right]P_n^1(\cos\theta_e^v) \\
&\quad + \frac{E_0}{\omega}\cos\theta_e^v\sum_{n=1}^{\infty}\left[a_n\hat{J}_n(\beta r)+b_n\hat{H}_n^{(2)}(\beta r)\right]\frac{\partial}{\partial\phi_i}\{P_n^1(\cos\theta_e^v)\}
\end{aligned} \tag{5.20}$$

The derivative of the term $\frac{\partial^2}{\partial r^2}A_r^v$ with respect to ϕ_i is

$$\begin{aligned}
&\frac{\partial}{\partial\phi_i}\left\{\frac{\partial^2}{\partial r^2}\{A_r^v\}\right\} \\
&= \frac{\partial}{\partial\phi_i}\left\{\frac{E_0\cos\phi_e^v}{\omega}\sum_{n=1}^{\infty}\left[a_n\frac{\partial^2}{\partial r^2}\left\{\hat{J}_n(\beta r)\right\}+b_n\frac{\partial^2}{\partial r^2}\left\{\hat{H}_n^{(2)}(\beta r)\right\}\right]P_n^1(\cos\theta_e^v)\right\} \\
&= \frac{E_0}{\omega}\frac{\partial}{\partial\phi_e^v}\{\cos\phi_e^v\}\sum_{n=1}^{\infty}\left[a_n\frac{\partial^2}{\partial r^2}\left\{\hat{J}_n(\beta r)\right\}+b_n\frac{\partial^2}{\partial r^2}\left\{\hat{H}_n^{(2)}(\beta r)\right\}\right]P_n^1(\cos\theta_e^v) \\
&+ \frac{E_0}{\omega}\cos\phi_e^v\sum_{n=1}^{\infty}\left[a_n\frac{\partial^2}{\partial r^2}\left\{\hat{J}_n(\beta r)\right\}+b_n\frac{\partial^2}{\partial r^2}\left\{\hat{H}_n^{(2)}(\beta r)\right\}\right]\frac{\partial}{\partial\phi_i}\{P_n^1(\cos\theta_e^v)\}
\end{aligned} \tag{5.21}$$

Equations 5.20 and 5.21 both require the derivatives of $\cos\phi_e^v$ and $P_n^1(\cos\theta_e^v)$ with respect to ϕ_i. These derivatives are found by substituting for $\cos\phi_e^v$ and $\cos\theta_e^v$. Recall $\cos\phi_e^v$ from Equation 3.30 and $\cos\theta_e^v$ from Equation 3.21.

$$\cos\phi_e^v = \frac{\cos(\phi_e-\phi i)\sin\theta_e\cos\theta_i-\cos\theta_e\sin\theta_i}{\sqrt{\sin^2\phi_e-\phi_i\sin^2\theta_e+(\cos(\phi_e-\phi_i)\sin\theta_e\cos\theta_i-\cos\theta_e\sin\theta_i)^2}} \tag{5.22}$$

$$\cos\theta_e^v = \cos(\phi_e-\phi_i)\sin\theta_e\sin\theta_i+\cos\theta_e\cos\theta_i \tag{5.23}$$

Substituting, the derivatives are

$$\frac{\partial}{\partial \phi_i}\{\cos\phi_e^v\} \tag{5.24}$$
$$= \frac{\partial}{\partial \phi_i}\left\{\frac{\cos(\phi_e-\phi_i)\sin\theta_e\cos\theta_i-\cos\theta_e\sin\theta_i}{\sqrt{[\sin(\phi_e-\phi_i)\sin\theta_e]^2+[\cos(\phi_e-\phi_i)\sin\theta_e\cos\theta_i-\cos\theta_e\sin\theta_i]^2}}\right\}$$
$$= \frac{\sin^2\theta_e[\cos\theta_i\sin\theta_e-\cos(\phi_e-\phi_i)\cos\theta_e\sin\theta_i]\sin(\phi_e-\phi_i)}{\left([\cos(\phi_e-\phi_i)\sin\theta_e\cos\theta_i-\cos\theta_e\sin\theta_i]^2+\sin^2\theta_e\sin^2(\phi_e-\phi_i)\right)^{\frac{3}{2}}}$$

$$\frac{\partial}{\partial \phi_i}\left\{P_n^1(\cos\theta_e^v)\right\}$$
$$= \frac{\partial}{\partial \phi_i}\left\{P_n^1[\cos(\phi_e-\phi_i)\sin\theta_e\sin\theta_i+\cos\theta_e\cos\theta_i]\right\}$$
$$= \frac{1}{1-\cos^2\theta_e^v}\left[(n+1)\cos\theta_e^v P_n^1(\cos\theta_e^v)-nP_{n+1}^1(\cos\theta_e^v)\right]$$
$$[\sin(\phi_e-\phi_i)\sin\theta_e\sin\theta_i] \tag{5.25}$$

As can be seen by the previous derivation, the chain rule permits symbolic calculation of the partial derivative of E_r^v with respect to ϕ_i. In a similar manner, the partial derivative of the horizontal component of the electric field E_r^h with respect to ϕ_i can be determined.

$$\frac{\partial E_r^h}{\partial \phi_i} = \frac{\partial}{\partial \phi_i}\left\{\frac{1}{j\omega\mu\epsilon}\left[\frac{\partial^2}{\partial r^2}A_r^h+\beta^2 A_r^h\right]\right\}$$
$$= \frac{1}{j\omega\mu\epsilon}\frac{\partial}{\partial \phi_i}\left\{\frac{\partial^2}{\partial r^2}A_r^h\right\}+\beta^2\frac{\partial}{\partial \phi_i}\left\{A_r^h\right\} \tag{5.26}$$

The derivative of the horizontal component of the magnetic vector potential A_r^h is

$$\begin{aligned}
&\frac{\partial}{\partial \phi_i}\left\{A_r^h\right\} \\
&= \frac{\partial}{\partial \phi_i}\left\{E_0 \frac{\cos\phi_e^h}{\omega}\sum_{n=1}^{\infty}\left[a_n \hat{J}_n(\beta r) + b_n \hat{H}_n^{(2)}(\beta r)\right] P_n^1(\cos\theta_e^h)\right\} \\
&= \frac{E_0}{\omega}\frac{\partial}{\partial \phi_i}\left\{\cos\phi_e^h\right\}\sum_{n=1}^{\infty}\left[a_n \hat{J}_n(\beta r) + b_n \hat{H}_n^{(2)}(\beta r)\right] P_n^1(\cos\theta_e^h) \\
&\quad + \frac{E_0}{\omega}\cos\theta_e^h \sum_{n=1}^{\infty}\left[a_n \hat{J}_n(\beta r) + b_n \hat{H}_n^{(2)}(\beta r)\right]\frac{\partial}{\partial \phi_i}\left\{P_n^1(\cos\theta_e^h)\right\} \qquad (5.27)
\end{aligned}$$

Likewise

$$\begin{aligned}
&\frac{\partial}{\partial \phi_i}\left\{\frac{\partial^2}{\partial r^2}\{A_r^h\}\right\} \qquad (5.28) \\
&= \frac{\partial}{\partial \phi_i}\left\{\frac{E_0\cos\phi_e^h}{\omega}\sum_{n=1}^{\infty}\left[a_n \frac{\partial^2}{\partial r^2}\left\{\hat{J}_n(\beta r)\right\} + b_n \frac{\partial^2}{\partial r^2}\left\{\hat{H}_n^{(2)}(\beta r)\right\}\right] P_n^1(\cos\theta_e^h)\right\} \\
&= \frac{E_0}{\omega}\frac{\partial}{\partial \phi_e^h}\left\{\cos\phi_e^h\right\}\sum_{n=1}^{\infty}\left[a_n \frac{\partial^2}{\partial r^2}\left\{\hat{J}_n(\beta r)\right\} + b_n \frac{\partial^2}{\partial r^2}\left\{\hat{H}_n^{(2)}(\beta r)\right\}\right] P_n^1(\cos\theta_e^h) \\
&+ \frac{E_0}{\omega}\cos\phi_e^h \sum_{n=1}^{\infty}\left[a_n \frac{\partial^2}{\partial r^2}\left\{\hat{J}_n(\beta r)\right\} + b_n \frac{\partial^2}{\partial r^2}\left\{\hat{H}_n^{(2)}(\beta r)\right\}\right]\frac{\partial}{\partial \phi_i}\left\{P_n^1(\cos\theta_e^h)\right\}
\end{aligned}$$

Again, the derivatives of A_r^h and $\frac{\partial^2}{\partial r^2}A_r^h$ are functions of the derivatives of $\cos\phi_e^h$ and $P_n^1\cos\theta_e^h$. Remember $\cos\phi_e^h$ and $\cos\theta_e^h$ from Equations 3.52 and 3.51 respectively.

$$\cos\phi_e^h = \frac{-\sin(\phi_e - \phi i)\sin\theta_e}{\sqrt{\sin^2\phi_e - \phi_i\sin^2\theta_e + (\cos(\phi_e - \phi_i)\sin\theta_e\cos\theta_i - \cos\theta_e\sin\theta_i)^2}} \qquad (5.29)$$

$$\cos\theta_e^h = \cos(\phi_e - \phi_i)\sin\theta_e\sin\theta_i + \cos\theta_e\cos\theta_i \qquad (5.30)$$

Substituting

$$\frac{\partial}{\partial\phi_i}\left\{\cos\phi_e^h\right\} \tag{5.31}$$

$$= \frac{\partial}{\partial\phi_i}\left\{\frac{-\sin(\phi_e-\phi_i)\sin\theta_e}{\sqrt{[\sin(\phi_e-\phi_i)\sin\theta_e]^2+[\cos(\phi_e-\phi_i)\sin\theta_e\cos\theta_i-\cos\theta_e\sin\theta_i]^2}}\right\}$$

$$= \sin\theta_e \cdot$$

$$\left\{\frac{\cos(\phi_e-\phi_i)\cos^2\theta_i\sin^2\theta_e+\cos(\phi_e-\phi_i)\cos^2\theta_e\sin^2\theta_i}{\left([\cos(\phi_e-\phi_i)\cos\theta_i\sin\theta_e-\cos\theta_e\sin\theta_i]^2+\sin^2(\phi_e-\phi_i)\sin^2\theta_e\right)^{\frac{3}{2}}}\right.$$

$$\left.-\frac{\frac{1}{4}\left(3+\cos[2(\phi_e-\phi_i)]\right)\cos\theta_i\sin 2\theta_e\sin\theta_i}{\left([\cos(\phi_e-\phi_i)\cos\theta_i\sin\theta_e-\cos\theta_e\sin\theta_i]^2+\sin^2(\phi_e-\phi_i)\sin^2\theta_e\right)^{\frac{3}{2}}}\right\}$$

$$\frac{\partial}{\partial\phi_i}\left\{P_n^1(\cos\theta_e^h)\right\}$$

$$= \frac{\partial}{\partial\phi_i}\left\{P_n^1[\cos(\phi_e-\phi_i)\sin\theta_e\sin\theta_i+\cos\theta_e\cos\theta_i]\right\}$$

$$= \frac{1}{1-\cos^2\theta_e^h}\left[(n+1)\cos\theta_e^h P_n^1(\cos\theta_e^h)\right]\left[\sin(\phi_e-\phi_i)\sin\theta_e\sin\theta_i\right] \tag{5.32}$$

5.2.2 Partial Derivative of E_r with Respect to θ_i

In the previous section, the partial derivative of E_r with respect to ϕ_i was symbolically calculated. The partial derivative of E_r with respect to θ_i can be found by an analogous method. Without further narration, this derivative is presented.

$$\frac{\partial E_r}{\partial\theta_i} = \frac{\partial}{\partial\theta_i}\left\{E_v^i E_r^v + E_h^i E_r^h\right\}$$

$$= E_v^i\frac{\partial E_r^v}{\partial\theta_i} + E_h^i\frac{\partial E_r^h}{\partial\theta_i} \tag{5.33}$$

$$\frac{\partial E_r^v}{\partial\theta_i} = \frac{\partial}{\partial\theta_i}\left\{\frac{1}{j\omega\mu\epsilon}\left[\frac{\partial^2}{\partial r^2}A_r^v+\beta^2 A_r^v\right]\right\}$$

$$= \frac{1}{j\omega\mu\epsilon}\frac{\partial}{\partial\theta_i}\left\{\frac{\partial^2}{\partial r^2}A_r^v\right\}+\beta^2\frac{\partial}{\partial\theta_i}\left\{A_r^v\right\} \tag{5.34}$$

$$\frac{\partial}{\partial\theta_i}\{A_r^v\}$$
$$= \frac{\partial}{\partial\theta_i}\left\{E_0\frac{\cos\phi_e^v}{\omega}\sum_{n=1}^{\infty}\left[a_n\hat{J}_n(\beta r)+b_n\hat{H}_n^{(2)}(\beta r)\right]P_n^1(\cos\theta_e^v)\right\}$$
$$= \frac{E_0}{\omega}\frac{\partial}{\partial\theta_i}\{\cos\phi_e^v\}\sum_{n=1}^{\infty}\left[a_n\hat{J}_n(\beta r)+b_n\hat{H}_n^{(2)}(\beta r)\right]P_n^1(\cos\theta_e^v)$$
$$+\frac{E_0}{\omega}\cos\theta_e^v\sum_{n=1}^{\infty}\left[a_n\hat{J}_n(\beta r)+b_n\hat{H}_n^{(2)}(\beta r)\right]\frac{\partial}{\partial\theta_i}\left\{P_n^1(\cos\theta_e^v)\right\} \tag{5.35}$$

$$\frac{\partial}{\partial\theta_i}\left\{\frac{\partial^2}{\partial r^2}\{A_r^v\}\right\} \tag{5.36}$$
$$= \frac{\partial}{\partial\theta_i}\left\{\frac{E_0\cos\phi_e^v}{\omega}\sum_{n=1}^{\infty}\left[a_n\frac{\partial^2}{\partial r^2}\left\{\hat{J}_n(\beta r)\right\}+b_n\frac{\partial^2}{\partial r^2}\left\{\hat{H}_n^{(2)}(\beta r)\right\}\right]P_n^1(\cos\theta_e^v)\right\}$$
$$= \frac{E_0}{\omega}\frac{\partial}{\partial\theta_e^v}\{\cos\phi_e^v\}\sum_{n=1}^{\infty}\left[a_n\frac{\partial^2}{\partial r^2}\left\{\hat{J}_n(\beta r)\right\}+b_n\frac{\partial^2}{\partial r^2}\left\{\hat{H}_n^{(2)}(\beta r)\right\}\right]P_n^1(\cos\theta_e^v)$$
$$+\frac{E_0}{\omega}\cos\phi_e^v\sum_{n=1}^{\infty}\left[a_n\frac{\partial^2}{\partial r^2}\left\{\hat{J}_n(\beta r)\right\}+b_n\frac{\partial^2}{\partial r^2}\left\{\hat{H}_n^{(2)}(\beta r)\right\}\right]\frac{\partial}{\partial\theta_i}\left\{P_n^1(\cos\theta_e^v)\right\}$$

$$\frac{\partial}{\partial\theta_i}\{\cos\phi_e^v\} \tag{5.37}$$
$$= \frac{\partial}{\partial\theta_i}\left\{\frac{\cos(\phi_e-\phi_i)\sin\theta_e\cos\theta_i-\cos\theta_e\sin\theta_i}{\sqrt{[\sin(\phi_e-\phi_i)\sin\theta_e]^2+[\cos(\phi_e-\phi_i)\sin\theta_e\cos\theta_i-\cos\theta_e\sin\theta_i]^2}}\right\}$$
$$= -\frac{\sin^2\theta_e[\cos\theta_e\cos\theta_i-\cos(\phi_e-\phi_i)\sin\theta_e\sin\theta_i]\sin^2(\phi_e-\phi_i)}{\left([\cos(\phi_e-\phi_i)\sin\theta_e\cos\theta_i-\cos\theta_e\sin\theta_i]^2+\sin^2\theta_e\sin^2(\phi_e-\phi_i)\right)^{\frac{3}{2}}}$$

$$\frac{\partial}{\partial\theta_i}\left\{P_n^1(\cos\theta_e^v)\right\}$$
$$= \frac{\partial}{\partial\theta_i}\left\{P_n^1[\cos(\phi_e-\phi_i)\sin\theta_e\sin\theta_i+\cos\theta_e\cos\theta_i]\right\}$$
$$= \frac{1}{1-\cos^2\theta_e^v}\left[(n+1)\cos\theta_e^vP_n^1(\cos\theta_e^v)-nP_{n+1}^1(\cos\theta_e^v)\right]\cdot$$
$$[\cos(\phi_e-\phi_i)\sin\theta_e\cos\theta_i-\cos\theta_e\sin\theta_i] \tag{5.38}$$

where

$$\cos\theta_e^v=\cos(\phi_e-\phi_i)\sin\theta_e\sin\theta_i+\cos\theta_e\cos\theta_i \tag{5.39}$$

Now, the horizontal case

$$\frac{\partial E_r^h}{\partial \theta_i} = \frac{\partial}{\partial \theta_i}\left\{\frac{1}{j\omega\mu\epsilon}\left[\frac{\partial^2}{\partial r^2}A_r^h + \beta^2 A_r^h\right]\right\}$$
$$= \frac{1}{j\omega\mu\epsilon}\frac{\partial}{\partial \theta_i}\left\{\frac{\partial^2}{\partial r^2}A_r^h\right\} + \beta^2\frac{\partial}{\partial \theta_i}\left\{A_r^h\right\} \tag{5.40}$$

$$\frac{\partial}{\partial \theta_i}\left\{A_r^h\right\}$$
$$= \frac{\partial}{\partial \theta_i}\left\{E_0\frac{\cos\phi_e^h}{\omega}\sum_{n=1}^{\infty}\left[a_n\hat{J}_n(\beta r) + b_n\hat{H}_n^{(2)}(\beta r)\right]P_n^1(\cos\theta_e^h)\right\}$$
$$= \frac{E_0}{\omega}\frac{\partial}{\partial \theta_i}\left\{\cos\phi_e^h\right\}\sum_{n=1}^{\infty}\left[a_n\hat{J}_n(\beta r) + b_n\hat{H}_n^{(2)}(\beta r)\right]P_n^1(\cos\theta_e^h)$$
$$+ \frac{E_0}{\omega}\cos\theta_e^h\sum_{n=1}^{\infty}\left[a_n\hat{J}_n(\beta r) + b_n\hat{H}_n^{(2)}(\beta r)\right]\frac{\partial}{\partial \theta_i}\left\{P_n^1(\cos\theta_e^h)\right\} \tag{5.41}$$

$$\frac{\partial}{\partial \theta_i}\left\{\frac{\partial^2}{\partial r^2}\{A_r^h\}\right\} \tag{5.42}$$
$$= \frac{\partial}{\partial \theta_i}\left\{\frac{E_0\cos\phi_e^h}{\omega}\sum_{n=1}^{\infty}\left[a_n\frac{\partial^2}{\partial r^2}\left\{\hat{J}_n(\beta r)\right\} + b_n\frac{\partial^2}{\partial r^2}\left\{\hat{H}_n^{(2)}(\beta r)\right\}\right]P_n^1(\cos\theta_e^h)\right\}$$
$$= \frac{E_0}{\omega}\frac{\partial}{\partial \theta_e^h}\left\{\cos\phi_e^h\right\}\sum_{n=1}^{\infty}\left[a_n\frac{\partial^2}{\partial r^2}\left\{\hat{J}_n(\beta r)\right\} + b_n\frac{\partial^2}{\partial r^2}\left\{\hat{H}_n^{(2)}(\beta r)\right\}\right]P_n^1(\cos\theta_e^h)$$
$$+ \frac{E_0}{\omega}\cos\phi_e^h\sum_{n=1}^{\infty}\left[a_n\frac{\partial^2}{\partial r^2}\left\{\hat{J}_n(\beta r)\right\} + b_n\frac{\partial^2}{\partial r^2}\left\{\hat{H}_n^{(2)}(\beta r)\right\}\right]\frac{\partial}{\partial \theta_i}\left\{P_n^1(\cos\theta_e^h)\right\}$$

$$\frac{\partial}{\partial \theta_i}\left\{\cos\phi_e^h\right\} \tag{5.43}$$
$$= \frac{\partial}{\partial \theta_i}\left\{\frac{-\sin(\phi_e-\phi_i)\sin\theta_e}{\sqrt{[\sin(\phi_e-\phi_i)\sin\theta_e]^2 + [\cos(\phi_e-\phi_i)\sin\theta_e\cos\theta_i - \cos\theta_e\sin\theta_i]^2}}\right\}$$
$$= -\sin\theta_e\sin(\phi_e-\phi_i)\cdot$$
$$\frac{[\cos(\phi_e-\phi_i)\cos\theta_i\sin\theta_e - \cos\theta_e\sin\theta_i]\,[\cos\theta_e\cos\theta_i + \cos(\phi_e-\phi_i)\sin\theta_e\sin\theta_i]}{\left([\cos(\phi_e-\phi_i)\cos\theta_i\sin\theta_e - \cos\theta_e\sin\theta_i]^2 + \sin^2(\phi_e-\phi_i)\sin^2\theta_e\right)^{\frac{3}{2}}}$$

$$\begin{aligned}
&\frac{\partial}{\partial\theta_i}\left\{P_n^1(\cos\theta_e^h)\right\} \\
&= \frac{\partial}{\partial\theta_i}\left\{P_n^1[\cos(\phi_e-\phi_i)\sin\theta_e\sin\theta_i+\cos\theta_e\cos\theta_i]\right\} \\
&= \frac{1}{1-\cos^2\theta_e^h}\left[(n+1)\cos\theta_e^h P_n^1(\cos\theta_e^h)\right] \\
&\qquad\qquad [\cos(\phi_e-\phi_i)\sin\theta_e\cos\theta_i-\cos\theta_e\sin\theta_i] \qquad (5.44)
\end{aligned}$$

where

$$\cos\theta_e^h = \cos(\phi_e-\phi_i)\sin\theta_e\sin\theta_i+\cos\theta_e\cos\theta_i \qquad (5.45)$$

5.2.3 Partial Derivative of E_r with Respect to ψ

The partial derivative of E_r with respect to ψ is much simpler to calculate than for ϕ_i or θ_i. Begin with the chain rule applied to E_r

$$\frac{\partial E_r}{\partial\psi} = E_r^v\frac{\partial E_v^i}{\partial\psi}+E_r^h\frac{\partial E_h^i}{\partial\psi} \qquad (5.46)$$

This time E_r^v and E_r^h are multiplication constants and the derivatives are taken of the vertical and horizontal components of the incident waveform E_v^i and E_h^i. Substitute for E_v^i with Equation 3.48 and take the derivative,

$$\begin{aligned}
\frac{\partial E_v^i}{\partial\psi} &= \frac{\partial}{\partial\psi}\left\{a_v\exp\left(j\frac{\delta}{2}\right)\right\} \\
&= \exp\left(j\frac{\delta}{2}\right)\frac{\partial a_v}{\partial\psi}+a_v\frac{\partial}{\partial\psi}\left\{\exp\left(j\frac{\delta}{2}\right)\right\} \qquad (5.47)
\end{aligned}$$

which leaves us to determine the partial derivative of the magnitude of the vertical component of the incident waveform a_v

$$\begin{aligned}
\frac{\partial a_v}{\partial\psi} &= \frac{\partial}{\partial\psi}\left\{\sqrt{\frac{1}{2}(1+\cos 2\psi\cos 2\chi)}\right\} \\
&= \frac{-\cos 2\chi\sin 2\psi}{\sqrt{2+2\cos 2\chi\cos 2\psi}} \qquad (5.48)
\end{aligned}$$

and the partial derivative of the phase of the vertical component of the incident waveform. δ is defined by Equation 3.50.

$$\begin{aligned}
&\frac{\partial}{\partial\psi}\left\{\exp\left(j\frac{\delta}{2}\right)\right\} \\
&= \frac{\partial}{\partial\psi}\left\{\exp\left[\frac{j}{2}\arcsin\left(\frac{\sin 2\chi}{\sqrt{1-\cos^2 2\psi\cos^2 2\chi}}\right)\right]\right\} \\
&= -j\frac{\exp\left[\frac{j}{2}\arcsin\left(\frac{\sin 2\chi}{\sqrt{1-\cos^2 2\chi\cos^2 2\psi}}\right)\right]\cos 2\psi\sin 2\chi\cos 2\chi}{1-\cos^2 2\chi\cos^2 2\psi}
\end{aligned} \tag{5.49}$$

The partial derivative of E_h^i with respect to ψ is

$$\begin{aligned}
\frac{\partial E_h^i}{\partial\psi} &= \frac{\partial}{\partial\psi}\left\{a_h\exp\left(-j\frac{\delta}{2}\right)\right\} \\
&= \exp\left(-j\frac{\delta}{2}\right)\frac{\partial a_h}{\partial\psi} + a_h\frac{\partial}{\partial\psi}\left\{\exp\left(-j\frac{\delta}{2}\right)\right\}
\end{aligned} \tag{5.50}$$

where the partial derivative of the magnitude of the horizontal component of the incident waveform is

$$\begin{aligned}
\frac{\partial a_h}{\partial\psi} &= \frac{\partial}{\partial\psi}\left\{\sqrt{\frac{1}{2}(1-\cos 2\psi\cos 2\chi)}\right\} \\
&= \frac{\cos 2\chi\sin 2\psi}{\sqrt{2-2\cos 2\chi\cos 2\psi}}
\end{aligned} \tag{5.51}$$

and the partial derivative of the phase is

$$\begin{aligned}
&\frac{\partial}{\partial\psi}\left\{\exp\left(-j\frac{\delta}{2}\right)\right\} \\
&= \frac{\partial}{\partial\psi}\left\{\exp\left[\frac{-j}{2}\arcsin\left(\frac{\sin 2\chi}{\sqrt{1-\cos^2 2\psi\cos^2 2\chi}}\right)\right]\right\} \\
&= j\frac{\exp\left[\frac{-j}{2}\arcsin\left(\frac{\sin 2\chi}{\sqrt{1-\cos^2 2\chi\cos^2 2\psi}}\right)\right]\cos 2\psi\sin 2\chi\cos 2\chi}{1-\cos^2 2\chi\cos^2 2\psi}
\end{aligned} \tag{5.52}$$

5.2.4 Partial Derivative of E_r with Respect to χ

The partial derivative of E_r with respect to χ can be found much like the previous derivative with respect to ψ. It is presented below with no further nar-

ration.

$$\frac{\partial E_r}{\partial \chi} = E_r^v \frac{\partial E_v^i}{\partial \chi} + E_r^h \frac{\partial E_h^i}{\partial \chi} \tag{5.53}$$

$$\begin{aligned}\frac{\partial E_v^i}{\partial \chi} &= \frac{\partial}{\partial \chi}\left\{a_v \exp\left(j\frac{\delta}{2}\right)\right\} \\ &= \exp\left(j\frac{\delta}{2}\right)\frac{\partial a_v}{\partial \chi} + a_v \frac{\partial}{\partial \chi}\left\{\exp\left(j\frac{\delta}{2}\right)\right\}\end{aligned} \tag{5.54}$$

$$\begin{aligned}\frac{\partial a_v}{\partial \chi} &= \frac{\partial}{\partial \chi}\left\{\sqrt{\frac{1}{2}(1+\cos 2\psi \cos 2\chi)}\right\} \\ &= \frac{-\cos 2\psi \sin 2\chi}{\sqrt{2+2\cos 2\chi \cos 2\chi}}\end{aligned} \tag{5.55}$$

$$\begin{aligned}&\frac{\partial}{\partial \chi}\left\{\exp\left(j\frac{\delta}{2}\right)\right\} \\ &\quad= \frac{\partial}{\partial \chi}\left\{\exp\left[\frac{j}{2}\arcsin\left(\frac{\sin 2\chi}{\sqrt{1-\cos^2 2\psi \cos^2 2\chi}}\right)\right]\right\} \\ &\quad= j\frac{\exp\left[\frac{j}{2}\arcsin\left(\frac{\sin 2\chi}{\sqrt{1-\cos^2 2\chi \cos^2 2\psi}}\right)\right]\sin 2\psi}{1-\cos^2 2\chi \cos^2 2\psi}\end{aligned} \tag{5.56}$$

$$\begin{aligned}\frac{\partial E_h^i}{\partial \chi} &= \frac{\partial}{\partial \chi}\left\{a_h \exp\left(-j\frac{\delta}{2}\right)\right\} \\ &= \exp\left(-j\frac{\delta}{2}\right)\frac{\partial a_h}{\partial \chi} + a_h \frac{\partial}{\partial \chi}\left\{\exp\left(-j\frac{\delta}{2}\right)\right\}\end{aligned} \tag{5.57}$$

$$\begin{aligned}\frac{\partial a_h}{\partial \chi} &= \frac{\partial}{\partial \chi}\left\{\sqrt{\frac{1}{2}(1-\cos 2\psi \cos 2\chi)}\right\} \\ &= \frac{\cos 2\psi \sin 2\chi}{\sqrt{2-2\cos 2\chi \cos 2\psi}}\end{aligned} \tag{5.58}$$

$$\begin{aligned}&\frac{\partial}{\partial \chi}\left\{\exp\left(-j\frac{\delta}{2}\right)\right\} \\ &\quad= \frac{\partial}{\partial \chi}\left\{\exp\left[\frac{j}{2}\arcsin\left(\frac{\sin 2\chi}{\sqrt{1-\cos^2 2\psi \cos^2 2\chi}}\right)\right]\right\} \\ &\quad= -j\frac{\exp\left[\frac{-j}{2}\arcsin\left(\frac{\sin 2\chi}{\sqrt{1-\cos^2 2\chi \cos^2 2\psi}}\right)\right]\sin 2\psi}{1-\cos^2 2\chi \cos^2 2\psi}\end{aligned} \tag{5.59}$$

5.2.5 Partial Derivative of $\ln|\Sigma_{R_n}|$ with respect to S_r and S_i

Recall, the covariance matrix Σ_{R_n} from Equation 4.25 is

$$\Sigma_{R_n} = \begin{bmatrix} S_r^2\sigma_1^2 + S_i^2\sigma_2^2 + \sigma_3^2 S_r S_i \sigma_1^2 - S_r S_i \sigma_2^2 \\ S_r S_i \sigma_1^2 - S_r S_i \sigma_2^2 S_i^2 \sigma_1^2 + S_r^2\sigma_2^2 + \sigma_3^2 \end{bmatrix} \tag{5.60}$$

The determinant of Σ_{R_n} is

$$|\Sigma_{R_n}| = S_i^4\sigma_1^2\sigma_2^2 + 2S_i^2 S_r^2 \sigma_1^2\sigma_2^2 + S_r^4\sigma_1^2\sigma_2^2 + S_i^2\sigma_1^2\sigma_3^2 + S_r^2\sigma_1^2\sigma_3^2 + S_i^2\sigma_2^2\sigma_3^2 + S_r^2\sigma_2^2\sigma_3^2 + \sigma_3^4 \tag{5.61}$$

The partial derivative of $\ln|\Sigma_{R_n}|$ with respect to S_r is

$$\frac{\ln|\Sigma_{R_n}|}{\partial S_r} = 2S_r \left[\frac{v_1}{(S_i^2 + S_r^2)v_1 + v_3} + \frac{v_2}{(S_i^2 + S_r^2)v_2 + v_3} \right] \tag{5.62}$$

and likewise, the partial derivative of $\ln|\Sigma_{R_n}|$ with respect to S_i is

$$\frac{\ln|\Sigma_{R_n}|}{\partial S_i} = 2S_i \left[\frac{v_1}{(S_i^2 + S_r^2)v_1 + v_3} + \frac{v_2}{(S_i^2 + S_r^2)v_2 + v_3} \right] \tag{5.63}$$

5.2.6 Partial Derivative of $(\mathbf{R}_n - \mathbf{m}_n)^T \Sigma_{\mathbf{R}_n}^{-1} (\mathbf{R}_n - \mathbf{m}_n)$ with respect to S_r and S_i

In some texts, the quantity

$$(\mathbf{R}_n - \mathbf{m}_n)^T \Sigma_{\mathbf{R}_n}^{-1} (\mathbf{R}_n - \mathbf{m}_n) \tag{5.64}$$

is known as the Mahalanobis Distance. The partial derivative of the Mahalanobis Distance with respect to S_r was determined using *Mathematica*® and is presented below. As can be seen, it is quite lengthy.

$$\frac{\partial}{\partial S_r} \left\{ (\mathbf{R}_n - \mathbf{m}_n)^T \Sigma_{\mathbf{R}_n}^{-1} (\mathbf{R}_n - \mathbf{m}_n) \right\} = a_1 R_r^2 + a_2 R_i^2 + a_3 R_r R_i + a_4 R_r + a_5 R_i + a_6 \tag{5.65}$$

where

$$a_1 = -2S_r \cdot \frac{S_i^4\sigma_1^2(2\sigma_1^2 - \sigma_2^2\sigma_2^2 + \sigma_1^2(S_r^2\sigma_2^2 + \sigma_3^2)^2 + S_i^2\left(2S_r^2\sigma_1^4\sigma_2^2 + (\sigma_1^4 + 2\sigma_1^2\sigma_2^2 - \sigma_2^4)\sigma_3^2\right)}{\left[(S_i^2 + S_r^2)\sigma_1^2 + \sigma_3^2\right]^2\left[(S_i^2 + S_r^2)\sigma_2^2 + \sigma_3^2\right]^2} \tag{5.66}$$

$$a_2 = 2S_r \cdot \frac{S_i^4\sigma_1^2(\sigma_1^2 - 2\sigma_2^2)\sigma_2^2 - \sigma_2^2(S_r^2\sigma_1^2 + \sigma_3^2)^2 - S_i^2\left(2S_r^2\sigma_1^2 + \sigma_2^4 + (-\sigma_1^4 + 2\sigma_1^2\sigma_2^2 + \sigma_2^4)\sigma_3^2\right)}{\left[(S_i^2 + S_r^2)\sigma_1^2 + \sigma_3^2\right]^2\left[(S_i^2 + S_r^2)\sigma_2^2 + \sigma_3^2\right]^2} \tag{5.67}$$

$$a_3 = -2S_i(\sigma_1^2 - \sigma_2^2) \cdot \frac{(S_i^2 - 3S_r^2)(S_i^2 + S_r^2)\sigma_1^2\sigma_2^2 + (S_i - S_r)(S_i + S_r)(\sigma_1^2 + \sigma_2^2)\sigma_3^2 + \sigma_3^4}{\left[(S_i^2 + S_r^2)\sigma_1^2 + \sigma_3^2\right]^2\left[(S_i^2 + S_r^2)\sigma_2^2 + \sigma_3^2\right]^2} \tag{5.68}$$

$$a_4 = \frac{-2\left[(S_i - S_r)(S_i + S_r)\sigma_1^2 + \sigma_3^2\right]}{\left[(S_i^2 + S_r^2)\sigma_1^2 + \sigma_3^2\right]^2} \tag{5.69}$$

$$a_5 = \frac{4S_iS_r\sigma_1^2}{\left[(S_i^2 + S_r^2)\sigma_1^2 + \sigma_3^2\right]^2} \tag{5.70}$$

$$a_6 = \frac{2S_r\sigma_3^2}{\left[(S_i^2 + S_r^2)\sigma_1^2 + \sigma_3^2\right]^2} \tag{5.71}$$

Later in this chapter, the expected value (over R) of the derivative of the Mahalanobis Distance (with respect to S_r) will be needed for a formula substitution. This expected value is found as follows:

$$\begin{aligned} &E\left[\frac{\partial}{\partial S_r}\left\{(\mathbf{R}_n - \mathbf{m}_n)^T\Sigma_{\mathbf{R}_n}^{-1}(\mathbf{R}_n - \mathbf{m}_n)\right\}\right] \\ &= E\left[a_1R_r^2 + a_2R_i^2 + a_3R_rR_i + a_4R_r + a_5R_i + a_6\right] \\ &= a_1E\left[R_r^2\right] + a_2E\left[R_i^2\right] + a_3E\left[R_rR_i\right] + a_4E\left[R_r\right] + a_5E\left[R_i\right] + a_6 \end{aligned} \tag{5.72}$$

The moments of R are found by applying what is sometimes called the moment theorem [10].

$$E\left\{R_r^mR_i^n\right\} = \frac{1}{j^{m+n}}\frac{\partial^m\partial^n}{\partial t_1^m\partial t_2^n}\left[\Psi(t_1, t_2)\right] \tag{5.73}$$

Here, Ψ is the joint characteristic function

$$\begin{aligned}
&\Psi(t_1, t_2) \\
&= \exp\left[j\mu_{\mathbf{R}}^T\mathbf{t} - \frac{1}{2}\mathbf{t}^T\Sigma_{\mathbf{R}}\mathbf{t}\right] \\
&= \exp\left[S_r t_1 + S_i t_2 - \frac{1}{2}t_1[t_2(S_i S_r\sigma_1^2 - S_i S_r\sigma_2^2) + t_1(S_r^2\sigma_1^2 + S_i^2\sigma_2^2 + \sigma_3^2)]\right. \\
&\qquad \left. -\frac{1}{2}t_2[t_1(S_i S_r\sigma_1^2 - S_i S_r\sigma_2^2) + t_2(S_i^2\sigma_1^2 + S_r^2\sigma_2^2 + \sigma_3^2)]\right] \qquad (5.74)
\end{aligned}$$

Application of the moment theorem yields the expected values.

$$\begin{aligned}
E\left[R_r^2\right] &= \frac{1}{j^2}\frac{\partial^2}{\partial t_1^2}\{\Psi(t_1, t_2)\} \\
&= S_r^2(1 + \sigma_1^2) + S_i^2\sigma_2^2 + \sigma_3^2 \qquad (5.75) \\
E\left[R_i^2\right] &= \frac{1}{j^2}\frac{\partial^2}{\partial t_2^2}\{\Psi(t_1, t_2)\} \\
&= S_i^2(1 + \sigma_1^2) + S_r^2\sigma_2^2 + \sigma_3^2 \qquad (5.76) \\
E\left[R_r R_i\right] &= \frac{1}{j^2}\frac{\partial^2}{\partial t_1 \partial t_2}\{\Psi(t_1, t_2)\} \\
&= S_i S_r(1 + \sigma_1^2 - \sigma_2^2) \qquad (5.77) \\
E\left[R_r\right] &= \frac{1}{j}\frac{\partial}{\partial t_1}\{\Psi(t_1, t_2)\} = S_r \qquad (5.78) \\
E\left[R_i\right] &= \frac{1}{j}\frac{\partial}{\partial t_2}\{\Psi(t_1, t_2)\} = S_i \qquad (5.79)
\end{aligned}$$

Substituting and simplifying, the expected value (over R) of the derivative of the Mahalanobis Distance (with respect to S_r) is

$$\begin{aligned}
&E\left[\frac{\partial}{\partial S_r}\left\{(\mathbf{R}_n - \mathbf{m}_n)^T\Sigma_{\mathbf{R}_n}^{-1}(\mathbf{R}_n - \mathbf{m}_n)\right\}\right] \\
&\qquad = -\frac{2S_r\sigma_1^2}{(S_i^2 + S_r^2)\sigma_1^2 + \sigma_3^2} - \frac{2S_r\sigma_2^2}{(S_i^2 + S_r^2)\sigma_2^2 + \sigma_3^2} \qquad (5.80)
\end{aligned}$$

The partial derivative of Mahalanobis Distance with respect to S_i was also determined by use of $Mathematica_{\textcircled{R}}$. It, too, is rather lengthy.

$$\frac{\partial}{\partial S_i}\left\{(\mathbf{R}_n-\mathbf{m}_n)^T\Sigma_{\mathbf{R}_n}^{-1}(\mathbf{R}_n-\mathbf{m}_n)\right\}$$

$$= b_1R_r^2 + b_2R_i^2 + b_3R_rR_i + b_4R_r + b_5R_i + b_6 \quad (5.81)$$

where:

$$b_1 = -2S_i \cdot \frac{S_i^4\sigma_1^4\sigma_2^2 + 2S_i^2\sigma_1^2\sigma_2^2(S_r^2\sigma_2^2+\sigma_3^2) + (S_r^2\sigma_2^2+\sigma_3^2)\left(-S_r^2\sigma_1^2(\sigma_1^2-2\sigma_2^2)+\sigma_2^2\sigma_3^2\right)}{\left[(S_i^2+S_r^2)\sigma_1^2+\sigma_3^2\right]^2\left[(S_i^2+S_r^2)\sigma_2^2+\sigma_3^2\right]^2} \quad (5.82)$$

$$b_2 = -\frac{2S_i^5\sigma_1^2\sigma_2^4 + 4S_i^3\sigma_1^2\sigma_2^2(S_r^2\sigma_1^2+\sigma_3^2) + 2S_i(S_r^2\sigma_1^2+\sigma_3^2)\left[S_r^2(2\sigma_1^2-\sigma_2^2)\sigma_2^2+\sigma_1^2\sigma_3^2\right]}{\left[(S_i^2+S_r^2)\sigma_1^2+\sigma_3^2\right]^2\left[(S_i^2+S_r^2)\sigma_2^2+\sigma_3^2\right]^2} \quad (5.83)$$

$$b_3 = 2S_r(\sigma_1^2-\sigma_2^2) \cdot \frac{3S_i^4\sigma_1^2\sigma_2^2 - (S_r^2\sigma_1^2+\sigma_3^2)(S_r^2\sigma_2^2+\sigma_3^2) + S_i^2\left(2S_r^2\sigma_1^2\sigma_2^2+(\sigma_1^2+\sigma_2^2)\sigma_3^2\right)}{\left[(S_i^2+S_r^2)\sigma_1^2+\sigma_3^2\right]^2\left[(S_i^2+S_r^2)\sigma_2^2+\sigma_3^2\right]^2} \quad (5.84)$$

$$b_4 = \frac{4S_iS_r\sigma_1^2}{\left[(S_i^2+S_r^2)\sigma_1^2+\sigma_3^2\right]^2} \quad (5.85)$$

$$b_5 = \frac{2S_i^2\sigma_1^2 - 2(S_r^2\sigma_1^2+\sigma_3^2)}{\left[(S_i^2+S_r^2)\sigma_1^2+\sigma_3^2\right]^2} \quad (5.86)$$

$$b_6 = \frac{2S_i\sigma_3^2}{\left[(S_i^2+S_r^2)\sigma_1^2+\sigma_3^2\right]^2} \quad (5.87)$$

In a short while, the expected value (over R) of the derivative of the Mahalanobis Distance (with respect to S_i) will also be needed for a formula substitution. This expected value is similar to the previous.

$$E\left[\frac{\partial}{\partial S_i}\left\{(\mathbf{R}_n-\mathbf{m}_n)^T\Sigma_{\mathbf{R}_n}^{-1}(\mathbf{R}_n-\mathbf{m}_n)\right\}\right] \quad (5.88)$$

$$= E\left[b_1R_r^2 + b_2R_i^2 + b_3R_rR_i + b_4R_r + b_5R_i + b_6\right] \quad (5.89)$$

$$= b_1E\left[R_r^2\right] + b_2E\left[R_i^2\right] + b_3E\left[R_rR_i\right] + b_4E\left[R_r\right] + b_5E\left[R_i\right] + b_6 \quad (5.90)$$

The moments of R are the same as those found previously. Substituting and simplifying, the expected value (over R) of the derivative of the Mahalanobis Distance (with respect to S_i) is

$$E\left[\frac{\partial}{\partial S_i}\left\{(\mathbf{R}_n-\mathbf{m}_n)^T\Sigma_{\mathbf{R}_n}^{-1}(\mathbf{R}_n-\mathbf{m}_n)\right\}\right] = -\frac{2S_i\sigma_1^2}{(S_i^2+S_r^2)\sigma_1^2+\sigma_3^2}-\frac{2S_i\sigma_2^2}{(S_i^2+S_r^2)\sigma_2^2+\sigma_3^2} \quad (5.91)$$

At this point, we are ready to multiply the two multiplicands of Equation 5.12 and find the expected value. Because $p(\mathbf{R}|\mathbf{A})$ is a conditional probability, the expectation is over both $\mathbf{R}$ and $\mathbf{A}$. The expectation over $\mathbf{R}$ will be performed first because it can be done symbolically. Recall Equation 5.12,

$$E\left[\frac{\partial \ln p(\mathbf{R}|\mathbf{A})}{\partial A_i}\frac{\partial \ln p(\mathbf{R}|\mathbf{A})}{\partial A_j}\right] \quad (5.92)$$

substituting for the partial derivatives

$$\begin{aligned} J_{ij}^R = E\Bigg\{ & \\ & \left[-\frac{1}{2}\sum_{n=1}^{N}\left(\left[\frac{\partial}{\partial S_r}\left\{(\mathbf{R}_n-\mathbf{m}_n)^T\Sigma_{\mathbf{R}_n}^{-1}(\mathbf{R}_n-\mathbf{m}_n)\right\}+\frac{\partial}{\partial S_r}\left\{\ln|\Sigma_{\mathbf{R}_n}|\right\}\right]\frac{\partial S_r}{\partial A_i}\right.\right. \\ & \left.\left.+\left[\frac{\partial}{\partial S_i}\left\{(\mathbf{R}_n-\mathbf{m}_n)^T\Sigma_{\mathbf{R}_n}^{-1}(\mathbf{R}_n-\mathbf{m}_n)\right\}+\frac{\partial}{\partial S_i}\left\{\ln|\Sigma_{\mathbf{R}_n}|\right\}\right]\frac{\partial S_i}{\partial A_i}\right)\right] \\ & \left[-\frac{1}{2}\sum_{m=1}^{N}\left(\left[\frac{\partial}{\partial S_r}\left\{(\mathbf{R}_n-\mathbf{m}_n)^T\Sigma_{\mathbf{R}_n}^{-1}(\mathbf{R}_n-\mathbf{m}_n)\right\}+\frac{\partial}{\partial S_r}\left\{\ln|\Sigma_{\mathbf{R}_n}|\right\}\right]\frac{\partial S_r}{\partial A_j}\right.\right. \\ & \left.\left.+\left[\frac{\partial}{\partial S_i}\left\{(\mathbf{R}_n-\mathbf{m}_n)^T\Sigma_{\mathbf{R}_n}^{-1}(\mathbf{R}_n-\mathbf{m}_n)\right\}+\frac{\partial}{\partial S_i}\left\{\ln|\Sigma_{\mathbf{R}_n}|\right\}\right]\frac{\partial S_i}{\partial A_j}\right)\right]\Bigg\} \end{aligned} \quad (5.93)$$

$$J_{ij}^{R} = \frac{1}{4}\sum_{n=1}^{N}\sum_{m=1}^{N} E\Big\{ \tag{5.94}$$
$$\left(\left[\frac{\partial}{\partial S_r}\left\{(\mathbf{R}_n-\mathbf{m}_n)^T\Sigma_{\mathbf{R}_n}^{-1}(\mathbf{R}_n-\mathbf{m}_n)\right\}+\frac{\partial}{\partial S_r}\left\{\ln|\Sigma_{\mathbf{R}_n}|\right\}\right]\frac{\partial S_r}{\partial A_i}\right.$$
$$\left.+\left[\frac{\partial}{\partial S_i}\left\{(\mathbf{R}_n-\mathbf{m}_n)^T\Sigma_{\mathbf{R}_n}^{-1}(\mathbf{R}_n-\mathbf{m}_n)\right\}+\frac{\partial}{\partial S_i}\left\{\ln|\Sigma_{\mathbf{R}_n}|\right\}\right]\frac{\partial S_i}{\partial A_i}\right)$$
$$\left(\left[\frac{\partial}{\partial S_r}\left\{(\mathbf{R}_n-\mathbf{m}_n)^T\Sigma_{\mathbf{R}_n}^{-1}(\mathbf{R}_n-\mathbf{m}_n)\right\}+\frac{\partial}{\partial S_r}\left\{\ln|\Sigma_{\mathbf{R}_n}|\right\}\right]\frac{\partial S_r}{\partial A_j}\right.$$
$$\left.+\left[\frac{\partial}{\partial S_i}\left\{(\mathbf{R}_n-\mathbf{m}_n)^T\Sigma_{\mathbf{R}_n}^{-1}(\mathbf{R}_n-\mathbf{m}_n)\right\}+\frac{\partial}{\partial S_i}\left\{\ln|\Sigma_{\mathbf{R}_n}|\right\}\right]\frac{\partial S_i}{\partial A_j}\right)\Big\}$$

$$J_{ij}^{R} = \frac{1}{4}\sum_{n=1}^{N}\sum_{\substack{m=1\\ m\neq n}}$$
$$E\Big\{\left[\frac{\partial}{\partial S_r}\left\{(\mathbf{R}_n-\mathbf{m}_n)^T\Sigma_{\mathbf{R}_n}^{-1}(\mathbf{R}_n-\mathbf{m}_n)\right\}+\frac{\partial}{\partial S_r}\left\{\ln|\Sigma_{\mathbf{R}_n}|\right\}\right]\frac{\partial S_r}{\partial A_i}$$
$$+\left[\frac{\partial}{\partial S_i}\left\{(\mathbf{R}_n-\mathbf{m}_n)^T\Sigma_{\mathbf{R}_n}^{-1}(\mathbf{R}_n-\mathbf{m}_n)\right\}+\frac{\partial}{\partial S_i}\left\{\ln|\Sigma_{\mathbf{R}_n}|\right\}\right]\frac{\partial S_i}{\partial A_i}\Big\}$$
$$E\Big\{\left[\frac{\partial}{\partial S_r}\left\{(\mathbf{R}_n-\mathbf{m}_n)^T\Sigma_{\mathbf{R}_n}^{-1}(\mathbf{R}_n-\mathbf{m}_n)\right\}+\frac{\partial}{\partial S_r}\left\{\ln|\Sigma_{\mathbf{R}_n}|\right\}\right]\frac{\partial S_r}{\partial A_j}$$
$$+\left[\frac{\partial}{\partial S_i}\left\{(\mathbf{R}_n-\mathbf{m}_n)^T\Sigma_{\mathbf{R}_n}^{-1}(\mathbf{R}_n-\mathbf{m}_n)\right\}+\frac{\partial}{\partial S_i}\left\{\ln|\Sigma_{\mathbf{R}_n}|\right\}\right]\frac{\partial S_i}{\partial A_j}\Big\}$$
$$+\frac{1}{4}\sum_{n=1}^{N}$$
$$E\Big\{\left(\left[\frac{\partial}{\partial S_r}\left\{(\mathbf{R}_n-\mathbf{m}_n)^T\Sigma_{\mathbf{R}_n}^{-1}(\mathbf{R}_n-\mathbf{m}_n)\right\}+\frac{\partial}{\partial S_r}\left\{\ln|\Sigma_{\mathbf{R}_n}|\right\}\right]\frac{\partial S_r}{\partial A_i}\right.$$
$$\left.+\left[\frac{\partial}{\partial S_i}\left\{(\mathbf{R}_n-\mathbf{m}_n)^T\Sigma_{\mathbf{R}_n}^{-1}(\mathbf{R}_n-\mathbf{m}_n)\right\}+\frac{\partial}{\partial S_i}\left\{\ln|\Sigma_{\mathbf{R}_n}|\right\}\right]\frac{\partial S_i}{\partial A_i}\right)$$
$$\cdot\left(\left[\frac{\partial}{\partial S_r}\left\{(\mathbf{R}_n-\mathbf{m}_n)^T\Sigma_{\mathbf{R}_n}^{-1}(\mathbf{R}_n-\mathbf{m}_n)\right\}+\frac{\partial}{\partial S_r}\left\{\ln|\Sigma_{\mathbf{R}_n}|\right\}\right]\frac{\partial S_r}{\partial A_j}\right.$$
$$\left.+\left[\frac{\partial}{\partial S_i}\left\{(\mathbf{R}_n-\mathbf{m}_n)^T\Sigma_{\mathbf{R}_n}^{-1}(\mathbf{R}_n-\mathbf{m}_n)\right\}+\frac{\partial}{\partial S_i}\left\{\ln|\Sigma_{\mathbf{R}_n}|\right\}\right]\frac{\partial S_i}{\partial A_j}\right)\Big\}$$

Continuing the simplification process

$$J_{ij}^{R} = \frac{1}{4}\sum_{n=1}^{N}\sum_{\substack{m=1\\m\neq n}}^{N} \tag{5.95}$$

$$\left(\left[E\left\{\frac{\partial}{\partial S_r}\left\{(\mathbf{R}_n-\mathbf{m}_n)^T\Sigma_{\mathbf{R}_n}^{-1}(\mathbf{R}_n-\mathbf{m}_n)\right\}\right\}+\frac{\partial}{\partial S_r}\left\{\ln|\Sigma_{\mathbf{R}_n}|\right\}\right]\frac{\partial S_r}{\partial A_i}\right.$$
$$\left.+\left[E\left\{\frac{\partial}{\partial S_i}\left\{(\mathbf{R}_n-\mathbf{m}_n)^T\Sigma_{\mathbf{R}_n}^{-1}(\mathbf{R}_n-\mathbf{m}_n)\right\}\right\}+\frac{\partial}{\partial S_i}\left\{\ln|\Sigma_{\mathbf{R}_n}|\right\}\right]\frac{\partial S_i}{\partial A_i}\right)$$
$$\cdot\left(\left[E\left\{\frac{\partial}{\partial S_r}\left\{(\mathbf{R}_n-\mathbf{m}_n)^T\Sigma_{\mathbf{R}_n}^{-1}(\mathbf{R}_n-\mathbf{m}_n)\right\}\right\}+\frac{\partial}{\partial S_r}\left\{\ln|\Sigma_{\mathbf{R}_n}|\right\}\right]\frac{\partial S_r}{\partial A_j}\right.$$
$$\left.+\left[E\left\{\frac{\partial}{\partial S_i}\left\{(\mathbf{R}_n-\mathbf{m}_n)^T\Sigma_{\mathbf{R}_n}^{-1}(\mathbf{R}_n-\mathbf{m}_n)\right\}\right\}+\frac{\partial}{\partial S_i}\left\{\ln|\Sigma_{\mathbf{R}_n}|\right\}\right]\frac{\partial S_i}{\partial A_j}\right)$$
$$+\frac{1}{4}\sum_{n=1}^{N}E\left\{\left[(w+x)\frac{\partial S_r}{\partial A_i}+(y+z)\frac{\partial S_i}{\partial A_i}\right]\left[(w+x)\frac{\partial S_r}{\partial A_j}+(y+z)\frac{\partial S_i}{\partial A_j}\right]\right\}$$

where:

$$w = \frac{\partial}{\partial S_r}\left\{(\mathbf{R}_n-\mathbf{m}_n)^T\Sigma_{\mathbf{R}_n}^{-1}(\mathbf{R}_n-\mathbf{m}_n)\right\} \tag{5.96}$$

$$x = \frac{\partial}{\partial S_i}\left\{\ln|\Sigma_{\mathbf{R}_n}|\right\} \tag{5.97}$$

$$y = \frac{\partial}{\partial S_i}\left\{(\mathbf{R}_n-\mathbf{m}_n)^T\Sigma_{\mathbf{R}_n}^{-1}(\mathbf{R}_n-\mathbf{m}_n)\right\} \tag{5.98}$$

$$z = \frac{\partial}{\partial S_i}\left\{\ln|\Sigma_{\mathbf{R}_n}|\right\} \tag{5.99}$$

$$
\begin{aligned}
J_{ij}^{R} = \frac{1}{4}\sum_{n=1}^{N}\sum_{\substack{m=1\\ n\neq m}}^{N}\Bigg(\Bigg[&- \frac{2S_r\sigma_1^2}{(S_i^2+S_r^2)\sigma_1^2+\sigma_3^2} - \frac{2S_r\sigma_2^2}{(S_i^2+S_r^2)\sigma_2^2+\sigma_3^2} \\
&+ \frac{2S_r\sigma_1^2}{(S_i^2+S_r^2)\sigma_1^2+\sigma_3^2} + \frac{2S_r\sigma_2^2}{(S_i^2+S_r^2)\sigma_2^2+\sigma_3^2}\Bigg]\frac{\partial S_r}{\partial A_i} \\
+\Bigg[&- \frac{2S_i\sigma_1^2}{(S_i^2+S_r^2)\sigma_1^2+\sigma_3^2} - \frac{2S_i\sigma_2^2}{(S_i^2+S_r^2)\sigma_2^2+\sigma_3^2} \\
&+ \frac{2S_i\sigma_1^2}{(S_i^2+S_r^2)\sigma_1^2+\sigma_3^2} + \frac{2S_i\sigma_2^2}{(S_i^2+S_r^2)\sigma_2^2+\sigma_3^2}\Bigg]\frac{\partial S_i}{\partial A_i}\Bigg) \\
\cdot\Bigg(\Bigg[&- \frac{2S_r\sigma_1^2}{(S_i^2+S_r^2)\sigma_1^2+\sigma_3^2} - \frac{2S_r\sigma_2^2}{(S_i^2+S_r^2)\sigma_2^2+\sigma_3^2} \\
&+ \frac{2S_r\sigma_1^2}{(S_i^2+S_r^2)\sigma_1^2+\sigma_3^2} + \frac{2S_r\sigma_2^2}{(S_i^2+S_r^2)\sigma_2^2+\sigma_3^2}\Bigg]\frac{\partial S_r}{\partial A_j} \\
+\Bigg[&- \frac{2S_i\sigma_1^2}{(S_i^2+S_r^2)\sigma_1^2+\sigma_3^2} - \frac{2S_i\sigma_2^2}{(S_i^2+S_r^2)\sigma_2^2+\sigma_3^2} \\
&+ \frac{2S_i\sigma_1^2}{(S_i^2+S_r^2)\sigma_1^2+\sigma_3^2} + \frac{2S_i\sigma_2^2}{(S_i^2+S_r^2)\sigma_2^2+\sigma_3^2}\Bigg]\frac{\partial S_i}{\partial A_j}\Bigg) \\
+\frac{1}{4}\sum_{n=1}^{N} E\Bigg\{ &\left[(w+x)\frac{\partial S_r}{\partial A_i} + (y+z)\frac{\partial S_i}{\partial A_i}\right] \\
&\left[(w+x)\frac{\partial S_r}{\partial A_j} + (y+z)\frac{\partial S_i}{\partial A_j}\right]\Bigg\}
\end{aligned}
\tag{5.100}
$$

$$
\begin{aligned}
J_{ij}^{R} = &\frac{1}{4}\sum_{n=1}^{N}\sum_{\substack{m=1\\ m\neq n}}^{N}\left[0\frac{\partial S_r}{\partial A_i} + 0\frac{\partial S_i}{\partial A_i}\right]\cdot\left[0\frac{\partial S_r}{\partial A_j} + 0\frac{\partial S_i}{\partial A_j}\right] \\
&+\frac{1}{4}\sum_{n=1}^{N} E\Bigg\{\left(w^2+2wx+x^2\right)\frac{\partial S_r}{\partial A_i}\frac{\partial S_r}{\partial A_j} \\
&\quad+\left(wy+xy+wz+xz\right)\cdot\left(\frac{\partial S_i}{\partial A_i}\frac{\partial S_r}{\partial A_j} + \frac{\partial S_r}{\partial A_i}\frac{\partial S_i}{\partial A_j}\right) \\
&\quad+\left(y^2+2yz+z^2\right)\frac{\partial S_i}{\partial A_i}\frac{\partial S_i}{\partial A_j}\Bigg\}
\end{aligned}
\tag{5.101}
$$

$$J_{ij}^{R} = 0 + \frac{1}{4}\sum_{n=1}^{N} \frac{\partial S_r}{\partial A_i}\frac{\partial S_r}{\partial A_j} E\{w^2 + 2wx + x^2\} + \left(\frac{\partial S_i}{\partial A_i}\frac{\partial S_r}{\partial A_j} + \frac{\partial S_r}{\partial A_i}\frac{\partial S_i}{\partial A_j}\right) E\{wy + xy + wz + xz\} + \frac{\partial S_i}{\partial A_i}\frac{\partial S_i}{\partial A_j} E\{y^2 + 2yz + z^2\} \quad (5.102)$$

$$J_{ij} = \frac{1}{4}\sum_{n=1}^{N} \frac{\partial S_r}{\partial A_i}\frac{\partial S_r}{\partial A_j} \left[E\{w^2\} + 2xE\{w\} + x^2\right] + \left(\frac{\partial S_i}{\partial A_i}\frac{\partial S_r}{\partial A_j} + \frac{\partial S_r}{\partial A_i}\frac{\partial S_i}{\partial A_j}\right) \left[E\{wy\} + xE\{y\} + zE\{w\} + xz\right] + \frac{\partial S_i}{\partial A_i}\frac{\partial S_i}{\partial A_j} \left[E\{y^2\} + 2zE\{y\} + z^2\right] \quad (5.103)$$

$$
\begin{aligned}
J_{ij}^{R} = \frac{1}{4}\sum_{n=1}^{N} \frac{\partial S_r}{\partial A_i}\frac{\partial S_r}{\partial A_j}\Bigg[& E\left\{\left[\frac{\partial}{\partial S_r}\left\{(\mathbf{R}_n-\mathbf{m}_n)^T\Sigma_{\mathbf{R}_n}^{-1}(\mathbf{R}_n-\mathbf{m}_n)\right\}\right]^2\right\} \\
& + 2\frac{\partial}{\partial S_r}\left\{\ln|\Sigma_{\mathbf{R}_n}|\right\} E\left\{\frac{\partial}{\partial S_r}\left\{(\mathbf{R}_n-\mathbf{m}_n)^T\Sigma_{\mathbf{R}_n}^{-1}(\mathbf{R}_n-\mathbf{m}_n)\right\}\right\} \\
& + \left[\frac{\partial}{\partial S_r}\left\{\ln|\Sigma_{\mathbf{R}_n}|\right\}\right]^2\Bigg] \\
+ \left[\frac{\partial S_i}{\partial A_i}\frac{\partial S_r}{\partial A_j} + \frac{\partial S_r}{\partial A_i}\frac{\partial S_i}{\partial A_j}\right] & \cdot \\
& \Bigg[E\Bigg\{\frac{\partial}{\partial S_r}\left\{(\mathbf{R}_n-\mathbf{m}_n)^T\Sigma_{\mathbf{R}_n}^{-1}(\mathbf{R}_n-\mathbf{m}_n)\right\} \\
& \qquad \frac{\partial}{\partial S_i}\left\{(\mathbf{R}_n-\mathbf{m}_n)^T\Sigma_{\mathbf{R}_n}^{-1}(\mathbf{R}_n-\mathbf{m}_n)\right\}\Bigg\} \\
& + \frac{\partial}{\partial S_r}\left\{\ln|\Sigma_{\mathbf{R}_n}|\right\} E\left\{\frac{\partial}{\partial S_i}\left\{(\mathbf{R}_n-\mathbf{m}_n)^T\Sigma_{\mathbf{R}_n}^{-1}(\mathbf{R}_n-\mathbf{m}_n)\right\}\right\} \\
& + \frac{\partial}{\partial S_i}\left\{\ln|\Sigma_{\mathbf{R}_n}|\right\} E\left\{\frac{\partial}{\partial S_r}\left\{(\mathbf{R}_n-\mathbf{m}_n)^T\Sigma_{\mathbf{R}_n}^{-1}(\mathbf{R}_n-\mathbf{m}_n)\right\}\right\} \\
& + \frac{\partial}{\partial S_r}\left\{\ln|\Sigma_{\mathbf{R}_n}|\right\}\frac{\partial}{\partial S_i}\left\{\ln|\Sigma_{\mathbf{R}_n}|\right\}\Bigg] \\
+ \frac{\partial S_r}{\partial A_i}\frac{\partial S_r}{\partial A_j}\Bigg[& E\left\{\left[\frac{\partial}{\partial S_r}\left\{(\mathbf{R}_n-\mathbf{m}_n)^T\Sigma_{\mathbf{R}_n}^{-1}(\mathbf{R}_n-\mathbf{m}_n)\right\}\right]^2\right\} \\
& + 2\frac{\partial}{\partial S_r}\left\{\ln|\Sigma_{\mathbf{R}_n}|\right\} E\left\{\frac{\partial}{\partial S_r}\left\{(\mathbf{R}_n-\mathbf{m}_n)^T\Sigma_{\mathbf{R}_n}^{-1}(\mathbf{R}_n-\mathbf{m}_n)\right\}\right\} \\
& + \left[\frac{\partial}{\partial S_r}\left\{\ln|\Sigma_{\mathbf{R}_n}|\right\}\right]^2\Bigg]
\end{aligned}
\tag{5.104}
$$

After finding the expected value over R, J_{ij}^{R} with Equation 5.104, it is time to find the expected value over A. Unfortunately, it cannot be found symbolically. It must be determined numerically.

$$
\begin{aligned}
J_{ij}^{data} &= E\left[\frac{\partial \ln p(\mathbf{R}|\mathbf{A})}{\partial A_i}\frac{\partial \ln p(\mathbf{R}|\mathbf{A})}{\partial A_j}\right] \\
&= \iiiint J_{ij}^{R} p(R|A)\, d\psi\, d\chi\, d\theta_i\, d\phi_i
\end{aligned}
\tag{5.105}
$$

Of course, the limits of integration need to be specified. Because the PDF's are known to be Gaussian, computational time can be reduced by limiting the Gaussian in the (y', z') plane to $\pm 3.25\sigma$ where σ is the standard deviation in the y' and z' directions. Of course, narrowing the limits of integration will affect the accuracy of the answer, so caution must be exercised when applying this timesaving technique. The author arrived at $\pm 3.25\sigma$ with a little intuition and a lot of trial-and-error. With limits of integration applied, the preceding expectation looks like

$$J_{ij}^{data} = \int_{\phi_i^{b1}}^{\phi_i^{b2}} \int_{\theta_i^{b1}}^{\theta_i^{b2}} p(\theta_i, \phi_i) \int_{-\frac{\pi}{4}}^{\frac{\pi}{4}} p(\chi) \int_{-\frac{\pi}{2}}^{\frac{\pi}{2}} p(\psi) J_{ij}^{R} d\psi d\chi d\theta_i d\phi_i \tag{5.106}$$

where ϕ_i^{b1} is from Equation 4.50, ϕ_i^{b2} is from Equation 4.51, θ_i^{b1} is from Equation 4.58, and θ_i^{b2} is from Equation 4.59. It is difficult to see where the 3.25σ is utilized. In ϕ_i^{b1} and ϕ_i^{b2}, 3.25σ is substituted for b. In θ_i^{b1} and θ_i^{b2}, 3.25σ is substituted for both a and b. With these limits, the numerical integration gives the Fisher's Information for one element in the Fisher's Information matrix.

5.3 Apriori Fisher's Information

The Fisher's Information Matrix for the a priori model can be extracted from Equation 5.11

$$J_{ij}^{apriori} = E\left[\frac{\partial \ln p(\mathbf{A})}{\partial A_i} \frac{\partial \ln p(\mathbf{A})}{\partial A_j}\right] \tag{5.107}$$

Remember the a priori PDF from Equation 4.76

$$p(\mathbf{A}) = -\frac{\cos 2\chi}{\pi} \frac{h^2}{\sin^2\theta_i \cos^2\phi_i} \frac{\exp\left[\frac{-(h\tan\phi_i)^2}{2\sigma_{y'}^2} - \frac{\left(\frac{h}{\cos\phi_i \tan\theta_i} + z_{off}\right)^2}{2\sigma_{z'}^2}\right]}{2\pi\sigma_{y'}\sigma_{z'}} \tag{5.108}$$

Take the natural logarithm of Equation 5.108

$$\ln p(\mathbf{A}) = j\pi - \ln 2 + 2\ln h - 2\ln \pi - \ln \sigma_{y'} - \ln \sigma_{z'} + \ln(\cos 2\chi) - 2\ln(\sin \theta_i) - 3\ln(\cos \phi_i) - \frac{h^2 \tan \phi_i}{2\sigma_{y'}} - \frac{\left(z_{off} + \frac{h}{\tan \theta_i \cos \phi_i}\right)^2}{2\sigma_{y'}} \quad (5.109)$$

With $\ln p(\mathbf{A})$ found, the partial derivative with respect to each element in state vector $\mathbf{A}$ must be determined. Beginning with the partial derivative with respect to ϕ_i,

$$\frac{\partial \ln p(\mathbf{A})}{\partial \phi_i} = 3\tan \phi_i - \frac{h^2 \tan \phi_i}{\cos^2 \phi_i \sigma_{y'}^2} - \frac{h \tan \phi_i \left(z_{off} + \frac{h}{\tan \theta_i \cos \phi_i}\right)}{\tan \theta_i \cos \phi_i \sigma_{z'}^2} \quad (5.110)$$

and then the partial derivative with respect to θ_i.

$$\frac{\partial \ln p(\mathbf{A})}{\partial \theta_i} = -\frac{2}{\tan \theta_i} + \frac{h\left(z_{off} + \frac{h}{\tan \theta_i \cos \phi_i}\right)}{\sin^2 \theta_i \cos \phi_i \sigma_{z'}^2} \quad (5.111)$$

The partial derivatives with respect to the ellipticity and rotation angles χ and ψ are

$$\frac{\partial \ln p(\mathbf{A})}{\partial \chi} = -2\tan 2\chi \quad (5.112)$$

$$\frac{\partial \ln p(\mathbf{A})}{\partial \psi} = 0 \quad (5.113)$$

Up to this point, all algebraic operations were accomplished symbolically. Unfortunately, the expectation over $\mathbf{A}$ cannot be found symbolically due to the required integrations. Therefore, numerical techniques must be employed. The expected value in Equation 5.107 is simply

$$E\left[\frac{\partial \ln p(\mathbf{A})}{\partial A_i}\frac{\partial \ln p(\mathbf{A})}{\partial A_j}\right] = \iiiint \frac{\partial \ln p(\mathbf{A})}{\partial A_i}\frac{\partial \ln p(\mathbf{A})}{\partial A_j} p(\mathbf{A}) d\psi d\chi d\theta_i d\phi_i \quad (5.114)$$

Again, the limits of integration need to be specified. Because the PDF's are Gaussian, valuable computer calculation time can be saved by narrowing the limits of integration and splitting the PDF $p(\mathbf{A})$

$$J_{ij}^{apriori} = E\left[\frac{\partial \ln p(\mathbf{A})}{\partial A_i}\frac{\partial \ln p(\mathbf{A})}{\partial A_j}\right] \tag{5.115}$$

$$= \int_{\phi_i^{b1}}^{\phi_i^{b2}} \int_{\theta_i^{b1}}^{\theta_i^{b2}} p(\theta_i, \phi_i) \int_{-\frac{\pi}{4}}^{\frac{\pi}{4}} p(\chi) \cdot \int_{-\frac{\pi}{2}}^{\frac{\pi}{2}} p(\psi)\frac{\partial \ln p(\mathbf{A})}{\partial A_i}\frac{\partial \ln p(\mathbf{A})}{\partial A_j} d\psi d\chi d\theta_i d\phi_i \tag{5.116}$$

where ϕ_i^{b1} is from Equation 4.50, ϕ_i^{b2} is from Equation 4.51, θ_i^{b1} is from Equation 4.58, and θ_i^{b2} is from Equation 4.59.

To arrive at total Fisher's Information, add the Fisher's Information of the a priori data to the Fisher's Information of the observations.

$$\mathbf{J_T} = \mathbf{J_D} + \mathbf{J_P} \tag{5.117}$$

where Equation 5.106 and Equation 5.115 represent the elements in $\mathbf{J_D}$ and $\mathbf{J_P}$ respectively.

Equation 5.117 is the total Fisher's Information at one point on the sphere. In order to make decisions concerning optimum element placement for array design, we will need to compute the total Fisher's Information around the entire surface of the sphere. We will gather this data in the Chapter 6.

Chapter 6

Results

6.1 Computing Fisher's Information

With the equations derived to compute Fisher's Information for the conducting sphere, the next step is to run the computer simulations and collect the Fisher's Information at selected intervals around the sphere.

Originally, the author assumed that the Fisher's Information determined with one monopole placed on the sphere would not be related to the case with two monopoles placed on the sphere. As it turns out, finding the Fisher's Information of two elements at the same time is the same as finding the Fisher's Information of each element separately and adding their respective Fisher's Information together. As a result of this observation, the Fisher's Information at every location on the sphere can be calculated once and only once. When additional elements are added to the array design, the Fisher's Information at each monopole location will simply be added together and inverted to find the variance.

The problem of finding Fisher's Information for the spherical antenna array requires the initial specification of several unknown quantities. The first of these quantities is a set of noise variances. Recall the noise covariance matrix from Equation 4.17. Because the multiplicative and additive noises are statistically independent, only the diagonals of the noise covariance matrix need to be

defined. The off diagonal elements are set to zero. The first diagonal element in that matrix, element (1,1), is defined as the variance of the real part of the multiplicative noise n_r. Recall it is designated σ_1^2. Element (2,2) is the variance of the imaginary part of the multiplicative noise n_i. It is denoted σ_2^2. Element (3,3) is the variance of the real part of the additive noise w_r and it is denoted by σ_3^2. Lastly, element (4,4) is the variance of the imaginary part of the additive noise w_i. It is designated in similar fashion as σ_4^2. Because the noise variances will be changed for different test cases, they will be defined in the next section.

In addition to the noise variances, several geometrical dimensions must be specified. The first of these dimensions is the radius of the sphere. This dimension is represented by the variable a from Figure 3.1. Because we wish to calculate the field at the surface of the sphere, the radius a and the distance r are equal. In the equations from chapter 2, both β and a and β and r appear together, one multiplying the other. Known as the electrical length, βr and βa have units of radians. If we arbitrarily assign β as 2π and r (and a since they are equal) as some number over 2π, then the 2π's will cancel and we're left with a quantity in radians. It will be easier to speak in terms of the electrical length in the test cases which follow.

In addition to defining parameters associated with the sphere, some parameters associated with the a priori beamspot require definition. These parameters, σ_x^2, σ_y^2, h, and z_{off}, are unique because the units attached to them are insignificant. The ratios between them are important but the units are not. Therefore, the units will be called units.

Because we have modeled the probability that an emitter is found at a given point within the beamspot as a bivariate Gaussian distribution, defining the beamspot requires both choosing the two variances of the bivariate and se-

lecting some limits for numerical integration. In choosing the variances for the bivariate, we would prefer them to be different. This will ensure that the bivariate distribution is not symetrical (to lend more credibility to the problem, we will avoid symmetry where it is easy to do so). Therefore, we choose σ_x^2 to have a variance of 1 unit and σ_z^2 to have a variance of 2 units. As a result, the beamspot will have a bivariate distribution twice as wide in the z direction as in the x direction.

The expected value integral calculations derived in Chapter 5 will require numerical methods. Because the bivariate Gaussian distribution can theoretically extend forever in the all directions of the $x - z$ plane, performing numerical integration over the area will be inefficient. We are forced to choose more pragmatic integration limits than $\pm\infty$. After some trial and error, these limits were set to $\pm 3.25\sigma$. Values higher than $\pm 3.25\sigma$ gain too little in accuracy at the expense of significantly extended integration time. 3.25σ was used as integration limits for both the x and z axis of the plane.

The last unknown quantities to furnish before we can solve for Fisher's Information are the distances h and z_{off}. Remember from Chapter 2 that h is defined as the distance from the sensor to the beamspot plane as shown in Figure 2.1. z_{off} is defined to be the offset distance from the sensor to the center of the beamspot plane, also shown in Figure 2.1. Both h and z_{off} will remain the same for all test cases. We define them here as 1 unit and -1 unit respectively.

6.2 Test Cases

The tables below show the input parameters for eight different test cases. Only the noise variances and the radius of the sphere are included in the table. All the other input parameters remained fixed to the values given above. Table 6.1 presents the variances as voltages. Table 6.2 presents the variances in dB.

Test Case	$\beta r(rad)$	$\sigma_1^2(V^2)$	$\sigma_2^2(V^2)$	$\sigma_3^2(V^2)$	$\sigma_4^2(V^2)$
1	1.3	0.01	0.005	0.2	0.2
2	1.3	0.01	0.005	0.001	0.001
3	1.3	0.0001	0.0001	0.2	0.2
4	1.3	0.0001	0.0001	0.001	0.001
5	2.3	0.01	0.005	0.2	0.2
6	2.3	0.01	0.005	0.001	0.001
7	2.3	0.0001	0.0001	0.2	0.2
8	2.3	0.0001	0.0001	0.001	0.001

Table 6.1: Input Parameters for the 8 Test Cases

Note that the test cases in the tables above differ only slightly by their input parameters. Each test case was designed to simulate a real world condition. For instance, test case one was given both large multiplicative (columns one and two) and additive (columns three and four) noises. In a real world situation, multiplicative noise could represent channel imbalance in the receiver while additive noise might represent interferers such as thermal noise. Therefore, test case one represents the real world situation of large channel imbalance and large thermal noise.

In test case two the additive noise is much smaller. One could conclude that this test case represents the situation of large channel imbalance and small thermal noise. Continuing, test case three represents small channel imbalance and large thermal noise while test case four represents small channel imbalance and small thermal noise.

In the first four test cases, the electrical radius of the sphere was set to 1.3 radians. Starting in test case five, the electrical radius is changed to 2.3 radians while all the other parameters are identical to test case one. In test case six, the radius is again 2.3 radians while the other parameters are copied from

Test Case	$\beta r(rad)$	$\sigma_1^2(dB)$	$\sigma_2^2(dB)$	$\sigma_3^2(dB)$	$\sigma_4^2(dB)$
1	1.3	0.01	0.005	0.2	0.2
2	1.3	0.01	0.005	0.001	0.001
3	1.3	0.0001	0.0001	0.2	0.2
4	1.3	0.0001	0.0001	0.001	0.001
5	2.3	0.01	0.005	0.2	0.2
6	2.3	0.01	0.005	0.001	0.001
7	2.3	0.0001	0.0001	0.2	0.2
8	2.3	0.0001	0.0001	0.001	0.001

Table 6.2: Input Parameters for the 8 Test Cases

test case two. The remaining test cases (seven and eight) are the same as test cases three and four with exception of the electrical radius. What is significant about the change in electrical radius? The change in radius simulates a change in the frequency of the incident radiation. A smaller radius represents a higher incident wave frequency. Likewise a larger radius represents a lower incident wave frequency.

Therefore, the eight test cases are designed to simulate two different frequencies and two different amounts of multiplicative and additive noise. The Fisher's Information was calculated for each of the eight test cases at 20 degree increments of ϕ and θ around the sphere. It is not presented here because it is merely an intermediate result.

6.3 Designing an array

The author has shown previously how to derive and compute Fisher's Information. However, one question remains. How to apply Fisher's Information to the design of an antenna array? When designing an array using Fisher's Information, there are several strategies one might choose to follow. One could implement an

N dimensional search algorithm to find the N best locations to place N elements. Alternately, one could use an iterative search where the first element in the array is placed at a location found to have the most information. Each additional element is placed at a location found to have the next best information. The process repeats until all N elements are placed. For the case where $N = 1$ (a one element array), the two methods are identical so we will consider this case first.

6.3.1 The One Element Array

The Fisher's Information calculated in the preceding section takes the form of a 4×4 matrix sampled at $20°$ intervals of ϕ and θ around the perimeter of the sphere. In the hypothetical case of a one element array design, the Fisher's Information Matrix at each location would be inverted. From these inverted matrices, each element along the diagonal is a CRLB for a corresponding element in the state vector $\hat{\mathbf{A}} = [\,\phi_i\ \theta_i\ \chi\ \psi\,]$. More specifically, element $(1,1)$ in the inverted Fisher's Information Matrix is the CRLB for the DOA angle ϕ_i. Element $(2,2)$ is the CRLB for the DOA angle θ_i. Element $(3,3)$ is the CRLB for the ellipticity angle χ. And last, element $(4,4)$ is the CRLB for the rotational angle ψ. To state again in a different way, the diagonals in the inverted Fisher's Information Matrix represent the lower bounds on the variance for each of the four parameters we want to estimate - ϕ_i, θ_i, χ, and ψ.

Matrix Element	parameter	description
1,1	CRLB on variance of ϕ	one of two DOA parameters
2,2	CRLB on variance of θ	the other DOA parameter
3,3	CRLB on variance of χ	polarization ellipticity angle
4,4	CRLB on variance of ψ	polarization rotation angle

Table 6.3: Identities of the Important CRLB Matrix Elements

It is important to note that DOA estimates are formulated from two angles - ϕ and θ. When determining where to place array elements to make better DOA estimates, start with the locations where the CRLB's for both angles (matrix positions $(1,1)$ and $(2,2)$) are smallest. This is logical because whenever the CRLB is small, the Fisher's Information is high. Because the goal is to maximize information when selecting locations for array elements, any points where the Fisher's Information is high become good candidates for placing an array element.

It is also important to note that if the CRLB for one of the DOA angles is small, this does not imply that the CRLB for the other angle will also be small. Therefore, it is possible, but not necessarily desirable, to develop estimators that are good at estimating one of the angles but poor at estimating the other. Obviously, for direction finding arrays, the CRLB's for both angles should be small at any potential locations for elements. One way to help ensure that the CRLB's for both angles are low is too add them together at each point calculated and then select the point with the smallest sum. A weighted sum could also be used if one desired to lessen the effect of one of the angles. Of course, one can always choose to ignore one of the angles. In this research, the sum of the angles will be used most frequently.

6.3.2 N Element Arrays

While the case of a single element array is interesting, the definition of an array implies more than one element. Therefore, we now consider arrays with N elements. The two strategies mentioned previously will produce different results with two or more elements. Let's consider the N dimensional search first.

6.3.2.1 N Dimensional Search

When $N = 2$, the N dimensional search requires that the Fisher's Information at the first sample point on the sphere be added to every point on the sphere, including itself. This creates a new set of matrices. Each of these matrices is inverted. The sum of the CRLB of both DOA angles is stored temporarily. Then, the Fisher's Information at the second sample point is added to every point on the sphere, including itself. This creates another new set of matrices which are also inverted. The sum of the CRLB of both DOA angles is stored. In a continued fashion, the Fisher's Information for the next sample point is added to every point and the resulting set of matrices are each inverted. This occurs for every sample point. The two points with the lowest sum of CRLB for both DOA angles are the two best locations to place the two elements.

This algorithm may be followed for $1 \leq N < \infty$. However, there is a practical constraint. As N grows increasingly large, the N dimensional search algorithm becomes more and more burdensome to calculate.

6.3.2.2 Iterative Search

The iterative search strategy alleviates much of the computational burden of the N dimensional search. In the iterative search, the best location for each element is found successively, one after another. The best location for the first element is determined exactly as was done for the single element case in Section 6.3.1. The position for the first element is fixed and we will call it location one. The Fisher's Information associated with location one is then added to the Fisher's Information of all the other points including location one. This set of matrices is inverted. The sum of the CRLB for the DOA angles is computed and the location

with the smallest sum becomes the best location to place element two. Element two is fixed at location two and the process repeats itself for all the remaining elements.

While the iterative search dramatically reduces the computational burden associated with finding optimum locations for all the elements in an array, the iterative search has one disadvantage. The algorithm itself is somewhat suboptimal. The best location for each additional element added to an array design is the best location for that element given the locations of the previously placed elements. An ideal algorithm, such as the N dimensional search, allows all N elements to be located freely about the sphere. Nonetheless, the iterative search algorithm is used for this research because of its computational savings.

6.4 Results

Results are presented in the form of contour plots for each of the eight test cases. These plots show either the CRLB of the angle ϕ versus the angles ϕ and θ, the CRLB of the angle θ versus ϕ and θ, or the sum of CRLB of the angles ϕ and θ versus ϕ and θ. The contour plots in some of test cases did not show enough detail with 12 equal range contours. Therefore the logarithm of the data was plotted instead of just the data. The result is that the data plotted becomes negative instead of positive (as Fisher's Information should be).

To help interpret the plots, relative locations on the sphere are shown on a blank contour plot in Figure 6.4. By revisiting Figure 3.3 from Chapter 3, one can easily see that the top of the sphere translates into coordinates $(\phi = 180, \theta = 90)$. Likewise, the bottom of the sphere is represented by coordinates $(\phi = 0, \theta = 90)$, the front is represented by $\theta = 0$, and so forth.

When looking at the plots for the eight test cases, the first thing to notice

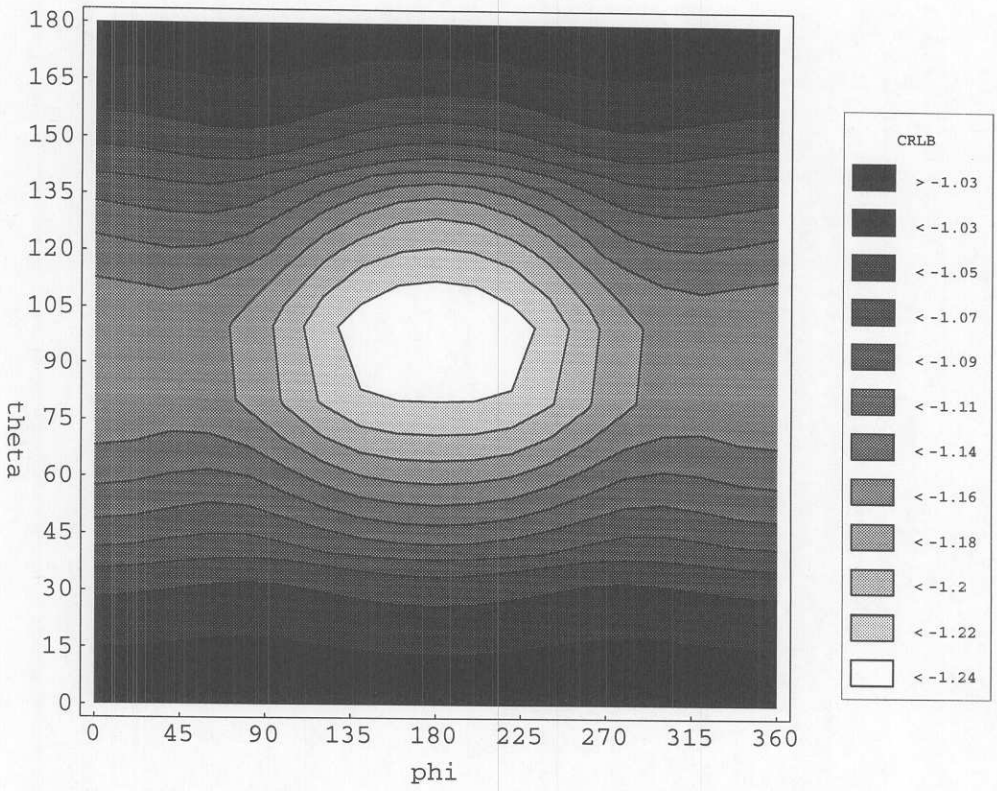

Figure 6.1: Test Case 1 - CRLB of ϕ in $\log radians^2$ vs. position ϕ and θ

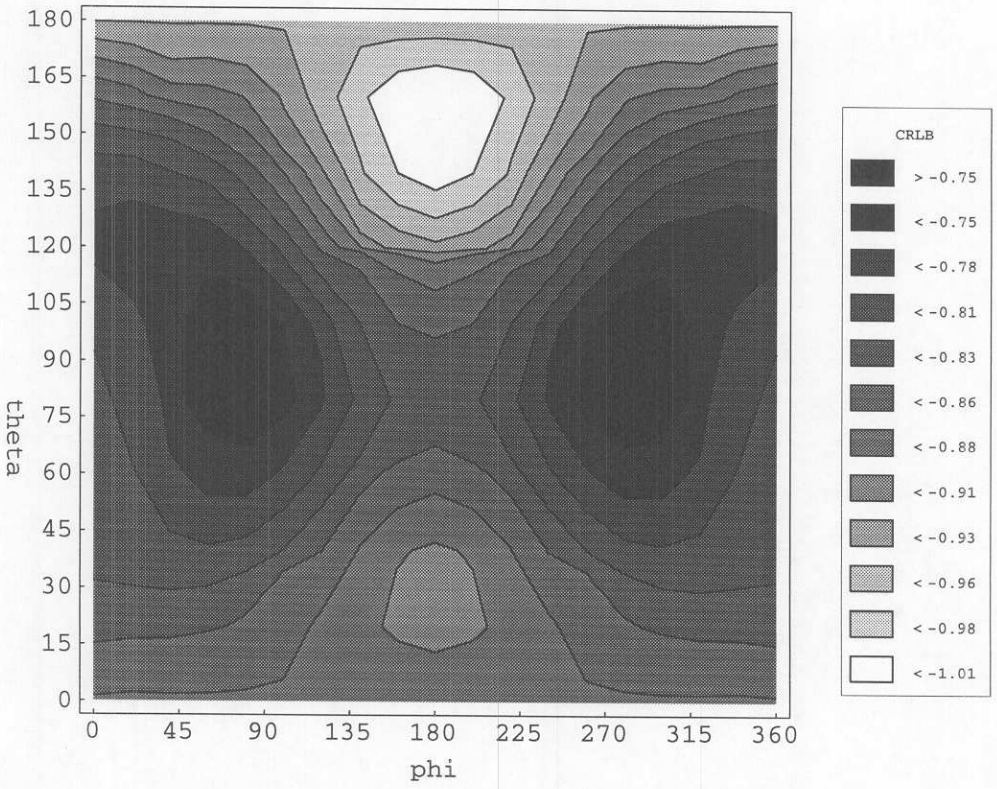

Figure 6.2: Test Case 1 - CRLB of θ in $\log radians^2$ vs. position ϕ and θ

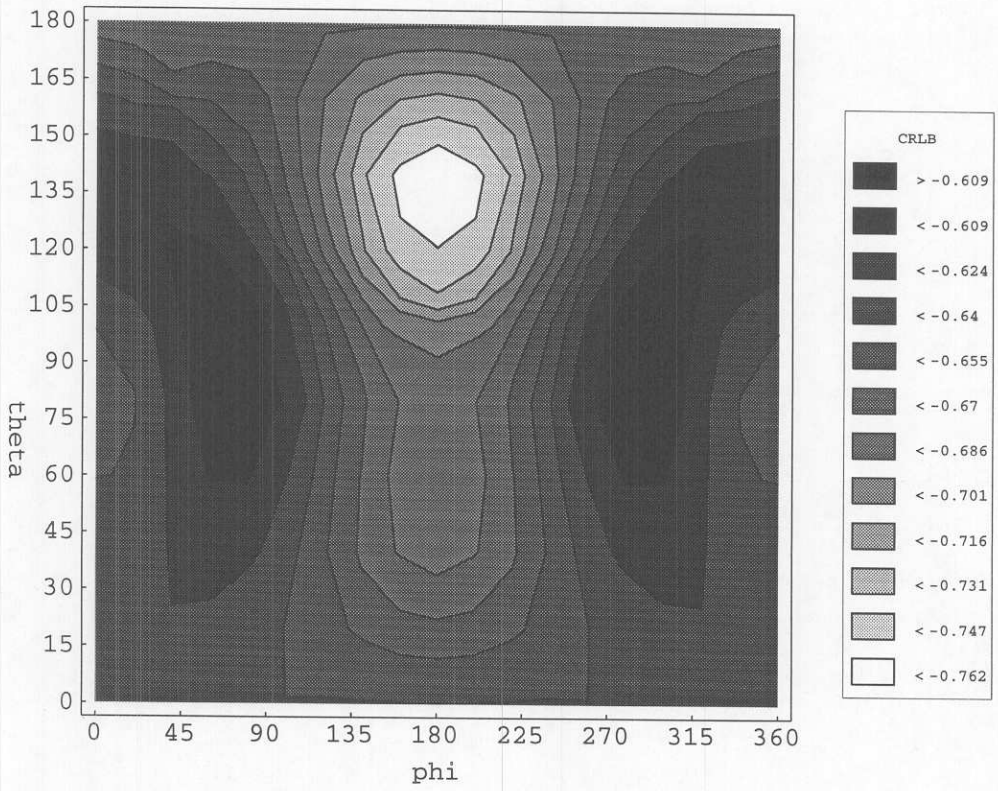

Figure 6.3: Test Case 1 - Sum of the CRLB's of ϕ and θ in $\log radians^2$ vs. position ϕ and θ

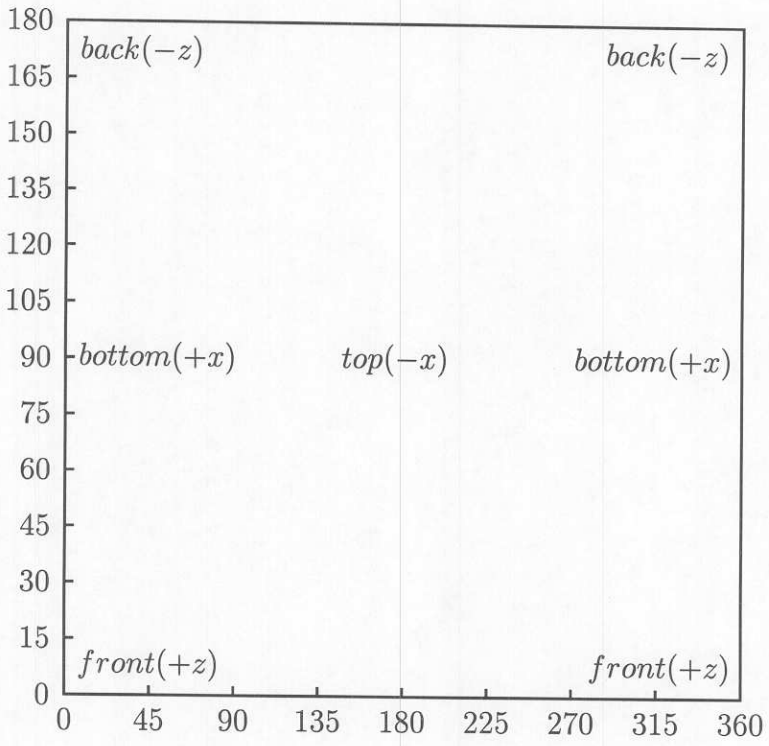

Figure 6.4: Angle-to-Relative Position Interpretation

is that the locations of the minimums (the white areas in the figures) are **not** necessarily intuitive. In fact, sometimes the minima locations are both intuitive and predictable, at other times, they are not. For instance, from Figure 6.3, there is one absolute minima at $(\phi = 180°, \theta = 135°)$. There are also two relative minima, one near $(\phi = 0°, \theta = 75°)$, the other near $(\phi = 180°, \theta = 60°)$. If array elements were placed at the minima locations, one could argue that the resulting array design is both intuitive and predictable in the angle ϕ, but not so intuitive or predictable in the angle θ. One might also say that the absolute minima (the location to place the first element in a design) is completely predictable. It lies on the back side of the sphere such that if one draws a line from the center of the beamspot through the center of the sphere and all the way out the back side of the sphere, the point where the line exits the sphere is the absolute minima. In this case, it seems logical that one could predict the location to place the first element, but it does not seem so easy to pick the locations for a second, third, or even fourth element.

Let us examine another example, that of test case four. From Figure 6.7, one can see that there are as many as five locations to place array elements. Three are relative minimas, while the other two are considered because they are in a band that shows high Fisher's Information (low CRLB) yet are separated from the relative minima a good distance.

Note that the minimas in test case four are in quite different locations than for the example of test case one. This can be attributed to the differences in the noise variances for the two test cases. As can be witnessed from Table 6.1, test case four has a lower noise variance than test case one.

If the sphere is bisected with a plane at $\phi = 180°$, the two best locations for placing elements are mirror images of each other. While these two locations,

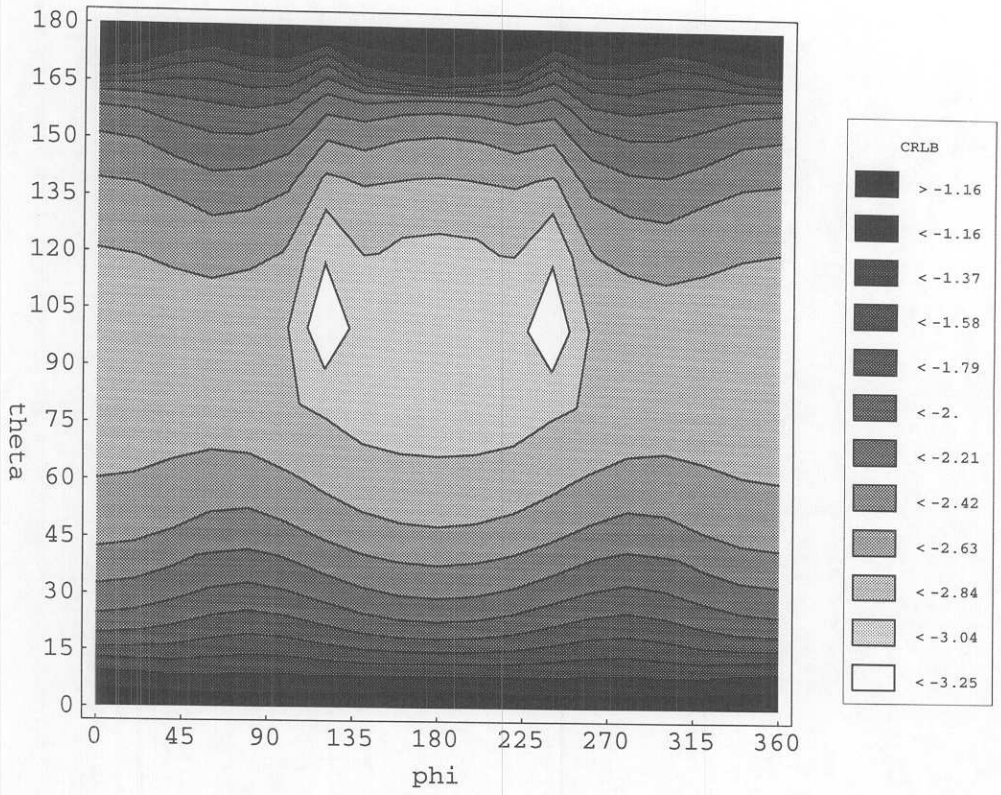

Figure 6.5: Test Case 4 - CRLB of ϕ in $\log radians^2$ vs. position ϕ and θ

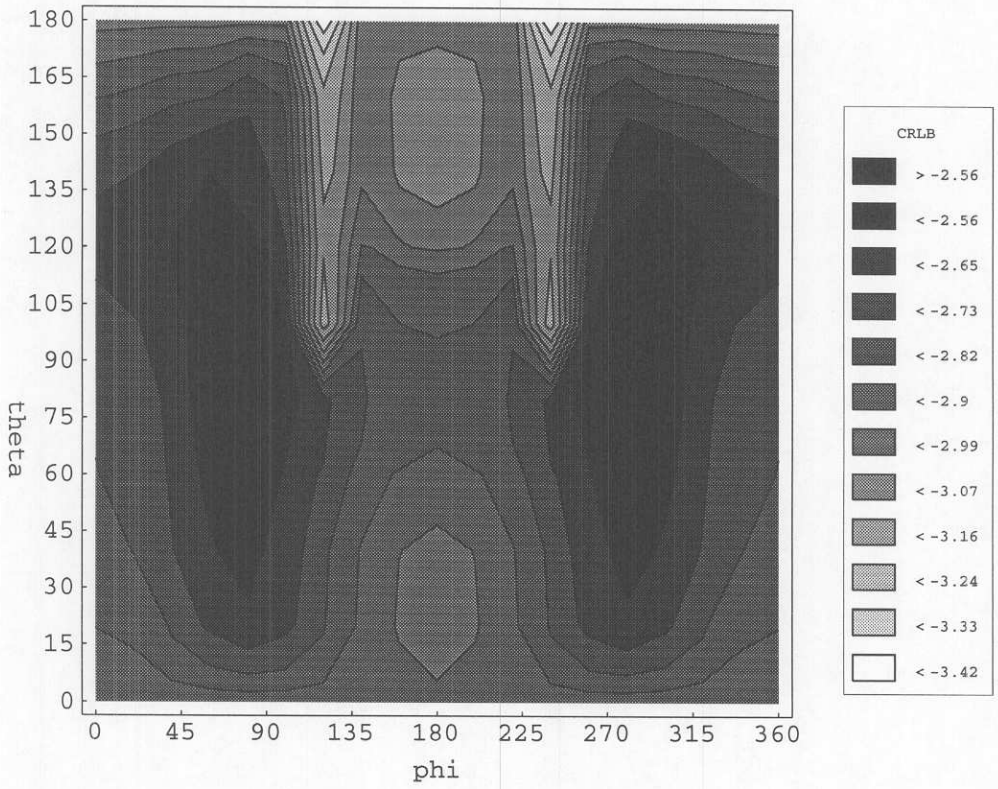

Figure 6.6: Test Case 4 - CRLB of θ in $\log radians^2$ vs. position ϕ and θ

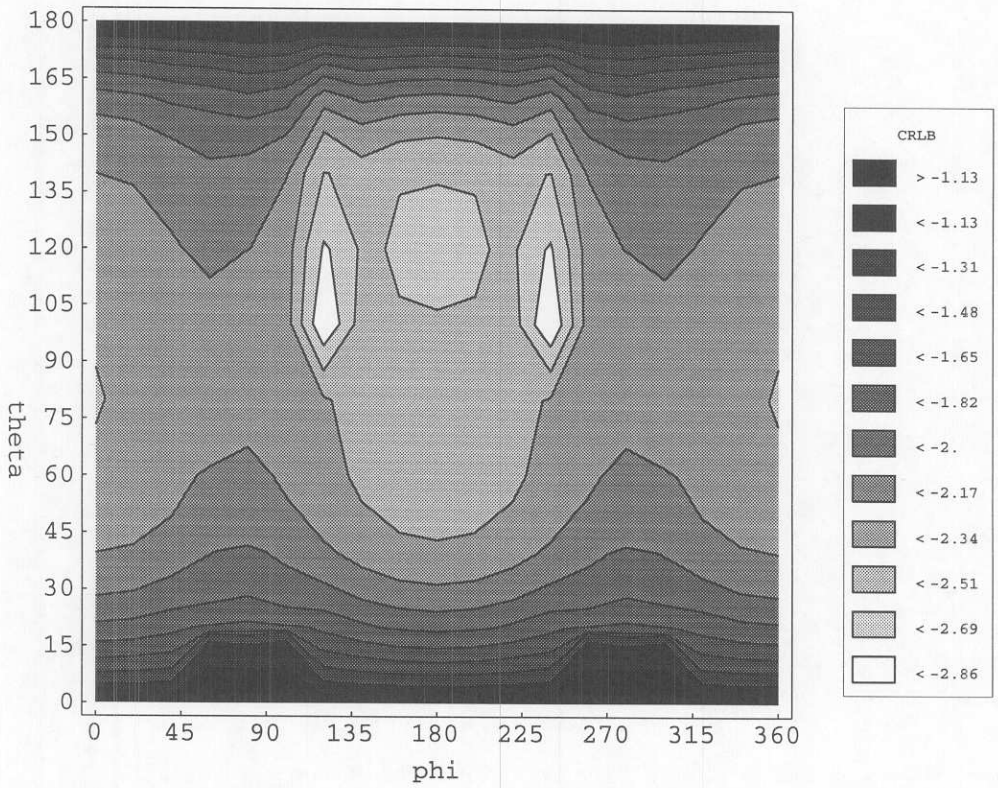

Figure 6.7: Test Case 4 - Sum of the CRLB's of ϕ and θ in $\log radians^2$ vs. position ϕ and θ

($\phi = 120°, \theta = 110°$) and ($\phi = 240°, \theta = 110°$), are symetrical, it is unlikely that one could have predicted the precise placement of those elements without Fisher's Information or more intensive trial and error.

In addition to the two above, there are three other promising locations to place elements. One is at ($\phi = 0°, \theta = 80°$). Two more could be placed at an azimuth of $\phi = 180°$, one with elevation $\theta = 55°$, the other with elevation of $\theta = 150°$. While the latter two are not relative minima, they are enough removed from the true minima to merit consideration.

The next test case we shall discuss is test case five. In this test case, the radius of the metallic sphere has been increased to $\frac{2.3}{\pi}$. The noise variances stay the same as test case one.

In the contour plot of Figure 6.10, there are three minima. All are located at $\phi = 0°$ or $\phi = 180°$, one at ($\phi = 180°, \theta = 80°$), one at ($\phi = 0°, \theta = 55°$), and one at ($\phi = 0°, \theta = 125°$). This test case is significant not only because it shows the drastic changes in the results due to a slight change in the radius of the sphere, but it is significant for another reason as well. Making the radius of the sphere larger will produce the same effect as making the wavelength of the incident waveform shorter, all other things being equal. Because frequency is the inverse of wavelength, a shorter wavelength incident wave is also a higher frequency incident wave. Therefore, as we might have guessed, the Fisher's Information about the sphere will change with variations in the frequency of the incident waveform.

The remaining five test cases follow. For these test cases, only the sum of the CRLB's of the angles ϕ and θ are shown.

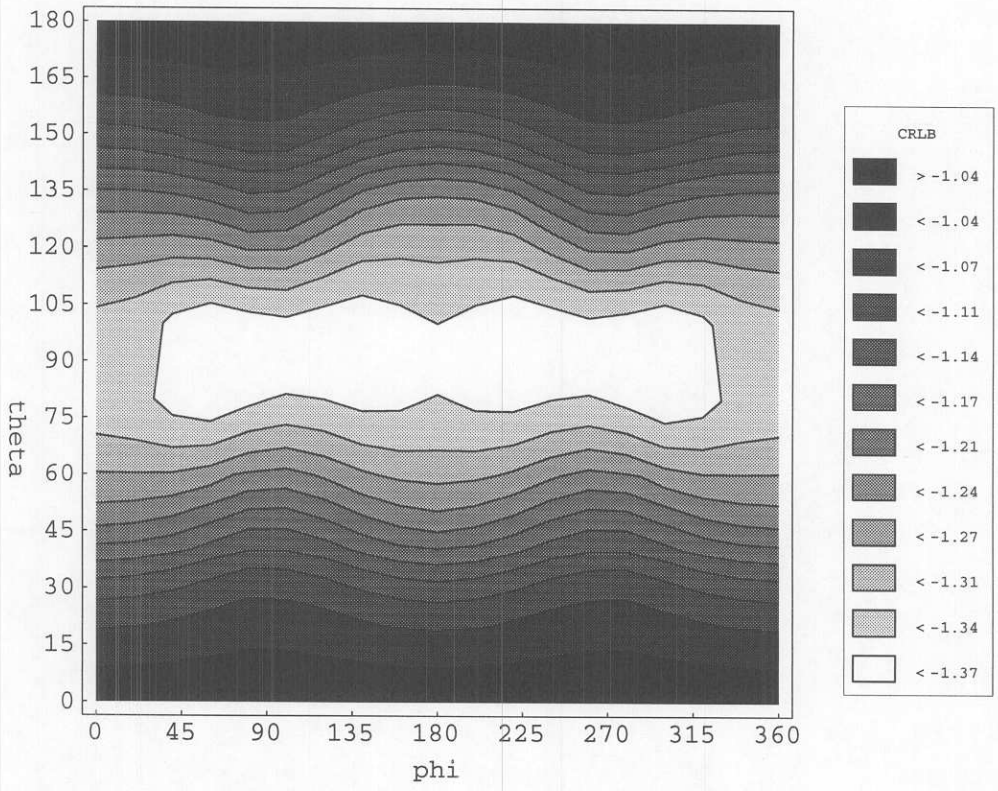

Figure 6.8: Test Case 5 - CRLB of ϕ in $\log radians^2$ vs. position ϕ and θ

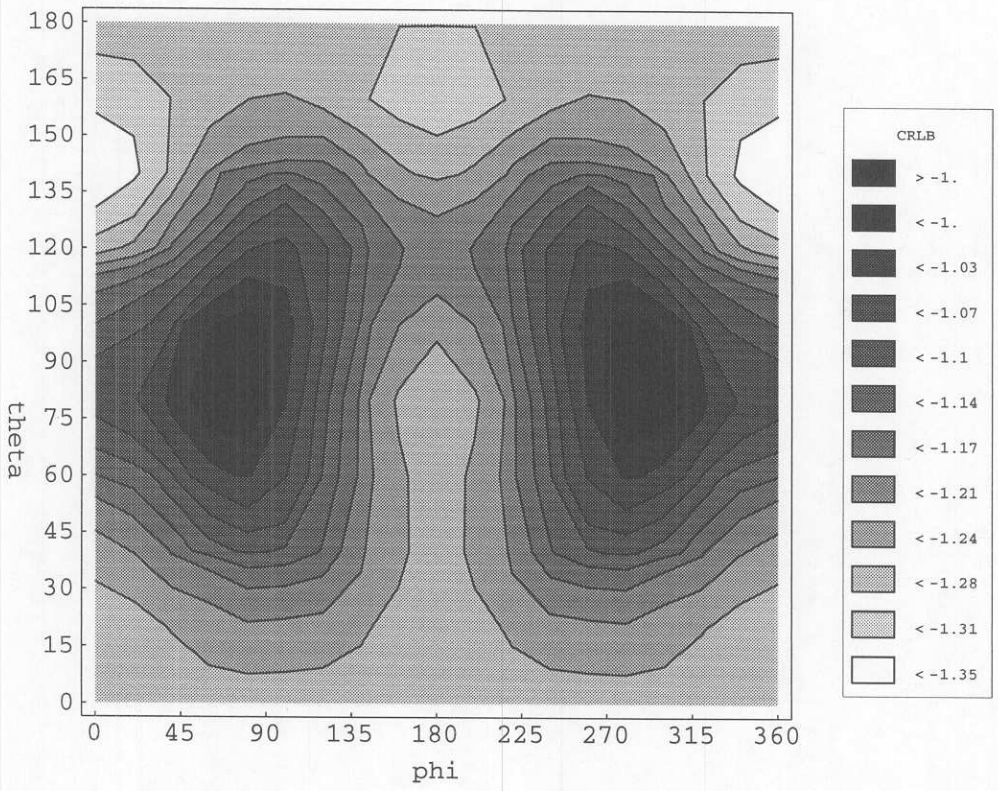

Figure 6.9: Test Case 5 - CRLB of θ in $\log radians^2$ vs. position ϕ and θ

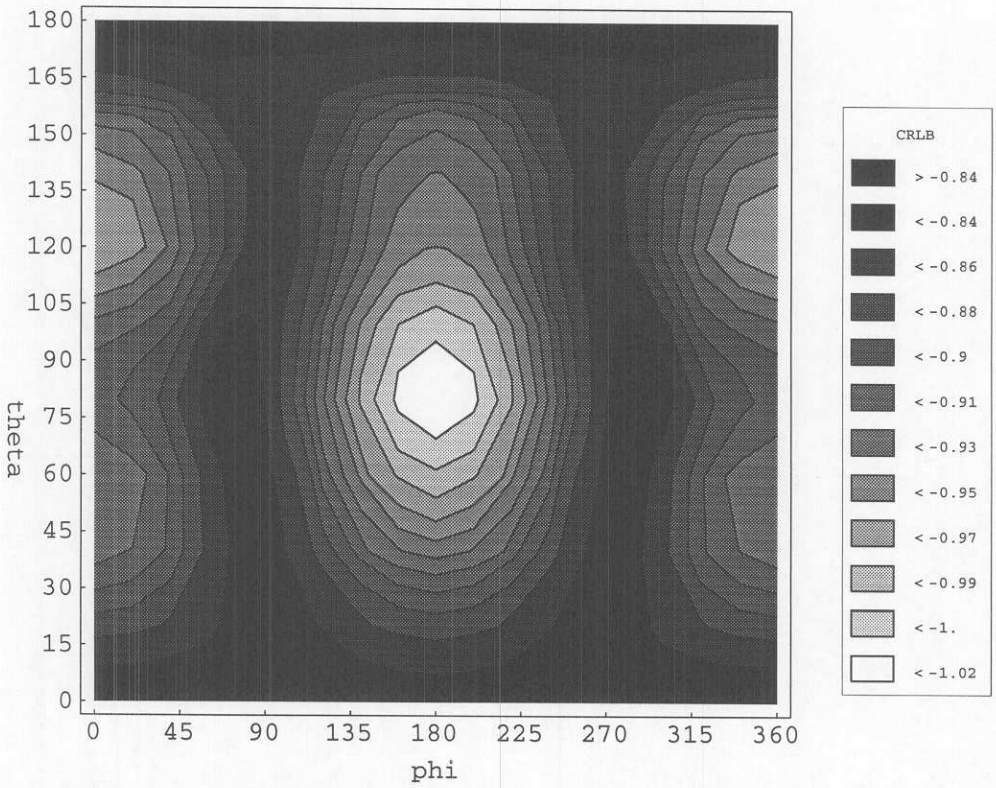

Figure 6.10: Test Case 5 - Sum of the CRLB's of ϕ and θ in $\log radians^2$ vs. position ϕ and θ

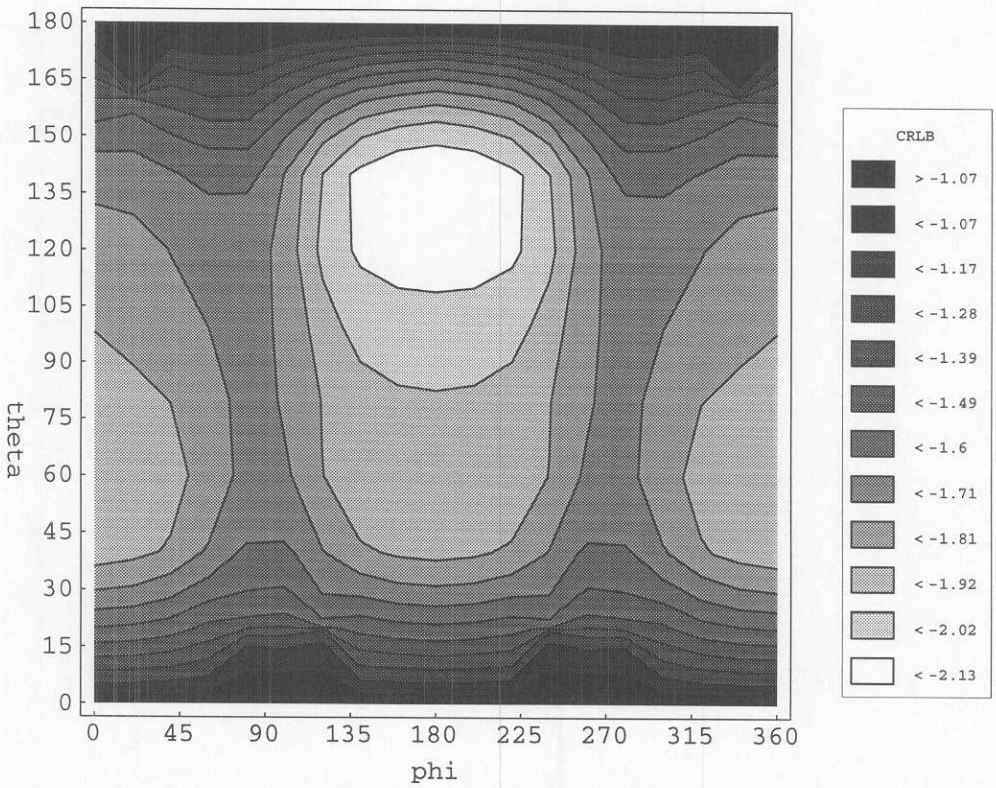

Figure 6.11: Test Case 2 - Sum of the CRLB's of ϕ and θ in $\log radians^2$ vs. position ϕ and θ

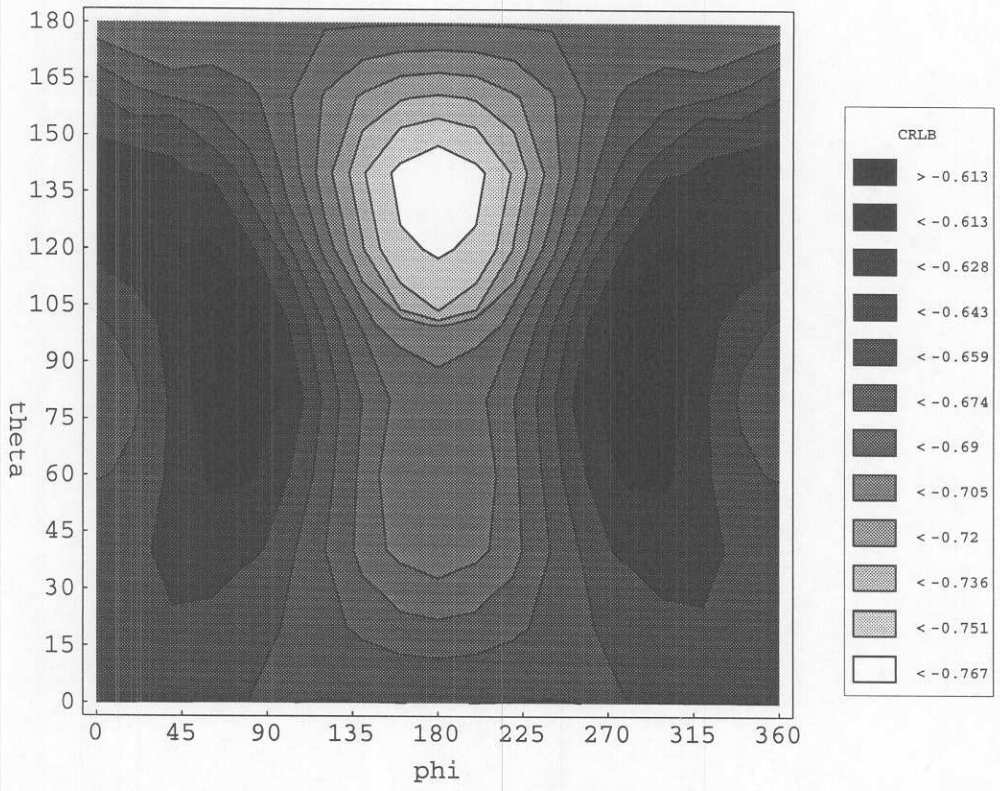

Figure 6.12: Test Case 3 - Sum of the CRLB's of ϕ and θ in $\log radians^2$ vs. position ϕ and θ

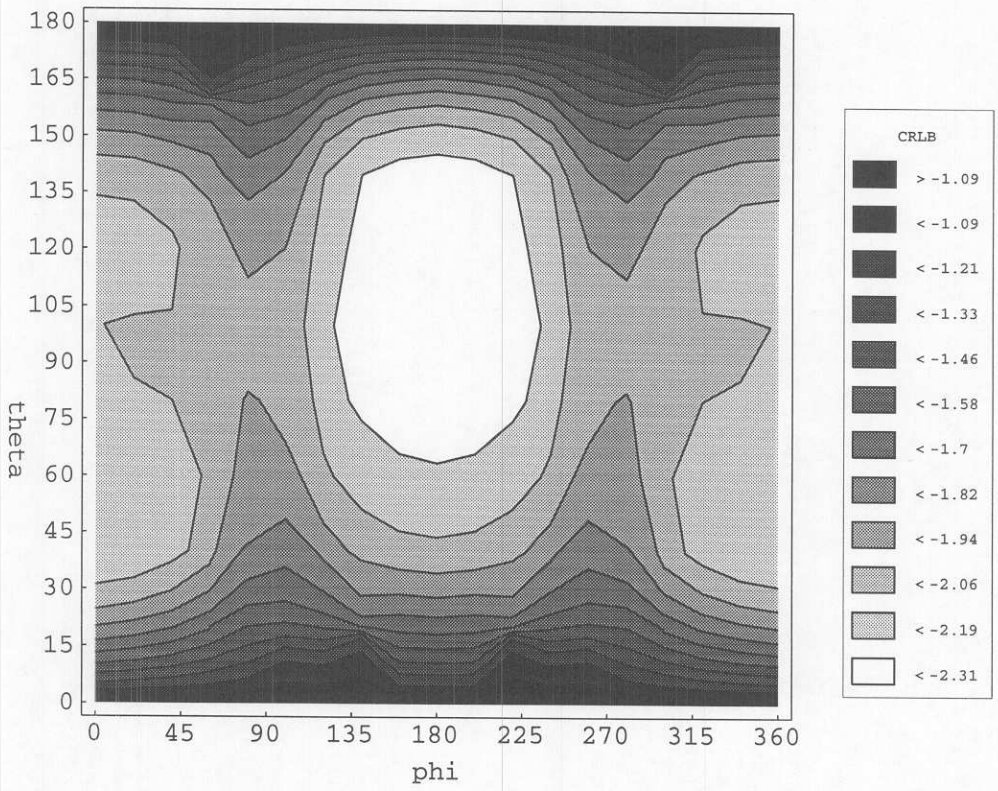

Figure 6.13: Test Case 6 - CRLB ($\log radians^2$) vs. element position ϕ and θ

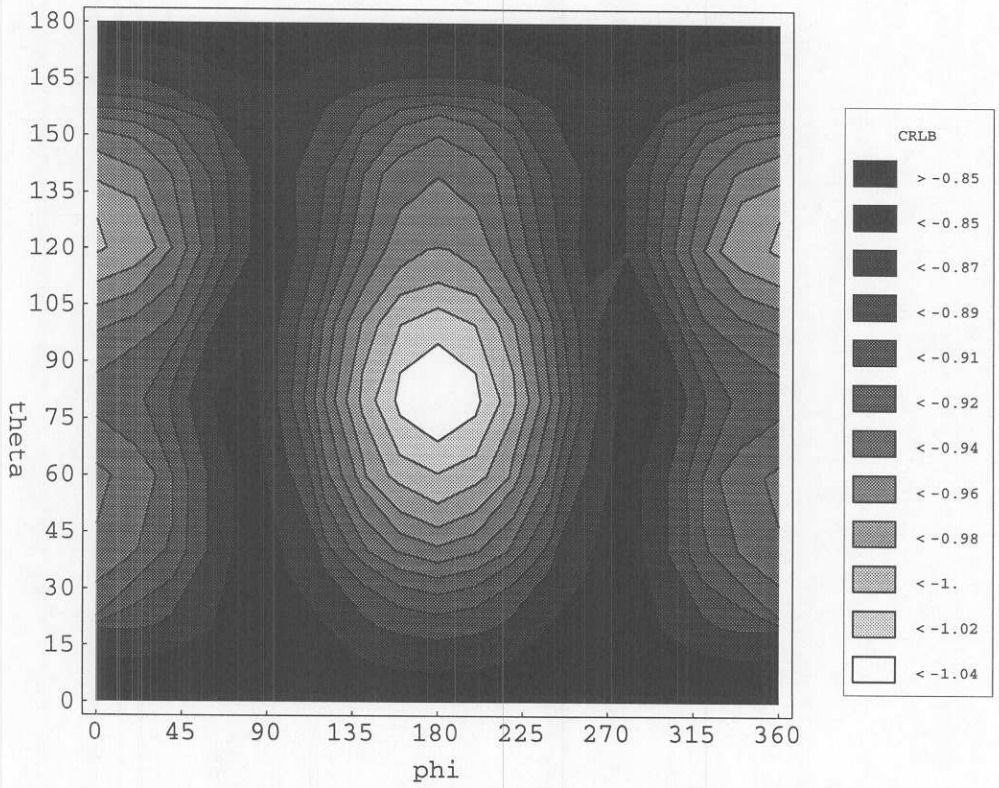

Figure 6.14: Test Case 7 - CRLB ($\log radians^2$) vs. element position ϕ and θ

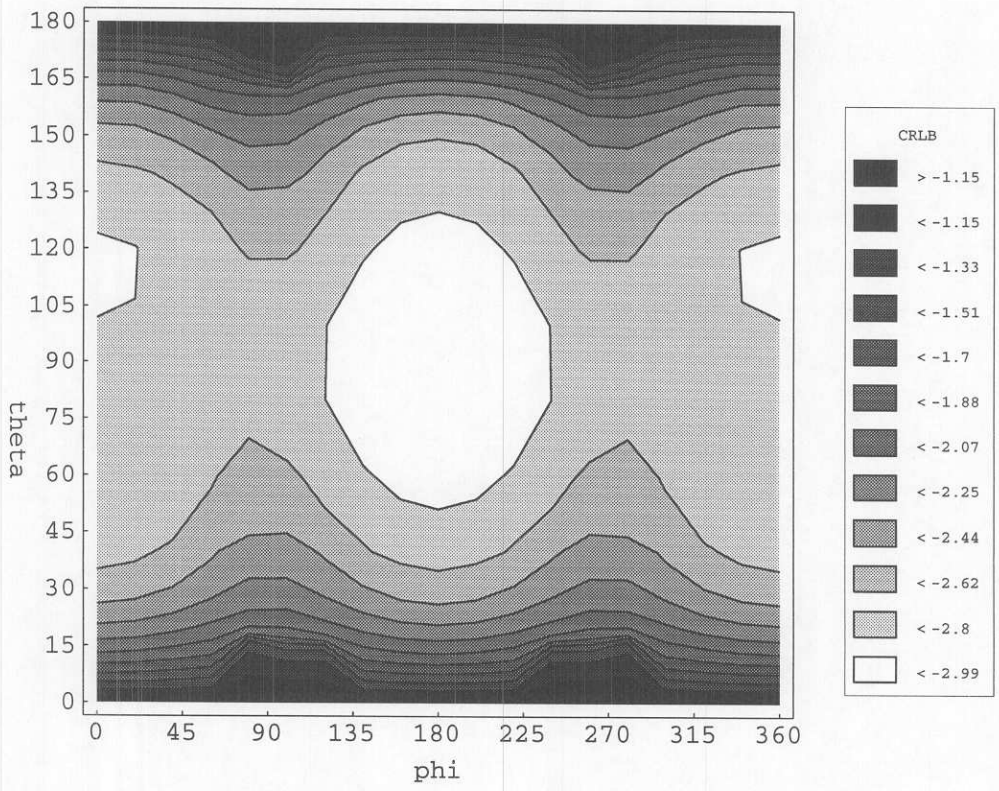

Figure 6.15: Test Case 8 - CRLB ($\log radians^2$) vs. element position ϕ and θ

6.5 Designing a Three Element Array

Up to this point, the contour plots have shown the best location to place only one element. But it takes more than one element to build an array. Using the iterative search procedure, let us build a three element direction finding array using the Fisher's Information data from test case two. Figure 6.11 is reprinted here as Figure 6.16 for ease of reference. The minima in this Figure is not precisely clear.

By choosing the contours nonlinearly, Figure 6.17 shows more detail at the expense of some added distortion. Since we are only interested in the minimums, this distortion will not be cause for concern. The remaining contour plots is this section will be plotted in this manner.

The minimum in Figure 6.17 is located at $(\phi = 180°, \theta = 140°)$. This mimimum is the best location to place the first element in our three element array.

Now we will find the best location to place element two by following the iterative search procedure described in Section 6.3.2.2. First, we add the Fisher's Information Matrix from the element one location to the Fisher's Information Matrices at all the other locations around the sphere. Next, we invert the matrices from step one. Last, we compute the sum of the CRLB of angles ϕ and θ and plot as in Figure 6.18. We can see that the best location to place a second element moves 20° in angle θ from element one to location $(\phi = 180°, \theta = 120°)$.

If we continued in a similar manner, we would find that the best location to place a third element in our array is the same location as element two. If we placed a fourth element, we would find its best location would be very near the first three elements. Logically, this is not what one would expect, and physically, it is

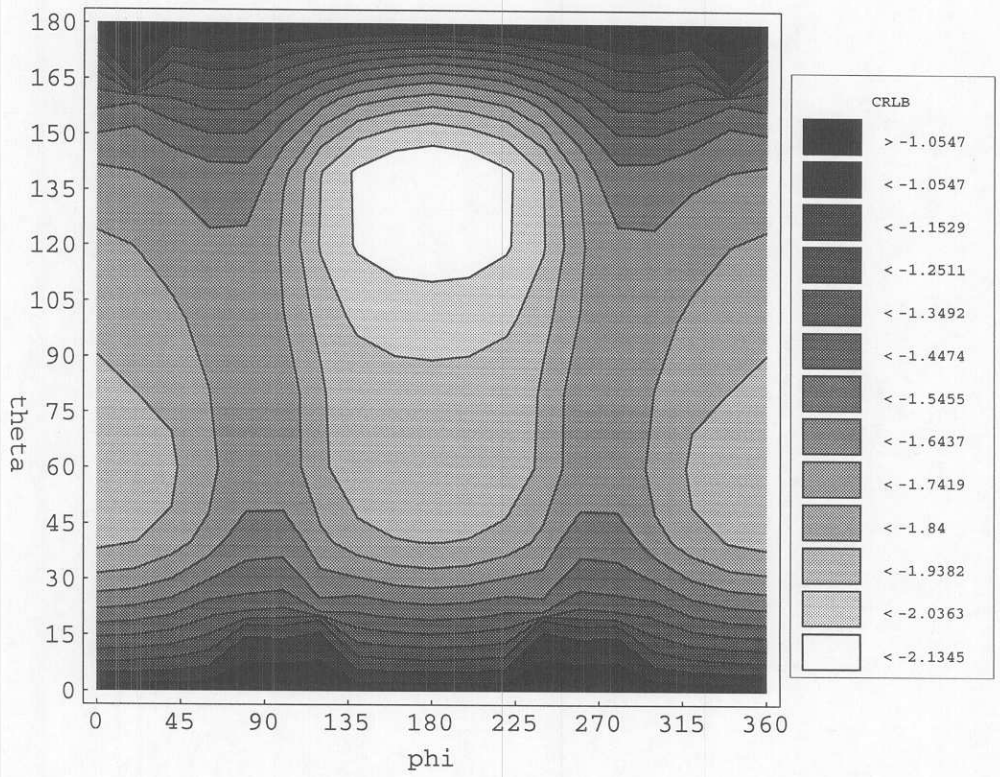

Figure 6.16: 1st Element - CRLB ($\log radians^2$) vs. element position ϕ and θ

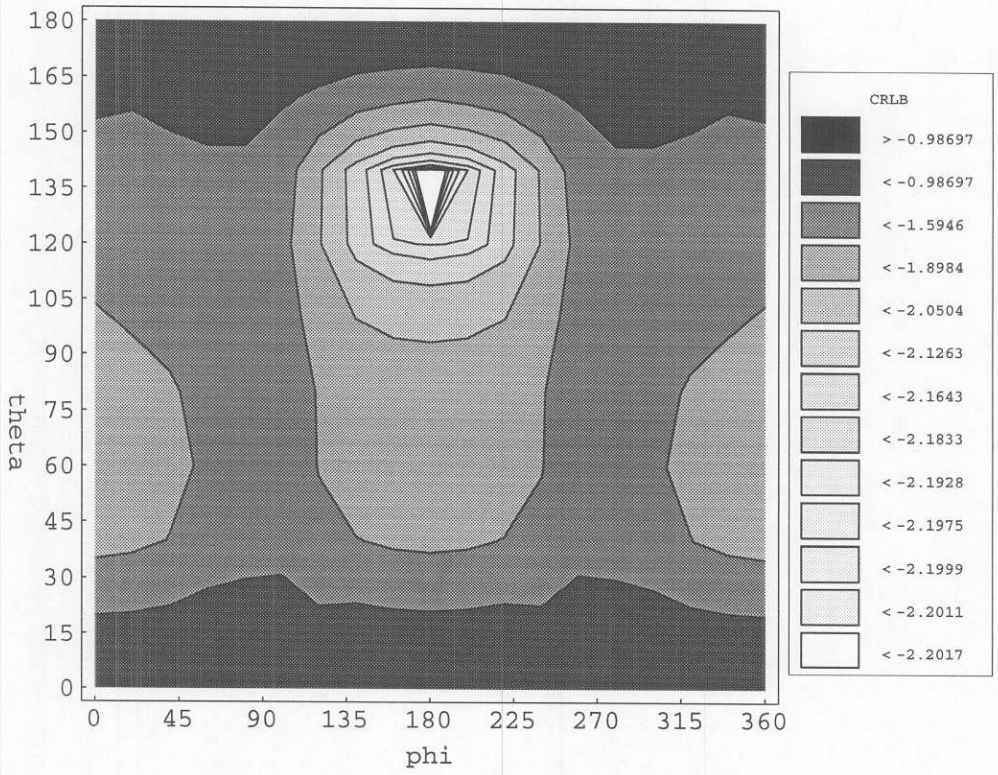

Figure 6.17: 1st Element - CRLB ($\log radians^2$) vs. element position ϕ and θ

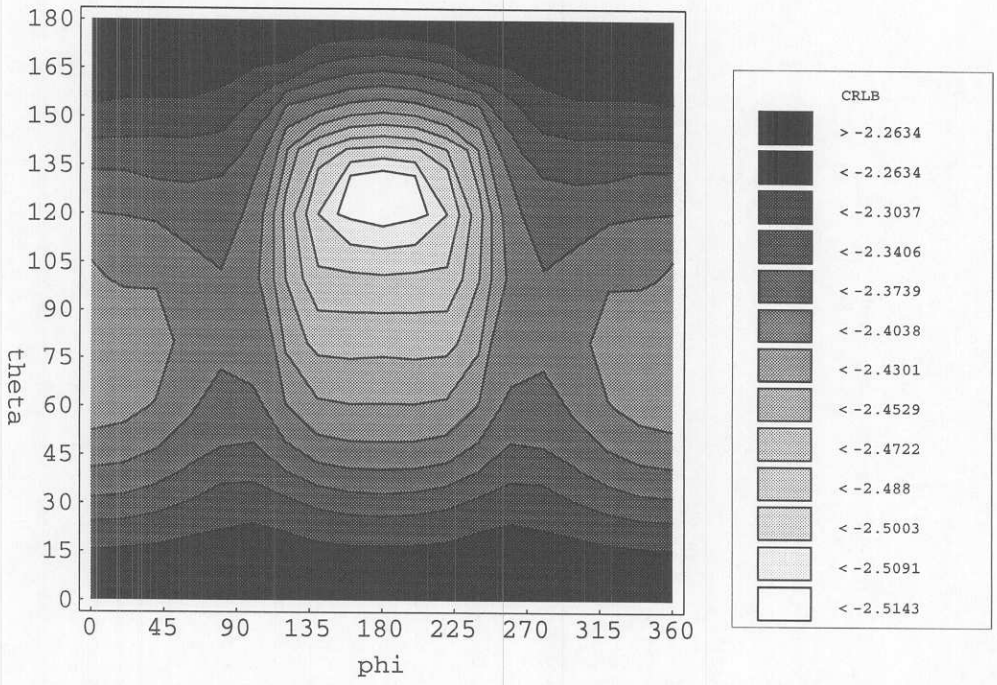

Figure 6.18: 2nd Element - CRLB ($\log radians^2$) vs. element position ϕ and θ

impossible to place one element on top of another. What is wrong? The elements keep going back to the same location because this location is super sensitive in terms of direction finding information. In other words, even though there already exists an element in this location, there is still more information to be gathered by placing the next element at this location than at any other location on the sphere. This behavior can best be explained by comparing the placement of additional elements in the same location to that of the mathematical operation known as integration.

By placing 10 elements at element location one ($\phi = 180°, \theta = 140°$), we can simulate this integration and find a genuinely new location to place a second element. If we add ten times the Fisher's Information Matrix from the element one location to the Fisher's Information Matrices at all the other locations around the sphere, invert, and compute the sum of the CRLB of angles ϕ and θ, we find that the best location to place the next element now moves significantly from element one. Because of the symmetry of the sphere, there is now a choice of two locations, each with identical CRLB's. They are ($\phi = 140°, \theta = 100°$) and ($\phi = 220°, \theta = 100°$). Let's pick ($\phi = 140°, \theta = 100°$) and continue.

Again, we will place 10 more elements at this second location, ($\phi = 140°, \theta = 100°$), and repeat the procedure just used to find location two. As one might expect, the best location for the third element turns out to be the unused location from the element two search. The two minima for this search are located at ($\phi = 140°, \theta = 100°$) and ($\phi = 220°, \theta = 100°$), same as the previous search. Since we don't want to place another element at ($\phi = 140°, \theta = 100°$) we will choose location ($\phi = 220°, \theta = 100°$).

As can be seen from the final element placement, it would have been difficult to find the optimum locations to place the three elements in this direction

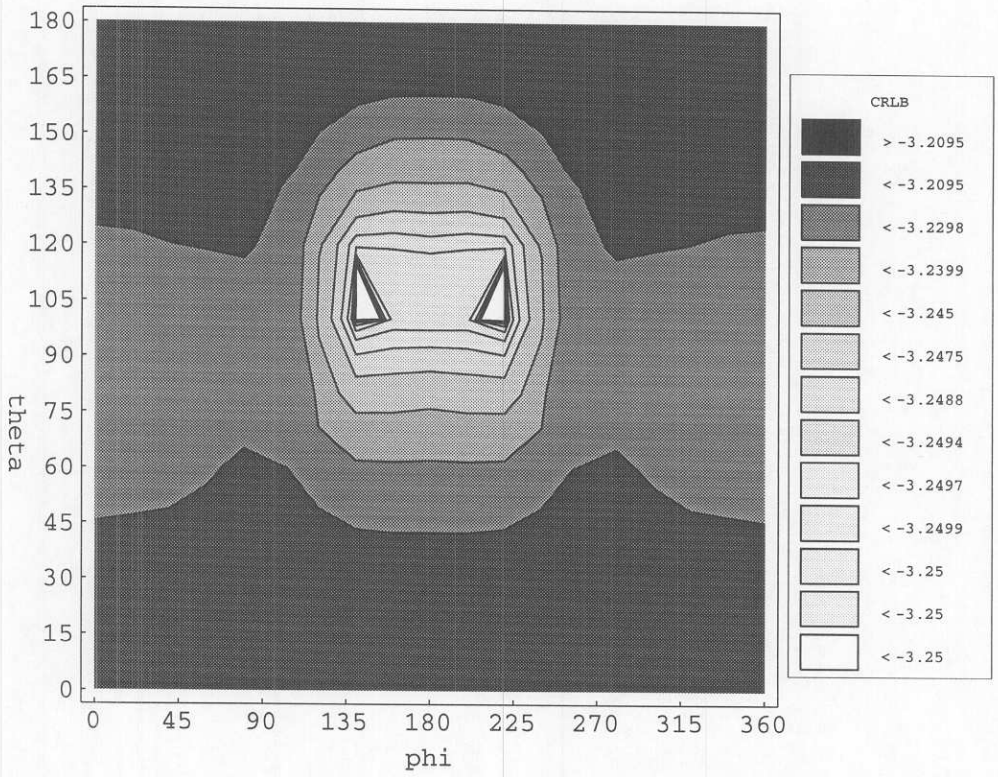

Figure 6.19: Best Location to Place Element 2 with More Detail

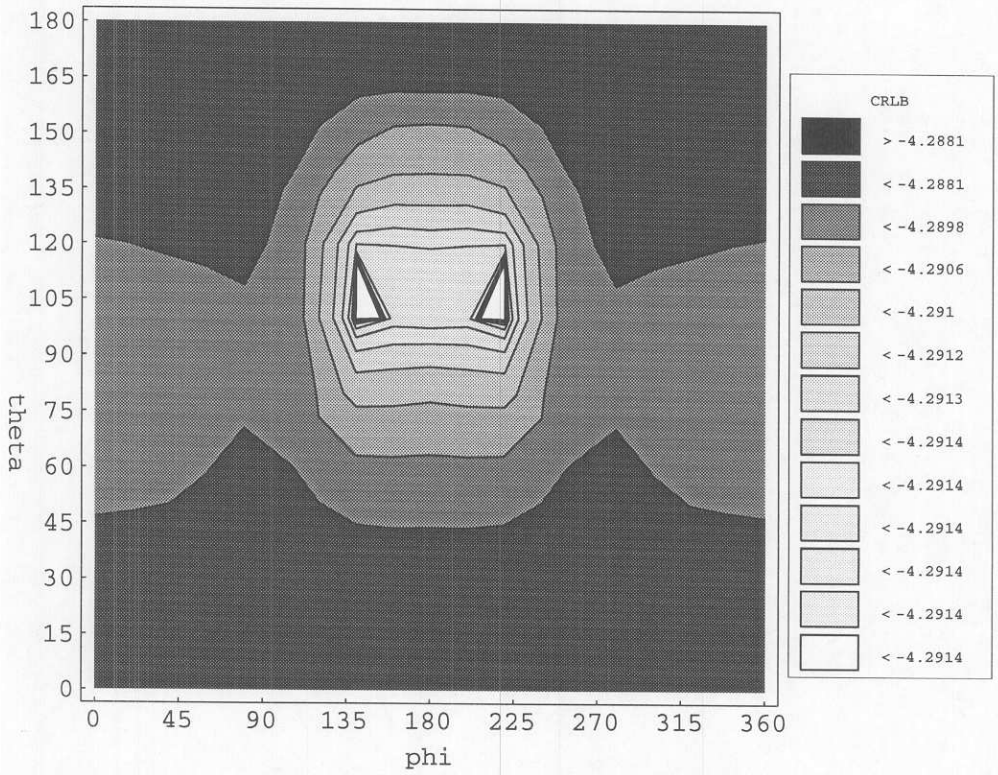

Figure 6.20: Best Location to Place Element 3 with More Detail

finding array with conventional array design methods. The positions of the elements in the Fisher's array, while symetric, are neither obvious or predictable. Therefore, Fisher's Information would seem to be a useful technique so far. But an unpredictable design such as the one just created is worthless if it doesn't work. Let us compare the Fisher designed array to a conventionally designed array to determine the Fisher technique's worth.

The array we will compare with will, of course, contain three elements. One element will be placed at $(\phi = 180°, \theta = 100°)$, one element at $(\phi = 60°, \theta = 100°)$, and one element at $(\phi = 300°, \theta = 100°)$. The design goal of this particular array is to maintain maximal separation of three elements in the $x - y$ plane. Maximal separation along a plane or line is a logical element placement which one might expect to find in a real world array. Therefore it makes since to compare our Fisher array to a maximally separated array.

Because the sum of CRLB's of the angles ϕ and θ is the information metric by which we want to compare arrays, we must calculate the sum of CRLB of the maximal separation array before continuing. This is accomplished in a manner similar to that in the Fisher's array design. The Fisher's Information array at the location for element one $(\phi = 180°, \theta = 100°)$ is first multiplied by ten to compensate for a similar multiplication in the Fisher's design. It is then added to the Fisher's Information arrays at every other location around the sphere. This creates a new set of Fisher's Information arrays. The calculation of the CRLB at this intermediate step is unnecessary. We do not need it to choose the next element location. It was chosen prior to starting - $(\phi = 60°, \theta = 100°)$. The Fisher's Information at the second element location is in turn multiplied by ten and then added to the Fisher's Information arrays at every other location around the sphere. This operation creates another new set of Fisher's Information

arrays. These arrays are all inverted and the sum of elements $(1,1)$ and $(2,2)$ is performed. While we calculated the sum at each location around the entire sphere and contour-plotted this data in the bottom half of Figure 6.21, we are only interested in the sum at one point, that of location three ($\phi = 300°, \theta = 100°$). Figure 6.21 compares the sum of the CRLB's of ϕ and θ for the Fisher's design and the conventional design.

The magnitude of the sum of the CRLB's at the last element in the Fisher's design must be compared to the magnitude of the sum of the CRLB's for the last element in the conventional design. The last element in the Fisher's design was placed at ($\phi = 220°, \theta = 100°$), so the log of the CRLB is somewhere between -4.2913 and -4.2914. The last element in the conventional array was predetermined to be ($\phi = 300°, \theta = 100°$). The log of the sum of the CRLB at this location is near -4.1409. Therefore the sum of the CRLB for the Fisher array is lower than the sum of the CRLB for the non-Fisher case. Because the Cramer-Rao Bound is a lower bound, a lower sum is better and could potentially provide more information for use in direction-finding. This lends credibility to the Fisher design procedure because it shows that arrays designed with Fisher's Information can potentially yield better angle-of-arrival estimates.

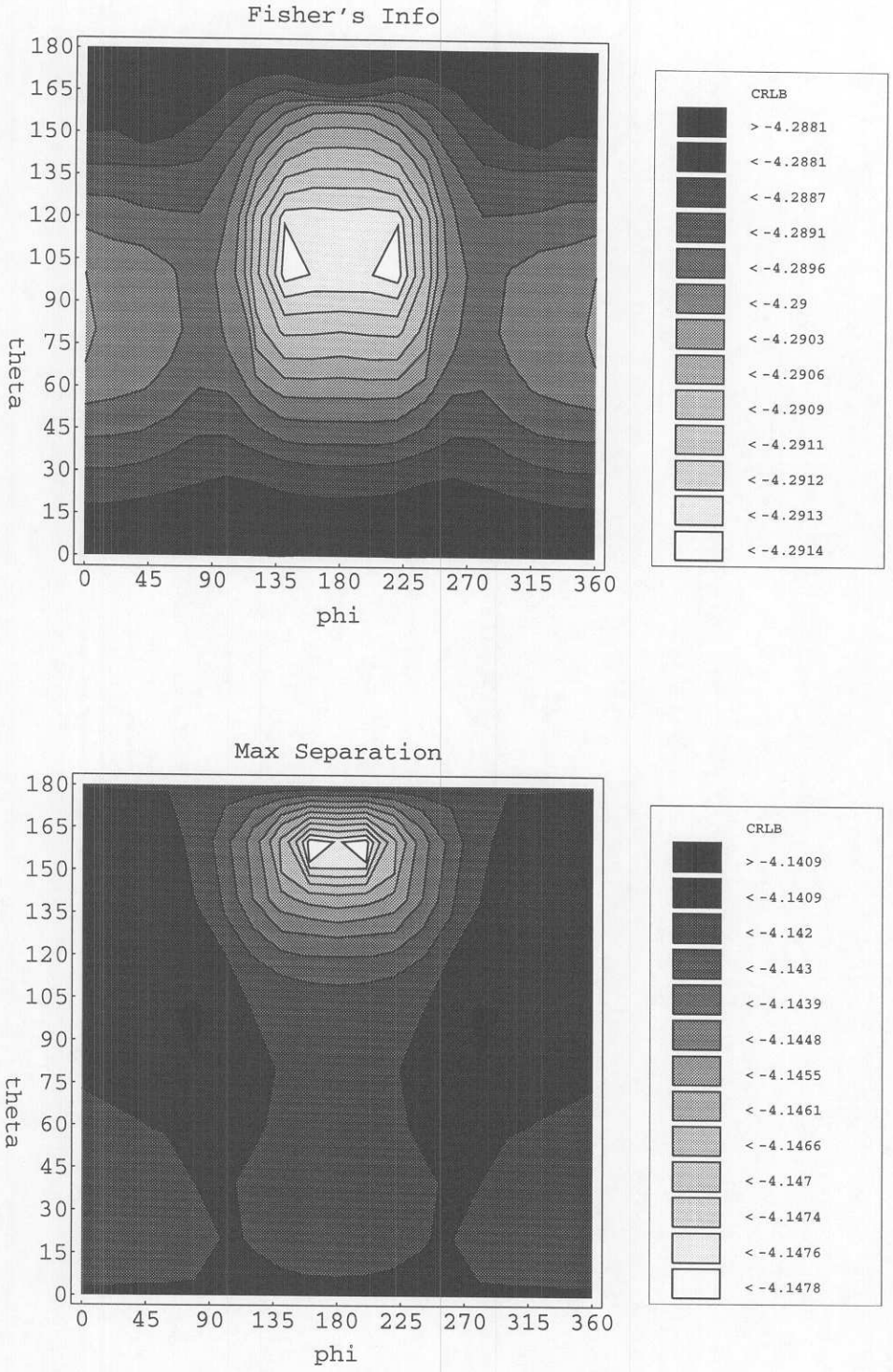

Figure 6.21: Comparing the sum of the CRLB's of Fisher and non-Fisher Designed Arrays

Chapter 7

Conclusions and Future Work

7.1 Conclusions

The plots from Chapter 6 illustrate some very important results. First, the locations of the sensors for arrays designed with Fisher's information are not always obvious or predictable. This indicates that previous methods of array design may not lead to arrays which are optimum for direction finding. Arrays designed with Fisher's information are potentially better in a direction finding sense. However, more work will be needed to quantify just how close these Fisher's arrays will approach an optimum condition.

The second conclusion we can infer from the results is that additive and multiplicative noise have different effects on DOA accuracy. This shows that modeling all channel inaccuracies as additive does not accurately represent some conditions such as imbalance. Therefore, a multiplicative noise model should be considered for inclusion in DOA estimation problems.

The third conclusion we can draw from this work is that we can use Fisher's Information to design arrays which complement our a priori knowledge of the direction finding problem. Stated another way, we can determine array designs that will maximize information about targets in the directions we know them to be a priori.

The last conclusion that can be made from this work is that Fisher's Information can be used as a metric for comparing different array designs. Because it can be calculated for all arrays (although maybe not so easily) and eliminates any dependencies on estimators, Fisher's Information allows us to compare one array to another without regard to the DOA processor. Thus, Fisher's Information gives us a design criteria which can be applied to direction finding arrays.

7.2 Future Work

The use of Fisher's Information in antenna array design is a promising technique. However, additional studies should be undertaken in order to fully characterize the value of this technique. Future work should address three items. First, future work should quantatively check the tightness of the Cramer-Rao Bound. By conducting a Monte-Carlo analysis whereby a number of different random arrays are connected to a MAP estimator, the performance of each of these arrays can be compared with the performance of the Fisher's array. If none of the random arrays perform better than the Fisher's array, the Cramer Rao Bound is a tight bound, and the Fisher's Information technique produces superior direction finding arrays. If even one of the random arrays performs better than the Fisher's array, the Cramer Rao Bound is not a tight bound, and Fisher's Information produces inferior direction finding arrays. The question then becomes how inferior and additional investigation would be required.

The second item of future work involves the amplitude and phase of the incident wave. In this study, the amplitude and phase of the incident wave were considered known quantities. The primary reason for this was the resulting simplification in the mathematics. If the amplitude and phase of the incident wave were considered unknown, then they would have had to be included in the list

of parameters to estimate. Instead of estimating four parameters $(\phi_i, \theta_i, \chi, \psi)$, the problem would have required estimation of six parameters (the original four plus amplitude and phase). This would have grown the Fisher's Information matrix from a four-by-four to a six-by-six and would have lengthened computation time considerably. Nonetheless, by fixing amplitude and phase, it is possible that some important information about direction of arrival is lost. Therefore, it is recommended that this experiment be performed in a future study.

The last item of study which should be undertaken is to repeat all the work in this paper using different conformal structures for the array. Simple structures such as a cylinder should be attempted first, graduating to more complex conformal shapes such as nose cones and aircraft wings. It is these more practical shapes which are of greater interest to the defense and aerospace industries. While more complex conformal arrays will likely require complete numerical solutions, the application of Fisher's Information to complex conformal array design will test the true merit of the technique.

Bibliography

[1] Constantine A. Balanis, Advanced Engineering Electromagnetics, New York:John Wiley & Sons, 1989.

[2] Yaakov Bar-Shalom and Xiao-Rong Li, Estimation and Tracking: Principles, Techniques, and Software, Boston:Artech House, 1993.

[3] E. T. Bayliss, "Design of Monopulse Antenna Difference Patterns with Low Side Lobes," BSTJ, Vol. 47, pp. 623-650, May-June 1968.

[4] C.L. Dolph, "A Current Distribution for Broadside Arrays which Optimizes the Relationship between Beam Width and Side-Lobe Level," Proc. IRE, Vol. 34, pp. 335-348, 1946.

[5] R.C. Hansen, Phased Array Antennas, New York:John Wiley & Sons, 1998.

[6] Roger F. Harrington, Time Harmonic Electromagnetic Fields, New York:McGraw Hill, 1970.

[7] H. Jasik and R.C. Johnson, Antenna Engineering Handbook, New York:McGraw Hill, 1993.

[8] Steven M. Kay, Fundamentals of Statistical Signal Processing, Upper Saddle River, NJ:Prentice Hall, 1993.

[9] Hamid Krim and Mats Viberg, "Two Decades of Array Signal Processing Research," IEEE Signal Processing Magazine, pp. 67-94, July 1996.

[10] Alberto Leon-Garcia Probability and Random Processes for Electrical Engineering, Reading, MA:Addison-Wesley, 1994.

[11] K. Sam Shanmugan, Random Signals: Detection, Estimation, and Data Analysis, New York:John Wiley & Sons, 1988.

[12] Ralph O. Schmidt, A Signal Subspace Approach to Multiple Emitter Location and Spectral Estimation, Ph.D. Thesis, Stanford University, Stanford, CA, November 1981.

[13] Ralph O. Schmidt, "Multiple Emitter Location and Signal Parameter Estimation," IEEE Trans. on Antennas and Propagation, Vol. AP-34, No. 3, March 1986.

[14] T.T. Taylor, "One Parameter Family of Line Sources Producing Modified $\frac{\sin \pi u}{\pi u}$ Patterns," Rep. TM 324, Hughes Aircraft Co., Culver City, CA, 1953.

[15] T.T. Taylor, "Design of Line-Source Antennas for Narrow Beamwidth and Low Sidelobes," Trans. IRE, Vol. AP-3, pp. 16-28, 1955.

[16] F.T. Ulaby, Fundamentals of Applied Electromagnetics, Upper Saddle River, NJ:Prentice Hall, 1997.

[17] F.T. Ulaby and C. Elachi, Radar Polarimetry for Geoscience Applications, Norwood, MA:Artech House, 1990.

[18] Harry L. Van Trees, Detection, Estimation, and Modulation Theory, Part I, New York:John Wiley & Sons, 1968.

[19] B.D. Van Veen and K.M. Buckley, "Beamforming: A Versatile Approach to Spatial Filtering," IEEE ASSP Magazine, pp. 4-24, April 1988.

[20] Anthony J. Weiss and Bejamin Friedlander, "Performance Analysis of Diversely Polarized Antenna Arrays," IEEE Transactions on Signal Processing, Vol. 39, No. 7, pp. 1589-1603, July 1991.